Low EMF Exposure Future Networks

LEXNET
Low EMF Exposure Future Networks

D4.2: Performance Evaluation of Low Exposure Index Solutions for Components and Transmission Techniques

Contractual delivery date: M24
Actual delivery date: M25

Document Information

Version	V1.0	**Dissemination level**	PU
Editor	E. Kocan (UoM)		
Other authors	Yenny Pinto(TPT), Xavier Begaud(TPT) Pat Chambers (UNIS) Yolanda Fernández (TTI), Adrián Sánchez (TTI) Massinissa Lalam (SAG) Dan Dragomir (UPB) Milica Pejanovic-Djurisic (UoM) Philippe CIBLAT (TPT) Yiwei Fang (FLE)		

	Antonio De Domenico, Antonio Clemente, Serge Bories (CEA)
Abstract	Based on a common evaluation 5-step methodology, initial performance assessments of the innovative solutions considered within WP4 are carried out. A dozen of radio components and transmission techniques solutions are developed and evaluated through ratio of the Exposure Index. The proposed intermediate performances assessments show a large range of exposure reduction from non-significant to ninety percent reduction, while keeping QoS constant. Despite a large diversity of solutions, the adopted methodology makes possible the comparison of their effectiveness but also allows to highlight some compatibility or at the opposite some conflicts between these solutions. This last point is a mandatory step to prepare solution prioritization and global exposure reduction assessment.
Key words	Exposure Index, evaluation methodology, transmission techniques, Components

Project Information

Grant Agreement n°	318273
Dates	1st November 2012 – 31th October 2015

Document approval

Name	Position in project	Organisation	Date	Visa
Joe Wiart	Coordinator	France Telecom	01/12/2014	OK

Document history

Version	Date	Modifications	Authors
V0.0	02/07/2014	Initial document template	E. Kocan (UoM)
V0.1	20/10/2014	Contribution submission from partners	All
V1.0	21/10/2014	Assembly of the Master document	E. Kocan (UoM)
V1.3	02/11/2014	Formatting and corrections	E. Kocan (UoM), M. Pejanovic-Djurisic (UoM) S. Bories (CEA)
V1.5	07/11/2014	Internal review	F. Cardoso (INOV)
V1.7	13/11/2014	Internal review	M. Lalam (SAG)
V1.9	14/11/2014	Revised contributions from partners	All
V2.0	14/11/2014	Assembly of the final document	E. Kocan (UoM), S. Bories (CEA)

Table of Contents

Executive Summary

The goal of the low EMF exposure future networks (LEXNET) project is to provide means of reducing human exposure to electromagnetic fields (EMF) that emanate from radio frequency (RF) communications devices. In the frame of “Smart Low EMF Radio” work package (WP), the aim is to recognize the innovative radio components and transmission techniques with the highest potential for Exposure Index (EI) reduction, among the different proposed solutions, as well to quantitatively asses the level of EI reduction they can achieve. The overall contribution of this deliverable is to present the intermediate performance assessment of different examined solutions that optimize exposure, all conducted in accordance to an adopted common evaluation methodology.

The objective this report is to summarize the initial performance assessment in terms of EI reduction of radio components and transmission techniques, and to present them in a comparable manner. Through using a five-step approach in a common evaluation methodology for EI assessment all the proposed solutions will provide results on EI reduction in a unified manner. Moreover, by examining the proposed solutions in the relevant scenarios defined in WP2, the obtained results ensure that as fair as possible comparison of the effectiveness between solutions can be attained. Using these results, and taking into account planed future research work, i.e. the potential for further EI reduction within each examined solution, selection can be made among the Low EMF technologies research work, and priority can be given to more effective ones. Also, the expected EI reduction after combining some of the proposed innovative techniques can be better assessed through having this kind of unified results.

Before presenting individual solutions, the deliverable provides a detailed explanation of the common evaluation methodology used for exposure assessment. The 5-step approach has been adopted by WP4 in order to deliver harmonized exposure improvements at the final step. They also aim to simplify discussions, to prepare the future global exposure reduction evaluation, and the most promising WP4 techniques selection.

The project is approaching the end of the second year, and most of the proposed solutions have made clear relation with the EI reduction, while some of them are still missing this step, necessary to obtain an insight in their potential for becoming “low EMF exposure techniques”. Even for the solutions where EI ratio has been calculated, and where the obtained results may justify their possible practical implementation for EI reduction, the results have to be consolidated whether by more realistic assumptions on the analysis, by further developments, by checking the impact of a solution on other system performances (energy consumption, complexity,..), or by widening the scenario to demonstrate a more general relevancy.

Some of the proposed solutions for EI reduction present the cutting edge of research, while the other analysed radio components and transmission solutions are partially (re)using known physical mechanisms developed to solve other issues in wireless communication systems (energy consumption, capacity increasing, antenna

decoupling). Their innovation is first in the adaptation of these mechanisms to the EM exposure lowering. Secondly the novelty of this work is in the analysis itself of a global assessment of the exposure (UL and DL, over a population) thanks to modified or specifically developed tools.

The obtained exposure index ratio results, which represents the level of EI reduction, range from the very low values (less than percent), up to ninety percent. Those solutions with promising EI reduction are generally considered in specific scenarios. They have to be further examined in order to obtain better insight into their potential for global EI reduction, as well as to assess the possibilities for combining them with the other proposed low EMF exposure solutions.

LIST OF ACRONYMS

Abbreviation	Meaning
3GPP	Third generation partnership project.
ACK	Acknowledgement
ADC	Analog to Digital Converter
AF	Amplify-and-forward
AMC	Artificial Magnetic Conductor
AP	Access point
ARQ	Automatic repeat request
AWGN	Additive white Gaussian noise
BB	Base Band
BCH	Broadcast Channel
BER	Bit error rate
BPF	Bandpass filter
BS	Base Station
CDF	Cumulative distribution function
CDM	Code division multiplexing
COMP	Coordinated multipoint transmission
COTS	Component of the shelf
CRS	Cell specific reference signal
CSI	Channel state information
CSIT	Channel state information at transmitter
CSMA/CA	Carrier sense multiple access with collision avoidance
CSRS	Cell-Specific Reference Signal
CW	Continuous wave
D	Destination terminal
DAC	Digital to Analog Converter
DCR	Direct Conversion Receiver
DDC	Digital Down Converter
DF	Decode-and-forward
DL	Downlink
DMRS	Demodulation reference signals
DT	Direct transmission
DTC	Digitally controlled capacitor
DTX	Discontinuous Transmission
DUC	Digital Up Converter
EBG	Electromagnetic Band Gap
EE	Energy efficiency
EI	Exposure Index
eICIC	Enhanced inter-cell interference coordination
EM	Electromagnetic
EMF	Electromagnetic field
eNB	Evolved Node B

FDD	Frequency Division Duplex
GaN	Gallium Nitride
HARQ	Hybrid automatic repeat request
HetNet	Heterogeneous Network
HIS	High Impedance Surface
HPA	High power amplifier
HPA	High Power Amplifier
HPF	Highpass filter
I/Q	In-phase and Quadrature components
IEEE	Institute of electrical and electronics engineers
IF	Intermediate frequency
IFA	Inverted F Antenna
ILA	Inverted L Antenna
ISD	Inter-site distance
ISM	industrial, scientific and medical
KPI	Key Performance Indicator
LDMOS	Laterally Diffused Metal Oxide Semiconductor
LNA	Low noise amplifier
LOS	Line of sight
LPF	Lowpass filter
LTE	Long term evolution
MAC	Medium access control
MC	Macro cell
MCS	Modulation and coding scheme
MEMS	Micro Electro-Mechanical Systems
MeNB	Macro eNB
MIMO	Multiple Input Multiple Output
MMIC	Monolithic Microwave Integrated Circuit
NACK	Negative acknowledgement
NF	Noise figure
OFDM	Orthogonal frequency division multiplexing
OFDMA	Orthogonal frequency division multiple access
PCB	Printed Circuit Board
PDSCH	physical downlink shared channel
PR	Primary receiver
PRR	Packet reception rate
PSS	Primary synchronization signals
QoS	Quality of service
R	Relay station
RAT	Radio access technology
RB	Resource block
RE	Resource element
REB	Range Expansion Bias
RF	Radio frequency

RHIS	Resistive High Impedance Surface
RL	Reinforcement learning
RSRP	Reference signal received power
RSS	Receive signal strength
Rx	Receiver
S	Source of information
SAR	Specific absorption rate
SC	Small Cell
SCeNB	Small Cell eNB
SCM	Subcarrier mapping
SINR	Signal to interference plus noise ratio
SIR	Stepped Impedance Resonator
SISO	Single Input Single Output
SNR	Signal to noise ratio
STA	Station
SotA	State of the art
TCP	Transmission control protocol
TDD	Time division duplex
TDM	Time-domain multiplexing
TDMA	Time division multiple access
TPC	Transmit power control
Tx	Transmitter
UE	User Equipment
UL	Uplink
UMTS	Universal mobile telecommunications system
VGA	Variable gain amplifier
WAN	Wide area network
WCDMA	Wideband code division multiple access
WiFi	Wireless fidelity
WiMAX	Worldwide interoperability for microwave access
WLAN	Wireless local area network
WMN	Wireless mesh network
WP	Work package
WSN	Wireless sensor network.
WWAN	Wireless wide area network

LIST OF FIGURES

LIST OF TABLES

INTRODUCTION

The LEXNET project, through its mission to reduce human exposure to EMF originating from RF communication devices, brings twofold novelties: First it aims to quantify the EMF exposure with a global approach, and then it introduces innovative techniques and demonstrates their quantitative impacts both on the exposure reduction and on the Quality of Service (QoS). A major step toward addressing the quantification to EMF exposure was definition of all the relevant parameters influencing Exposure Index (EI), irrespective of the type of the RF device, or RF technology it emanates, and putting them together in single formula defining the EI. On the other hand, when different innovative solutions for EI reduction are considered, almost of the same importance like EI formula definition was adoption of the common EI evaluation methodology. Such an approach will provide unified results on EI reduction for different proposed solutions. It will also ensure as fair as possible comparison between the various solutions for EI reduction, including various radio components and different transmission techniques considered in the frame of WP4. Based on this, each of the technologies developed in the project is examined by similar criteria and therefore making it possible to compare the effectiveness of the technologies developed and to prioritise certain ones in the long term planning of the LEXNET project. However, it should be born in mind that different proposed solutions do not compete among each other, and cannot be compared in completely fair conditions, as they may be solutions for different communications systems, in different communications scenarios, for different traffic types, etc., and at least different parameters may be taken as the QoS performance measures. Thus, many of the analysed innovative solutions may be actually complementary and can be combined to achieve higher global EI reduction.

This deliverable presents intermediate performance assessment of the six solutions for RF components and five solutions at the radio transmission techniques, which should reduce the EI. All the solutions are examined using the adopted common exposure evaluation methodology. In this way, different proposed solutions for EI reduction could be compared. The obtained results have shown that some of the analysed solutions do not have significant impact on lowering EI, as they reduce EI for less than 1%, or for several percent. On the other side, some very promising radio component's solutions can bring EI reduction up to 80% (beamforming techniques in indoor scenario), or even up to 90% (interference mitigation in wireless sensor network) of EI reduction when we talk about radio transmission techniques.

The content of the deliverable is as follows. Chapter 1 is a summary chapter to describe the common exposure evaluation framework that the WP4 has agreed on. Under this framework, effectiveness of each technology developed by the partner organization will be examined by similar criteria. The five-step harmonized evaluation framework will provide unified exposure reduction results, which will enable to prepare the future global exposure reduction evaluation that will consist in an integration of the improvements of the WP4 solutions. Moreover the most promising WP4 techniques selection will be partially based on this performances assessment, but also taking into account potential of each proposed solution for further EI reduction through the planned future research work.

Chapter 2 comprises the assessment of the six technical solutions for RF components design aimed for EI reduction, and presents the planned future research works of each partner. The considered solutions include: Antenna on terminal for low exposure index, Beamforming techniques, Small and directive antenna, Low noise receiver architecture, Cell DTX (Discontinuous Transmission) amplifier deactivation and Sleep/Idle mode in a mesh gateway deployment.

In Chapter 3, assessment of the five transmission technologies for exposure reduction is presented, jointly with the planned future research work and foreseen potential for further effectiveness improvement of the each solution. The analysed transmission technologies are: Enhanced efficiency in reference symbol usage, Interference mitigation in Zigbee and WiFi, Radio link allocation, Low exposure cooperative communication techniques and Interference management in heterogeneous network.

In the final chapter, concluding remarks on WP4 work progress are given, as well as future objectives.

1 COMMON WP4 EXPOSURE EVALUATION

This chapter gives an update on the exposure evaluation process regarding the previous one detailled in Chapter 4 of deliverable D4.1 [1]. The Exposure Index (EI) formula is now consolidated and first practical implementations have been demonstrated in the deliverable D2.4 [2] and in [3]. Meanwhile, the WP4 individual studies have independently progressed and devoted effort to the exposure evaluation practical assessment which has highlighted some common and some specific issues.

Despite a large diversity of technical domains, whatever the scenario or the Radio Access Technologies (RAT), this chapter presents a single strategy to organize and align the different WP4 exposure evaluations. A 5-step approach has been established in order to evaluate and harmonize the overall exposure improvement for each technology in the future. These steps also attempt to provide the basis for global exposure reduction evaluation in order to determine the most promising WP4 techniques based on fair and relevant comparisons.

The step-1 (section 1.1) identifies how the individual WP4 techniques contribute towards the overall LEXNET use case scenarios from WP2. Specifically to WP4 evaluations, we have introduced four sub-scenarios to assist in separating the different techniques under investigation. WP4 studies have been structured based on those sub-scenario highlighting which ones are complementary and which ones will require further analysis to determine potential conflicts.

The step-2 (section 1.2) clearly identifies the Key Performance Indicators (KPIs) being addressed by individual technique investigation. To facilitate this process, a limited numbers of Key Performances Indicators (KPI) for the exposure and for the QoS are used in the evaluation of each technique. As detailed in section 1.2, the second step is to clearly identify the KPIs being addressed by individual technique investigations.

The step-3 (section 1.3) concerns the evaluation itself of a partial EI ratio, in comparison with a baseline scenario without implementing the studied solution.

The step-4 (section 1.4) aims to ensure that capacity or QoS improvements are converted into exposure reduction. An objective of our research is to reduce exposure without impacting QoS.

At last the step-5 (section 1.5) estimates the absolute global EI reduction from the previous steps partial EI results throught the 24 hours LEXNET reference scenario.

1.1 Step-1: Sub-scenarios Description

By pursuing the objective of evaluating the global EI of the WP4 solutions [1], a top-down process is first applied in order to assess the performance of each individual solution. A partial evaluation is undertaken by selecting one or more branches of the tree of exposure (e.g. , location, choice of RAT and specific time of day) for which a

specific WP4 solution can be applied. This 'solution-specific' assessment for a given mechanism simplifies the evaluation by only considering the relevant parameters to a specific scenario.

1.1.1 Step-1 a: Sub-scenario compatibility

Thus, it has been decided to define four 'sub-scenarios':

- Small Cell (SC)
- Macro Cell (MC)
- Rural
- Wi-Fi & Wireless Sensor Network (WSN)

Each WP4 solution has to specify whether it is compatible or not with the sub-scenarios. The compatibility decision is based on technical compatibility with a context or a standard but could also consider other criteria (relevancy regarding EI reduction amount, energy consumption…). Practically a so called 'sub-scenario table' is mentioned for the sub-scenarios being addressed by the technology under investigation. For all the solutions analysed within WP4,Table 1 describes the sub-scenario considered.

Table 1 WP4 Sub-scenario table

Solution title	Small Cell	Macro Cell	Rural	Wi-Fi & WSN
Antenna on terminal for low exposure index	x	x	x	x
Beamforming techniques	x			x
Small and directive antenna for low exposure index	x			x
Low noise receiver architecture	x			
Cell DTX amplifier deactivation		x		
Sleep/idle mode in a mesh gateway deployment				x
Enhanced efficiency in reference symbols usage	x	x		

Interference mitigation in Zigbee & WiFi				x
Radio link allocation in WSNs				x
Low exposure cooperative communication techniques		x	x	
Interference management in heterogeneous network	x	x		

1.1.2 Step-1 b: Inputs description

In order to harmonize the evaluations of the different solutions studies, it is crucial to describe properly and extensively each assumption and each input parameter values related to the context study.

The important parameters, their range of values, and references, in which these parameters are defined, have to be mentioned in a dedicated table for each studied solution. Table 2 gives an example of inputs description for the small and directive Small-Cell (SC) Base Station (BS).

Table 2 Example of Inputs description for the small and directive antenna for the SC BS

Inputs	Description	Values (or range)	Reference
Environment	Spatial deployment (ISD…)	250 meters radius for the Macro Cell	[24]
EU or source density	EMF sources number	90 active user equipment (UE) in the MC	[24]
	Antenna gain	27 SC BS (9/MC sector)	[24]
	Max. Tx Power at MC	46 dBm (13 dBi ant. gain)	[24]
	Max. Tx Power at SC	30 dBm (5 dBi ant. gain)	[24]
Frequency	Central frequency/ Bandwidth	800 MHz / 5 MHz 2 GHz /10 MHz	[24]
Signal duration	Typical duration (duty cycle)	LTE Frame:10us	[24]
Traffic load	Throughput (low, medium, high)	Medium to high (UL:0.1-1 Mbps)	[24]
Path loss	Fast fading model	Winner phase 2	[25]

model, indoor/outdoor	Shadowing model Directional model	Winner phase 2 Winner phase 2	
Protocols	Any process managing Ptx, transmit duration or SAR	-Association: Best SINR+CRE* (CRE={0,3,6})	[24]

1.2 Step-2: Exposure and QoS Metrics Identification

The final objective of WP4 evaluation is to consider the EI as a global exposure reduction KPI. The definition of the EI in (1.1) is fully detailed and analysed in [1]. Nevertheless it is more convenient to work with one of the following three simpler metrics or KPIs derived from the EI formula.

$$\mathrm{EI} = \sum_{i}^{N_{\mathrm{Periods}}} \sum_{j}^{N_{\mathrm{Individuals}}} \sum_{k}^{N_{\mathrm{Locations}}} \sum_{l}^{N_{\mathrm{RATs}}} \left[\left(\sum_{m}^{\mathrm{N_{Usages}}} t_{i,j,k}^{\mathrm{UL}} \beta_{i,j,k,l,m}^{\mathrm{UL}} . \mathrm{SAR}_{l,m}^{\mathrm{Tx}} . \frac{P_{\mathrm{Tx}}}{P_{\mathrm{Tx|Ref}}} \right) + t_{i,j,k}^{\mathrm{DL}} \alpha_{i,j,k,l}^{\mathrm{DL}} . \mathrm{SAR}_{l}^{\mathrm{Rx}} . \frac{P_{\mathrm{Rx}}}{P_{\mathrm{Rx|Ref}}} \right] \quad (1.1)$$

For brevity, only Uplink (UL) KPIs are detailed hereafter; but Downlink (DL) ones are quasi equivalent.

- The first metric is the **Specific Absorption Rate** ($\mathrm{SAR}_{l,m}^{\mathrm{Tx}}$) which describes the amount of Electromagnetic (EM) energy absorbed into the user's body via the spatial distribution of the EM field from the source. Thus SAR is particularly relevant for antenna solutions.
- The second metric is the **mean duration of exposure** ($t_{i,j,k}^{\mathrm{UL}}$) which indicates the amount of time the user is exposed. It impacts the EI which is defined as a dose. A dose corresponds to the integration of instantaneous exposure (e.g. SAR) over the exposition duration. For example the duration is impacted by the amount of transmitted data. Reduced retransmission, improved interference management, and signalling reduction strategies are all ways of decreasing this metric. The duration used to calculate the mean is selected regarding the time constant of the studied technique.
- The third metric is the **mean transmitted power** (P_{Tx}) during the considered mean exposure duration. Again the duration used to calculate the mean is selected regarding the time constant of the studied technique.

Near Field distribution, frame-level transmission mean duration and mean transmitted power are three metrics typically handled by hardware and radio link design tools.

Each investigation provided a table for the KPIs being addressed by the technology under investigation, as shown in Table 3. Moreover due to the strong asymmetry of the exposure between the UL and DL, this information is provided in the dedicated column of the "Exposure KPIs" identification table.

Concerning the QoS, no metric has been imposed but each study has selected a parameter which is an alternative performance measure of QoS. The objective is to ensure that the implementation of the envisaged solution maintains the QoS compared to the case where this solution is not implemented.

Table 3 Exposure KPIs identification in the WP4 solution evaluation

Solution title	UL/DL	Exposure KPIs			QoS KPI
		SAR	Mean Tx power	Mean Tx duration	
Antenna on terminal for low exposure index	UL/DL	x			Impedance matching Total efficiency Radiation pattern
Beamforming techniques	UL/DL	x			BeR
Small and directive antenna for low exposure index	UL/DL		x		SiNR at Rx side
Low noise receiver architecture	UL		x		Noise Figure
Cell DTX amplifier deactivation	DL		x		
Sleep/idle mode in a mesh gateway deployment	DL		x		Coverage
Enhanced efficiency in reference symbols usage	DL			x	The probability of channel estimation error
Interference mitigation in Zigbee & WiFi	DL		x	x	Packet Reception Rate
Radio link allocation in WSNs	DL		x	x	Packet Reception Rate
Low exposure cooperative communication techniques	DL		x		Capacity
Interference management in heterogeneous network	DL		x		Throughput

1.3 Step-3: EI Ratio Evaluation

1.3.1 Exposure Evaluation

This step corresponds to the exposure evaluation itself but by considering only a given sub-scenario. The exposure reduction is evaluated through the calculation of an EI ratio ($\mathrm{Ratio}_{\mathrm{EI}}(\%)$) by comparing the 'with LEXNET' versus the 'without LEXNET' (i.e., SotA or standard) baseline configurations as shown in (1.2).

$$\mathrm{Ratio}_{\mathrm{EI}}(\%) = \frac{\mathrm{EI}_{\mathrm{partial}}(\mathrm{w\ LEX}) - \mathrm{EI}_{\mathrm{partial}}(\mathrm{wo\ LEX})}{\mathrm{EI}_{\mathrm{partial}}(\mathrm{wo\ LEX})} \times 100 \quad (1.2)$$

The three KPIs detailed in section 1.2 are variables independent of each other. This means that if a solution succeeds in decreasing one of the three KPIs, the two other will stay constant. Thus, All other things being equal, the EI ratio is thus equal to the identified KPI ratio as shown in (1.3). This approach brings a major advantage to simplify exposure reduction evaluation because it is easily matched with a typical RF front-end or PHY layer evaluation studies. By convention the EI ratio is negative when a reduction of exposure is reached.

The equation (1.2) is simplified when a specific sub-scenario is considered:

$$\mathrm{Ratio}_{\mathrm{EI}}(\%) = \frac{\mathrm{KPI}_{\mathrm{partial}}(\mathrm{w\ LEX}) - \mathrm{KPI}_{\mathrm{partial}}(\mathrm{wo\ LEX})}{\mathrm{KPI}_{\mathrm{partial}}(\mathrm{wo\ LEX})} \times 100 \quad (1.3)$$

where:
$\mathrm{EI}_{\mathrm{partial}}$ is the Exposure Index for a specific sub-scenario; $\mathrm{KPI}_{\mathrm{partial}}$ is the metric identified in step-2 calculated in the sub scenario context. The subscript 'w LEX' correspond to the LEXNET solution implementation, and the subscript 'wo LEX' correspond to the SotA or baseline (without the solution implementation).

At last, it is important to check that the improvement on DL exposure has no impact on the UL exposure, and vice versa.. General trade-off governing interactions between both kinds of exposure can be found in the SotA of [1]. Thus both UL and DL EI ratio should be evaluated.

1.3.2 QoS evaluation

Meanwhile the QoS metric identified in step-2 is also evaluated with and without LEXNET solution. One of the LEXNET objectives is to maintain the QoS level while reducing exposure.

1.4 Step-4: Capacity/QoS Improvements Convertion into EI Reduction

The step-4 has to be considered only if the implementation of the evaluated solution improves other performances, like are capacity or QoS (Figure 1). Actually this usually happens because lots of the considered hardware solutions or radio links techniques have been initially designed in order to increase either capacity or QoS. The idea is to convert this QoS improvement in term of EI reduction for example by reducing the transmit power level.

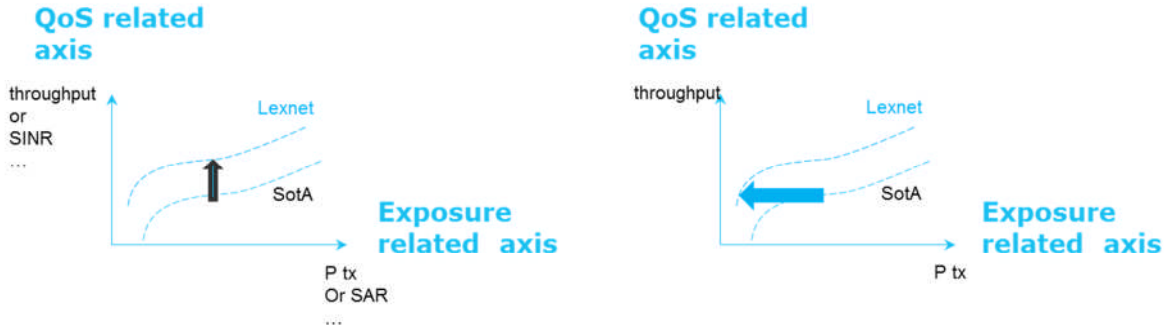

a) Study where QoS is improved b) Study where exposure is reduced

Figure 1 Capacity/QoS improvements conversion into Exposure metric reduction

1.5 Step-5: Global EI Reduction Assessment

From the previous steps, a relative EI reduction is assessed for a specific sub-scenario. However the final goal of LEXNET is to propose techniques that achieve absolute EI reduction taking into account the absolute exposure level and dose per day. The impact of proposed solution has to be evaluated regarding the 24h activities breaking down. The so-called dilution factor [1] is taken into account during this step-5. The usage statistics are used to weight the calculated partial EI reduction in order to assess the global EI reduction for a given solution.

To conclude this chapter,

Figure 2 summarizes the common EI evaluation methodology. This process is sufficiently generic to be applied by any of the WP4 proposed solutions. In the next chapters, the described approach for EI reduction evaluation it is implemented by following it steps by steps. Step-5 is not addressed yet according to the current progress of the WP4.

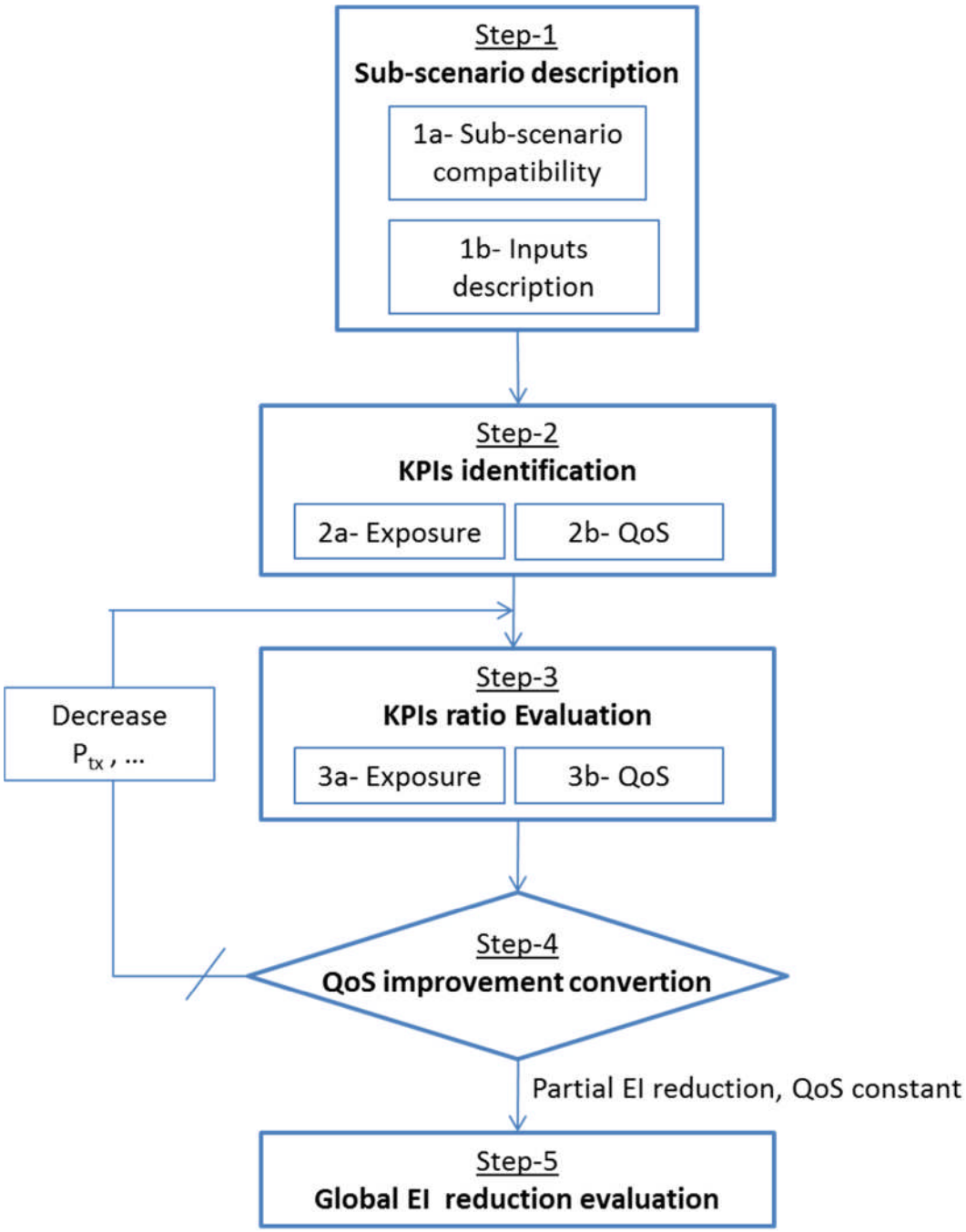

Figure 2 Common EI evaluation methodology for WP4 solutions

2 PERFORMANCE EVALUATION OF LOW EXPOSURE RADIO COMPONENTS

2.1.1 Antenna on terminal for low exposure index

The antenna characteristics and location have an influence on the SAR. The exposure can be reduced by applying some techniques in the antenna design. The main techniques are focused on the separation of the antenna (handset, laptop) and the human organ (head, hand, etc...) by either, increasing the distance [4] or using an electromagnetic shield, between the antenna and the user [5]. Another technique [6] is to suppress the current flowing in the handset box by using a ferrite sheet attached to the antenna. Despite the good performance of these techniques, these are expensive and require complex manufacturing.

Today, mobile and wireless industry requires a low cost and easy implementation solution to reduce human exposure. In this way, recent researches are focused on the use of metamaterials because they can be easily fabricated using Printed Circuit Board (PCB) processes.

2.1.2 Remind on the concept

The challenge is to show the benefits of using metamaterials in order to minimize the surface waves on the PCB of the devices. These metamaterials are usually composed of tailored and tiny (size ~ 0.1 wavelength) structures in metallic/dielectric materials. They have interesting properties when a sufficient number of metamaterials cells are used. So the objective is to prove that it is possible to have an improvement even if the PCB is small. Dimensions of the PCB are around 12.5 cm by 6 cm (classical smartphone dimensions).

Three different structures of metamaterials have been studied: the AMC (Artificial Magnetic Conductor), the EBG (Electromagnetic Band Gap) and the RHIS (Resistive High Impedance Surface). These artificial materials have the capability to act as a magnetic conductor to reduce surface currents (AMC), to reduce surface waves (EBG) and to absorb currents (RHIS) [7], [8], [9], [10].

2.1.3 Evaluation methodology

The evaluation method is to compare the metamaterial solution (the LEXNET solution) with a reference antenna. First, the method is focused on the antenna radiation characteristics comparison: surface currents, radiation patterns (far field and near field) given by EM simulations and validated by prototype measurements. Only the improved solutions will be realised.

As previously mentioned in D4.1 [1] the methodology is the following: Radiating characteristics of monopole and IFA (Inverted-F Antenna) will be analysed for each

antenna position (first at centre, then close to the edge). All these configurations are summarized in the Figure 3.

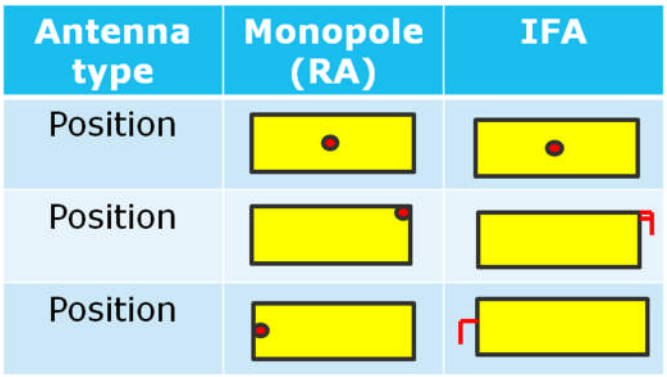

Figure 3 Antenna positions and configurations

Each study is composed of four steps:

1. Antenna design at 5 GHz, over a metallic ground plane;
2. Metamaterial design: AMC, EBG and RHIS;
3. Antenna with metamaterial design;
4. Radiation characteristics analysis;

The best solution will be kept after analysis of all the radiation characteristics and after measurement-based validation.

Finally, the SAR is calculated by performing simulations using a simplified model of the phantom, and the benefit of the LEXNET solution or exposure reduction is calculated comparing the SAR obtained with the reference antenna and the metamaterial antenna. The exposure reduction is evaluated through the calculation of an EI ratio (as mentioned in Chapter 1) by comparing the 'with LEXNET' (i.e. Antenna with best metamaterial solution) versus the 'without LEXNET' (i.e. Monopole Antenna) baseline configurations, Eq. (2.1).

$$\text{Ratio}_{\text{EI}}(\%) = \frac{\text{EI}_{\text{partial}}(\text{w LEX}) - \text{EI}_{\text{partial}}(\text{wo LEX})}{\text{EI}_{\text{partial}}(\text{wo LEX})} \times 100 \qquad (2.1)$$

2.1.3.1 Sub-scenario description

The mobile terminal antenna solution, based on metamaterials, is compatible with the four sub-scenarios: Small Cell, Macro Cell, Rural and WiFi & WSN.

The antennas will work at 2.6 GHz and 5 GHz bands. These bands corresponds to LTE (2.5-2.69 GHz) and one of the wireless standard 802.11n band (5 GHz). They can be implemented on terminals that are used indistinctly on both SC and MC; in the same way, terminals with metamaterial antennas can perform in a rural sub-scenario.

A first antenna solution is designed to work at 5GHz, compatible with Wi-Fi. Methodology and conclusions of this solution can be used as a guideline for a future study focused on 2.6GHz antennas.

2.1.3.2 Exposure and QoS metrics identification

The SAR is the metric used to evaluate the EI in the case of the terminal mobile antennas. The simplified model to calculate the SAR by simulations using CST software[1] is described in Figure 4. A flat phantom is illuminated by the mobile terminal antenna. The terminal is located on the center of the phantom. The model of the phantom consists on a homogeneous equivalent liquid with electrical properties: $\varepsilon_r = 39.29$, $\sigma = 3.479$ S/m and $\rho = 1030$ Kg/m^3 at 5 GHz.

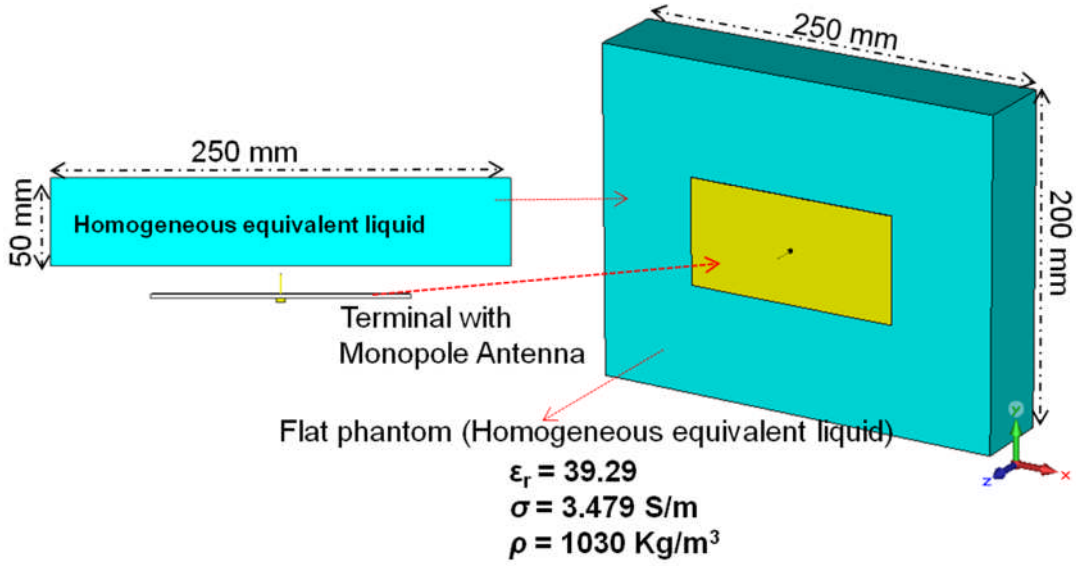

Figure 4 Simplified model for exposure simulation

Concerning QoS, the proposed antenna solution has to preserve the performance of the reference antenna. Then, QoS is evaluated by comparing the radiation characteristics of the reference antenna to the metamaterial antenna.

The first step is to verify that the antenna is matched, then, it's necessary to calculate the radiation of each antenna. The radiation efficiency has to be preserved and the radiation of the antenna has to be as omnidirectional as possible, this implies that realised gain has not to be higher than few dB. The KPIs for the terminal antenna solution are impedance matching, total efficiency and radiation pattern. The EI evaluation is not depending on the UL or the DL, in the case of the terminal mobile antenna solution.

2.1.3.3 EI ratio evaluation (or Capacity/QoS improvements converting into EI reduction)

As described on the methodology, two antennas solutions are analysed. The first solution is the monopole antenna, as reference case, and the second is the IFA antenna that is similar to a realistic case. The antenna is located on three different positions of a ground plane whose dimensions (~125mm x 60mm) are similar to

[1] CST-Computer Simulation Technology (https://www.cst.com)

standard smart mobile phones. Then, the antenna is surrounded with a metamaterial structure (AMC, EBG and RHIS).

In this document, results of the two cases, reference case (monopole antenna on the center) and realistic case (IFA antenna on the middle of the edge) are described.
All analysed solutions are presented in Appendix 2.

2.1.3.3.1 Monopole Antenna on the center

The QoS KPI parameters are displayed in Figure 5. If all parameters are taken into account (impedance matching, omnirectionnal pattern, and sufficient gain) it appears that a solution using an EBG structure seems to be not appropriated because the impedance matching (criteria: $|\Gamma|$ < -10dB) of the antenna with EBG is not achieved. In fact the EBG structure changes the omnidirectional radiation pattern in a directive one.

Solutions with AMC and two RHIS[2] give some shifts in frequency bandwidth but keep antenna matched. With the RHIS solutions, the gain changes and the total efficiency decreases due to the presence of resistors, but they remain acceptable in the operating bandwidth. Then the exposure is evaluated for these three structures.

[2] Two RHIS structures are analysed, one is optimised to absorb waves at normal incidence (angle of incidence equals to 0°) and the other absorbs waves at oblique incidence (angle of incidence equals to 85°, in this study)

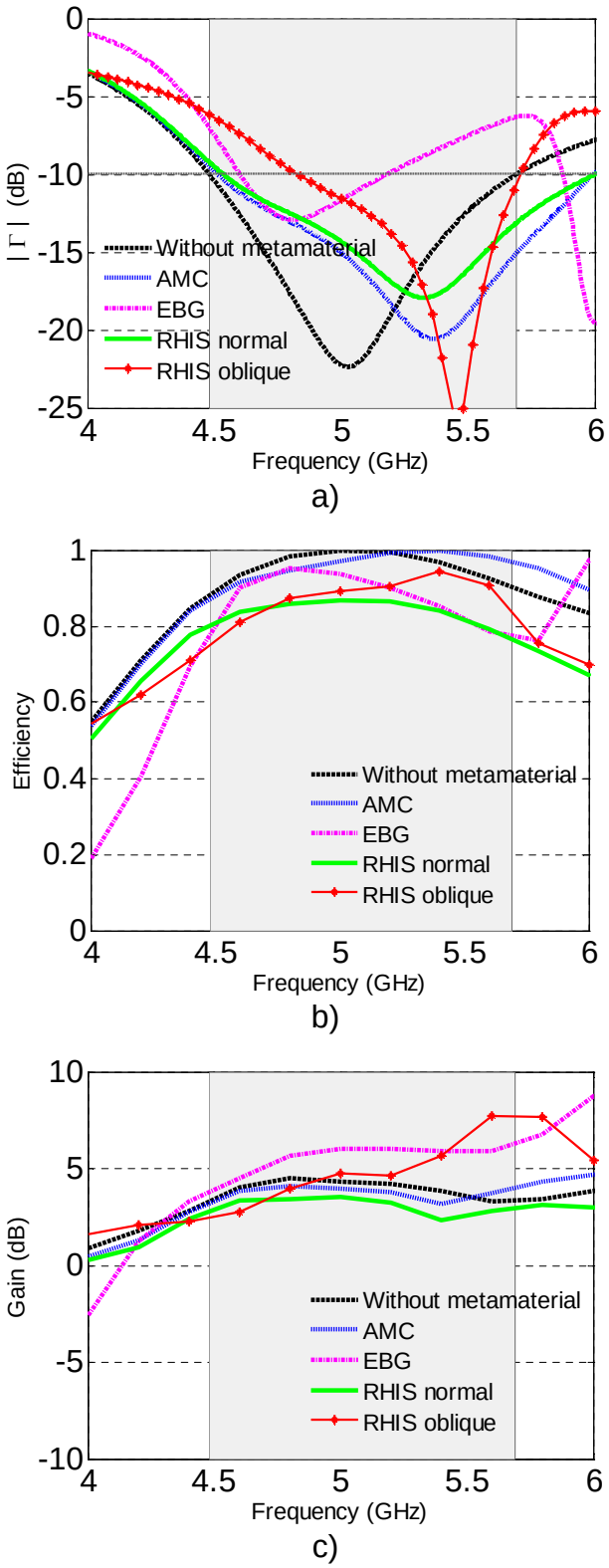

Figure 5 QoS KPI Monopole Antenna a) Antenna matching b) Total efficiency c) Gain

The power loss density is calculated for the four solutions (without metamaterial, AMC, RHIS normal incidence and RHIS oblique incidence), before calculating the SAR. In the previous report [10], the surface current distribution was used to identify

the best solution but the interpretation of results was not easy. In order to improve reading of the results, we have decided to present power loss density where the impact of the metamaterial solution clearly appears. Figure 7 displays the spatial distribution of the power loss density.

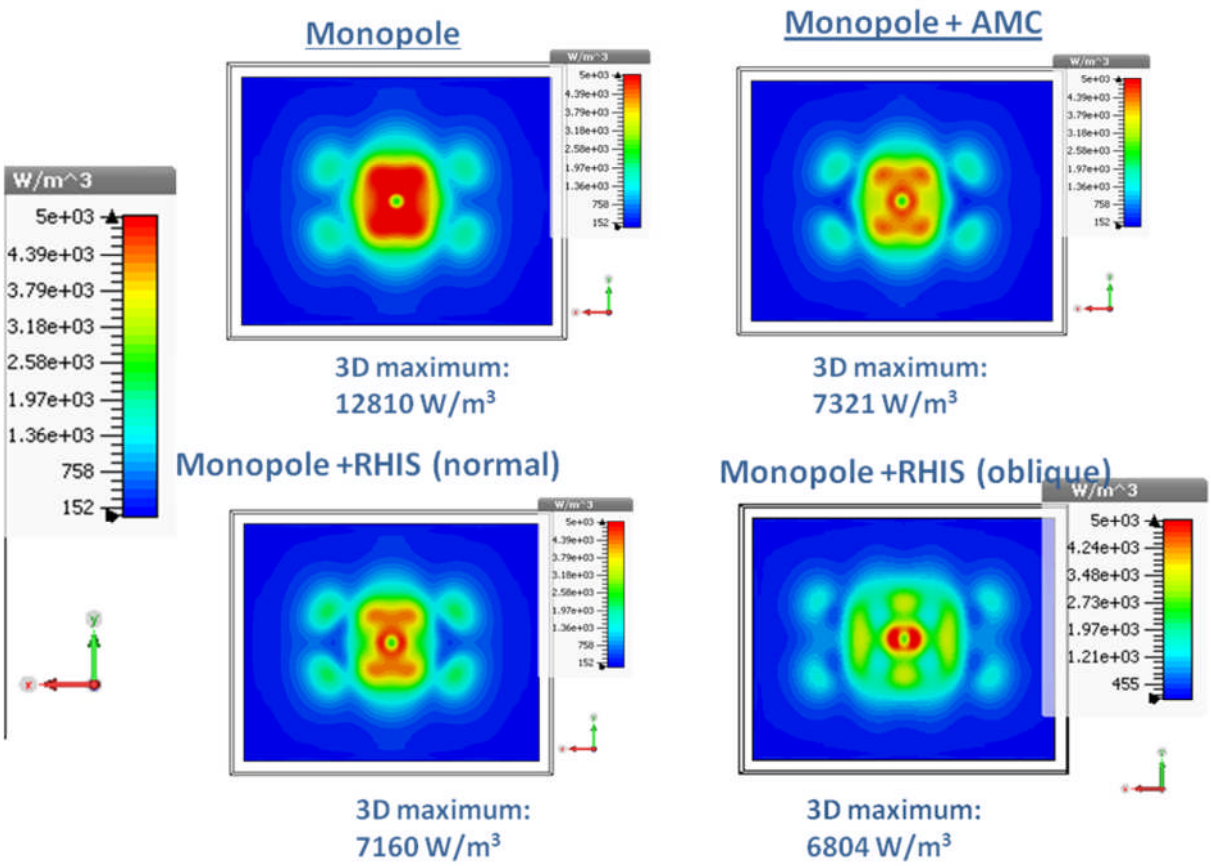

Figure 6 Power loss density, spatial distribution, Monopole Antenna

The power loss density is reduced in all cases, however the best result is obtained when the RHIS optimised to absorb waves in oblique incidence is used. Then, the SAR is calculated only for the best solution (RHIS optimised for incidence at 85 °). Results are displayed in Table 4; it is observed that the proposed solution (monopole antenna with RHIS optimised for oblique incidence) gives an EI reduction. A SAR 10g reduction of 23.6% is obtained and 11% for the Total SAR.

Table 4 Reduction Exposure, Monopole Antenna

	Monopole Antenna	Monopole Antenna +RHIS	Ratio EI [%]
Total SAR (rms) [W/kg]	0.106	0.094	-11.3
Max. point SAR (rms) [W/kg]	7.07	6.84	-3.25
Maximum SAR (rms,10g) [W/kg]	1.4	1.07	-23.6

The reference case (monopole antenna without metamaterials) and the best solution to reduce the exposure (RHIS optimised for incidence at 85 °) have been fabricated. The experimental results validate the antenna characteristics (matching and radiation characteristics). Experimental results are presented in Appendix 3.

2.1.3.3.2 IFA Antenna- results

The analysis of the IFA antenna is not ended so the described results are not complete. The QoS KPI for IFA antenna on the middle of edge are shown in Figure 7.

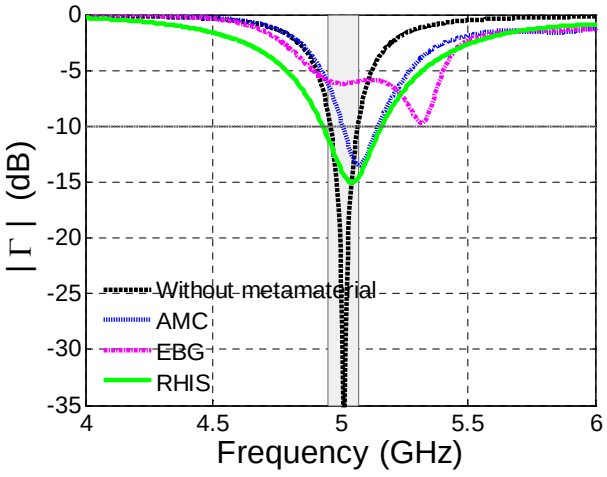

a)

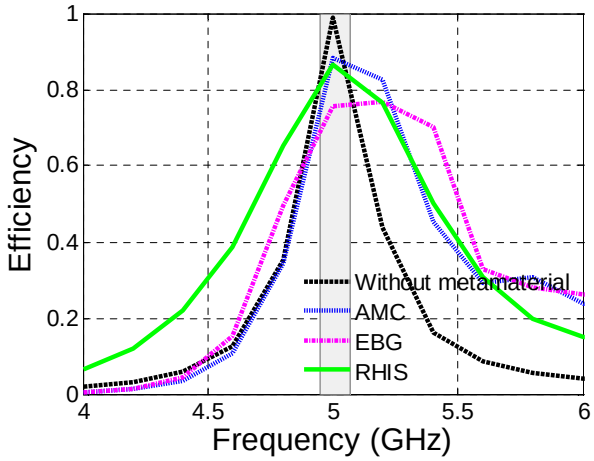

b)

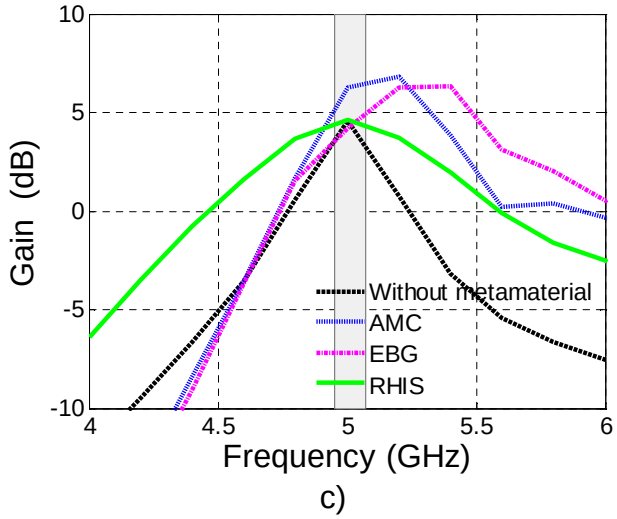

c)

Figure 7 QoS KPI IFA Antenna a) Antenna matching b) Total efficiency c) Gain

Like in the case of monopole antenna, the EBG solution is rejected because it does not accomplish the QoS KPI parameters: the antenna is not matched, the gain is increased and the efficiency is decreased. The AMC solution seems to be not appropriated too, because the frequency band (criteria: $|\Gamma| < -10dB$) shifts and the gain increase. In the RHIS solution case, the impedance matching, the gain, and the efficiency are acceptable, this is the only solution considered to evaluate the exposure.

The exposure is evaluated as described in the previous paragraph. The spatial distribution of the power loss density is shown in Figure 8. This results shows that the exposure is reduced by using a RHIS structure around the antenna.

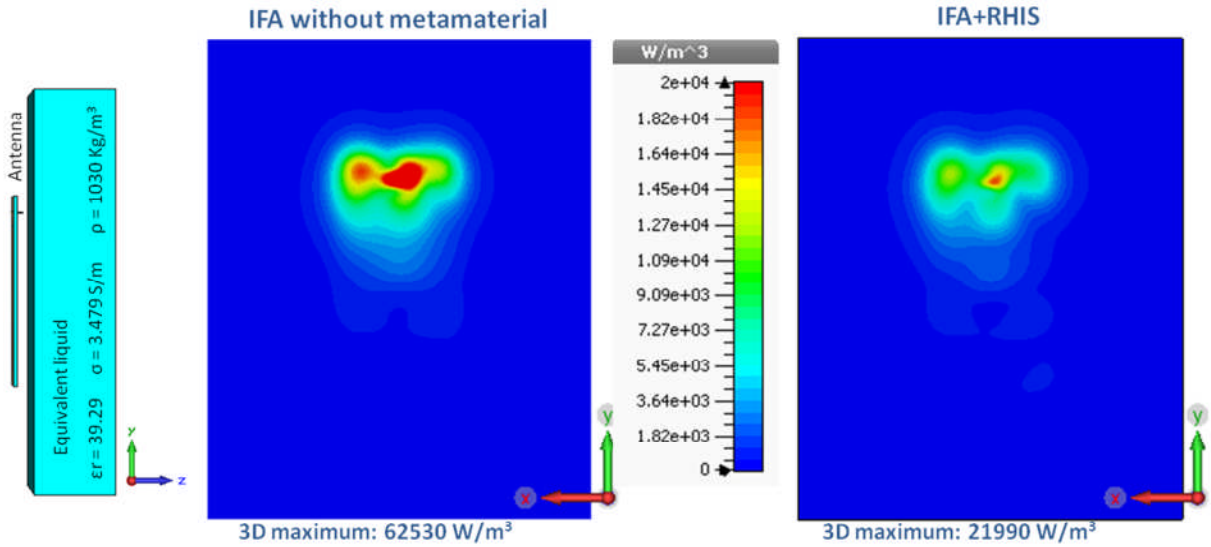

Figure 8 Power loss density, spatial distribution, IFA Antenna

This result is confirmed by the ratio of the exposure index evaluation, a SAR 10g reduction of -38.5% is obtained when a RHIS solution is used as shown in Table 5.

Table 5 Reduction Exposure, IFA Antenna

	IFA Antenna without metamaterial	IFA Antenna +RHIS	Ratio EI [%]
Total SAR (rms) [W/kg]	0.10	0.08	-20
Max. point SAR (rms) [W/kg]	67.4	23.4	-65.3
Maximum SAR (rms,10g) [W/kg]	4.6	2.83	-38.5

The antenna IFA will be realized in order to validate these results by measurement of antenna characteristics (matching and radiation characteristics).

2.1.3.4 Global EI reduction assessment

The previous results are valid for the Global EI assessment, in the case of the antenna evaluation the metric is based on the SAR 10g and it is not depending on the time, so we will obtain same results regarding 24h.

2.2 Beamforming techniques

2.2.1 Overview of the beamforming concept

In order to limit exposure to EM transmissions, an ideal solution would be to somehow reduce the emission power while maintaining the same signal-to-noise ratio (SNR) at the receiver. This has the effect of reducing the SAR. Some current approaches in [11], consider a hardware based approach where antennas are designed in conjunction with phase shifters to steer a null towards the user. In [13], a signal processing approach, referred to as SAR codes, is proposed based on the idea that a portable device placed in a 'talk position', i.e. placed at the user's skull, can reduce its user-imparted power by setting a phase offset of $\pi/3$ radians (or 60^{o}) between the transmit spatial samples. This phase offset was calculated based on CST microwave studio software simulations, which incorporate dual antennas in conjunction with a human skull phantom.

For this work, these ideas are extended to a scenario where a user is sitting at a laptop and it is desired to reduce the exposure to that user by examining, using a combination of measurement and simulation based approaches, the channels that would exist between the user and laptop. These channels are measured using probe antennas situated on the user's chest.

2.2.2 Evaluation methodology

The evaluation of the technique is measurement based. The object is to develop a calibration procedure that a manufacturer can use in order to assess the phase angle offset between transmit spatial samples, θ_2, that should be chosen to develop the necessary SAR modulation alphabet. The calibration procedure is necessary as this angle would vary depending on the geometry of the antennas as mounted on the laptop as well as the type of antenna that the manufacturer would use in the laptop. As described, as well as the probe antennas on the user's chest, the receiver of a channel sounder, which is an array of linear patch antennas, acts as a Wi-Fi access point while the transmitter is an array of omnidirectional patch antennas that are mounted on a ground plane, which is in turn mounted in a laptop. This evaluation procedure comprises a number of features:

- An extensive measurement campaign where the user is placed at three positions in a furnished laboratory environment is conducted to ensure repeatability of the concept.
- As well as placing the user and laptop in different positions within the laboratory environment, the user is rotated around the transmit laptop to examine exposure variation should a user not be sitting in front of the laptop.

In Figure 9, measurements of the channel between the user's probe antennas and the laptop antennas are made for one of the positions in the laboratory and the angle is assessed over a measurement time, t_{Meas}. It is clear that there is a significant reduction in exposure at approximately 180^{o}. In contrast, Figure 10 considers a similar scenario but where the angle is assessed at the linear patch array, i.e. the access point. It is clear that the angle at which there is a reduction in receive power has changed. This is due to the difference in the channels that would exist between the laptop-probes and the laptop-access point. It is the dissimilarity of these channels that underpins the viability of this approach as having highly similar channels would cause a reduction in SNR at the access point when applying the transmit spatial angle separation $\boldsymbol{\theta_2}$ to invoke user exposure reduction.

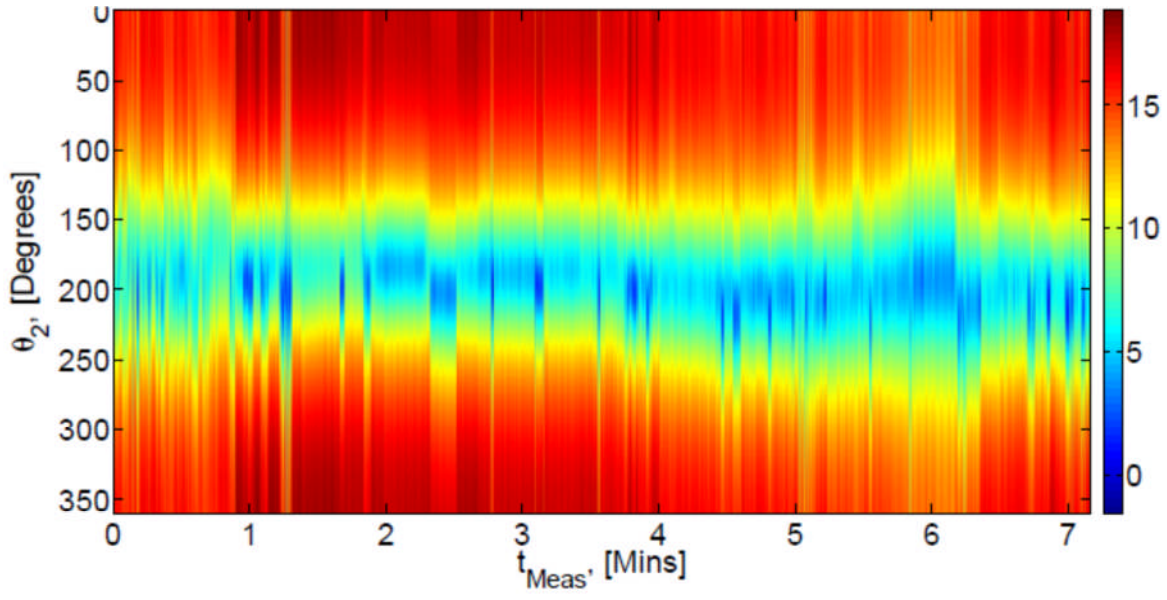

Figure 9: Receive power in dBm over time, t_{Meas}, as measured at probes as function of angle between transmit samples: θ_2, for the channel laptop-probes

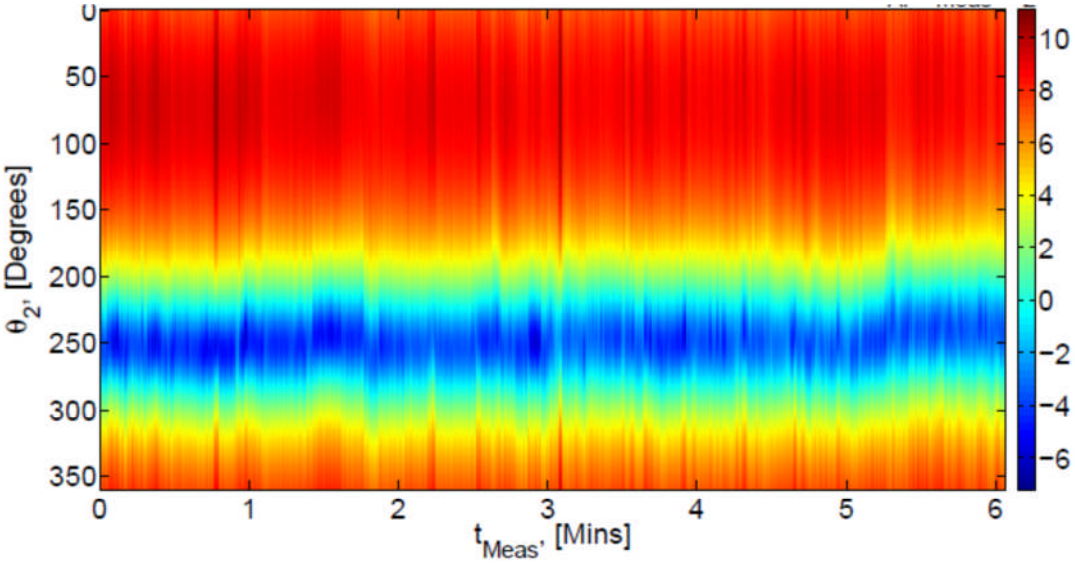

Figure 10: Receive power in dBm over time, t_{Meas}, as measured at probes as function of angle between transmit samples: θ_2, for the channel laptop-access point.

In order to further verify the fact that these channels are dissimilar, consider the co-linearity metric introduced in [14]. This is effectively a normalised measure of different the scattering in channels are. It varies between 1, indicating two equivalent channels and 0, indicating two orthogonal or highly dissimilar channels, and is invariant to scale factors. The fact that the co-linearity of these two channels varies between approximately 0.4 and 0.6 indicates that channels: laptop-probes and the laptop-access point, exhibit highly distinct scattering characteristics. This is reasonable since the laptop-probes channel should be highly AWGN in nature whereas signals traveling in the laptop-access point channel would have undergone more scattering.

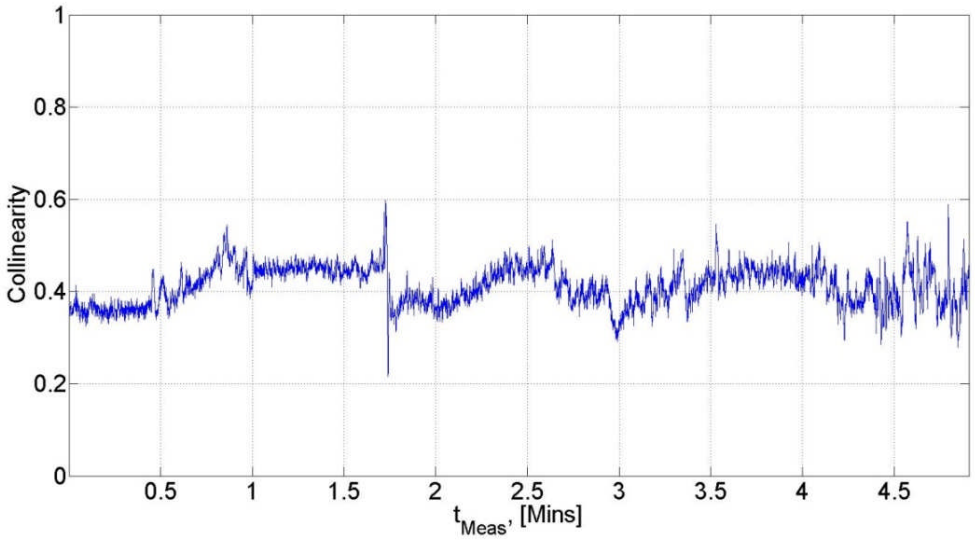

Figure 11: Collinearity of channels: laptop-probes and laptop-access point over time, t_{Meas}.

Future work involving post-processing the measurements that examine the effect of user various positions with respect to the laptop is currently being undertaken.

2.2.2.1 Sub-scenario description

The work specifically considers a 5 MHz bandwidth long term evolution signal, derived from the simulators in [14], being convolved with a measured channel impulse response in order to derive results. The focus is primarily on UL channels and thus has no implications for the DL. A summary of relevant parameters is given in Table 6.

Table 6 Table of scenario parameters

Scenario parameter	Value
Carrier frequency [GHz]	2.3
Tx Power [dBm]	23
LTE signal bandwidth [MHz]	5
LTE signal fame length [msec]	10
Fast Fourier transform (FFT) size	512

As can be seen by appropriate comparison with LEXNET deliverable 2.3, [16], these parameters, along with the evaluation methodology description outlined thus far, are in line with the scenario, 'Indoor scenario: Office in an urban environment' and the appropriate radio access technology is, 'UMTS'. The appropriate sub-scenario here is 'WiFi & WSN'.

2.2.2.2 Exposure and QoS metrics identification

From the choice of 3 KPIs for exposure reduction, which are namely SAR, mean duration exposure and mean transmit power, this work will focus on SAR. This will be quantified by converting the receive probe power levels to 10g whole body SAR (SARwb10g) levels. In order to do this, the statistical framework described in [15] was adapted to the sub-scenario context of this work. Figure 12 shows the effect of using this technique on SARwb10g where $\boldsymbol{\theta_2}$ was assumed to be 180 degrees for the LEXNET case. There is clearly a relative decrease in SAR when this technique is applied.

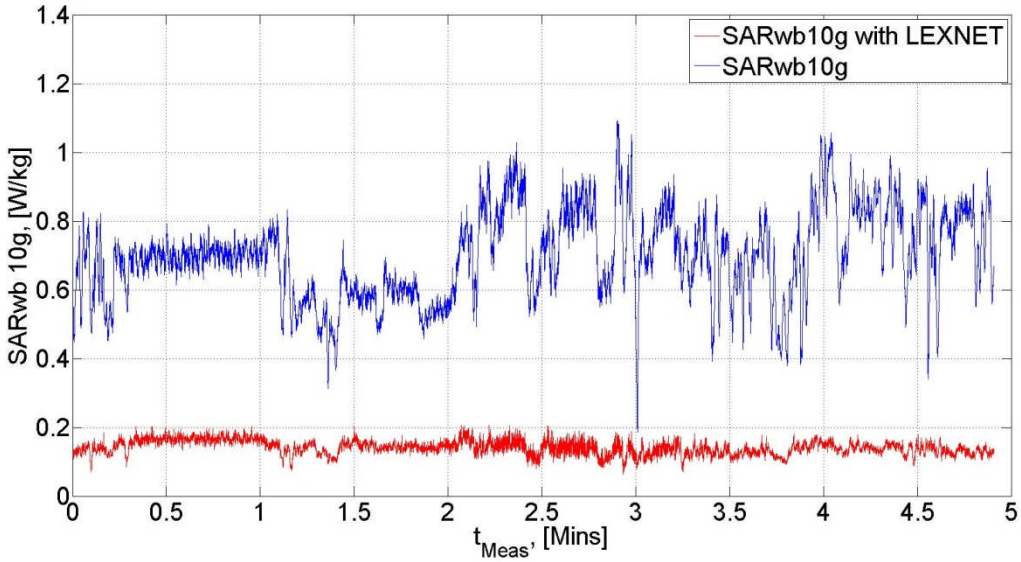

Figure 12: SARwb10g calculations with and without LEXNET.

2.2.2.3 EI ratio evaluation (or Capacity/QoS improvements converting into EI reduction)

The EI ratio evaluation is given as:

$$\text{Ratio}_{\text{EI}}(\%) = \frac{\text{EI}_{\text{partial}}(\text{w LEX}) - \text{EI}_{\text{partial}}(\text{wo LEX})}{\text{EI}_{\text{partial}}(\text{wo LEX})} \times 100 \qquad (2.2)$$

where in this context, $\text{EI}_{\text{partial}}$ is SARwb10g. The means of the two curves in Figure 12 are now given in

Table 7 and thus applying these figures to (2.2), a 79.78% reduction in exposure is predicted based on the implementation of SAR codes.

Table 7 Mean values of $\text{EI}_{\text{partial}}$ with and without LEXNET

$\text{EI}_{\text{partial}}$	**Mean value**
SARwb10g	0.6970
SARwb10g with LEXNET	0.1409

As described in [13], the exposure reduction due to the SAR modulation alphabet comes at the expense of throughput. The implementation of the SAR modulation alphabet requires an Alamouti space-time (or frequency) block coding scheme. Thus in terms of the LTE standard, this technology would be implemented when an LTE system is operating in 'diversity mode' since this uses Alamouti space-frequency block codes (SFBCs). In [13], it is was stipulated that if two QPSK alphabets (2 + 2 = 4 bits/transmission) are in operation on either transmit RF chain in conjunction with a SFBC then implementing SAR codes reduces this to a single equivalent 8-PSK (3 bits/transmission) scheme thus there is 25 % throughput (QoS) reduction. However, given that the emphasis of diversity in LTE is more on reliability than on throughput,

this may not be too prohibitive in terms of proposing implementation into a future standard.

2.2.2.4 Global EI reduction assessment

Since this exposure reduction does not come from a scheduling algorithm approach, the global EI reduction should be equivalent to the exposure reduction figure of 79.78% reduction as stated previously.

2.3 Small and directive antenna for low exposure index

This section presents the development of a novel antenna and evaluates its performance within the common methodology framework.

2.3.1 Remind on the concept

The proposed antenna solution is based on super directive compact parasitic arrays [19] with beam-steering capability in order to focus transmitted or received energy only where useful. The key of our approach is the optimization of the compact antenna array using the spherical modal expansion [20] and introducing the optimal amplitude and phase weight by integration of complex loads on each array elements. Compared to classical omnidirectional (360° angular resolution) antenna solutions available commercially, a directive antenna introduces spatial selectivity. In our proposition, a directivity around 10 dBi (-3dB beamwidth around 60°) is specified. This directivity level can be obtained using a three-element array separated by a distance of $0.1\lambda_0$. In order to achieve 360° beam-steering capability, a planar array composed of six electric dipoles will be designed.

In our case, the radiation efficiency degradation due to the super directivity is balanced thanks to the antenna spatial filtering properties. Consequently, the interference level decreases. In conclusion, our approach consists in keeping the same QoS of a classical network architecture while reducing the transmitted power level thanks to the higher antenna angular selectivity. This power reduction will lead to an efficient decrease of the EM exposure at the UL that is at the UE.

2.3.2 Super directive compact antenna arrays design & characterisation

A simple block diagram of a conventional digital beamforming system is presented in Figure 13. The signal received from each antenna is digitalized (ADC - Analog to Digital Converter) and combined with the signals received from the others antennas in order to form a desired beam pattern. Generally, the antennas are separated by a distance $\lambda_0/2$ in order to reduce the mutual coupling effects. The conventional digital beam-forming system is composed of four principal blocks: i) the antenna and the radiofrequency front-end (Tx/Rx), ii) the digital-analog or analog-digital converter (DAC/ADC), iii) the Digital Up or Down Conversion (DUC/DDC) system, and iv) the adaptive algorithm. It is important to notice that each antenna has a dedicated radiofrequency module, a DAC/ADC system, and a DUC/DDC.

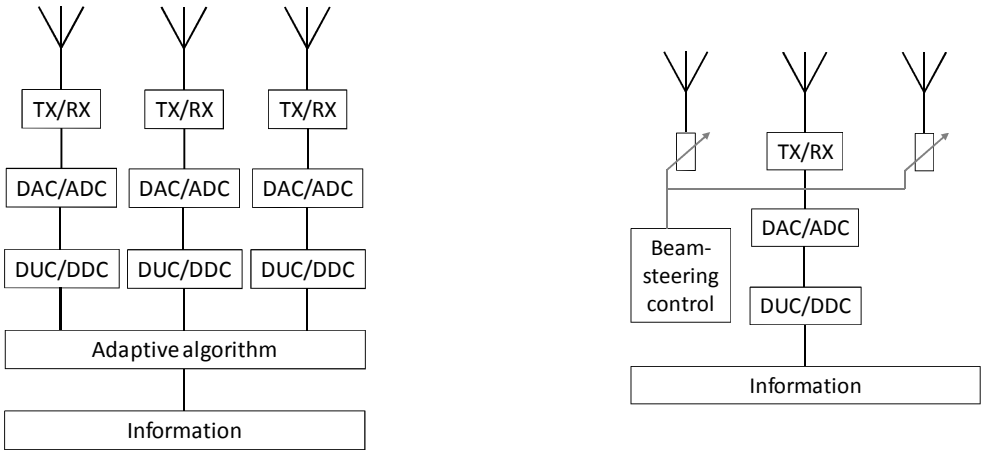

Figure 13 Block diagram of a conventional digital beam-forming transmitter/receiver system (a) and the architecture based on electronically reconfigurable parasitic array antenna (b).

The proposed solution is to integrate a super directive compact parasitic antenna array with beam-steering capability on the small cell (Figure 13 (b)). In this case, the antenna is composed of one fed element and a number of parasitic elements loaded by complex impedance loads. The elements are separated by a distance of $\lambda_0/10$ and the beam-steering is achieved by controlling the input impedance of the parasitic elements. Our approach limits the antenna size (reduction of the total surface of a factor five as compared to the digital beam-forming architecture with same angular resolution) and the system complexity compared to the classical beamforming architecture.

The proposed antenna design is based on super directivity theory which makes theoretically possible to reach any desired directivity for a given antenna array volume at the cost of a degradations on the bandwidth and efficiency. As consequence, a trade-off between electrical size (physical size regarding the wavelength), directivity, efficiency, and bandwidth must be done.

For a correct understanding, it is important to recall some antenna parameter definitions. The antenna gain (G) takes into account the directional properties and the antenna total efficiency η ($G = \eta D$, where D is the antenna directivity), while the directivity takes into account only the antenna directional properties.

A super directive compact antenna array can be designed and optimized using an *ad-hoc* procedure developed at CEA-LETI [21]. The schematic diagram of the procedure is presented in Figure 14. The algorithm implementing the proposed technique consists of four steps:

- STEP 1 Electric field calculation or measurement. The 3D electric field can be calculated using full-wave simulations, analytical model or measurements. In the case of parasitic array antennas composed of a number P of elements, one electric field associated to each array element must be extracted ($\vec{E}_p(r,\theta,\varphi)$).
- STEP 2 Spherical wave coefficients extraction [20]. Starting from the electric field calculated in the first step of the procedure, the spherical

wave expansion is applied in order to calculate the spherical wave coefficients (Q_{smnp}) of each array element.

- STEP 3 Optimal weights extraction. Starting from the spherical wave coefficients calculated during the second step of the procedure, the optimal (in terms of maximum directivity) weights (α_p) associated to each array element are calculated.
- STEP 4 Complex loads extraction. The complex loads associated to each antenna element are calculated starting from the optimal weights derived at the step 3 of the procedure.

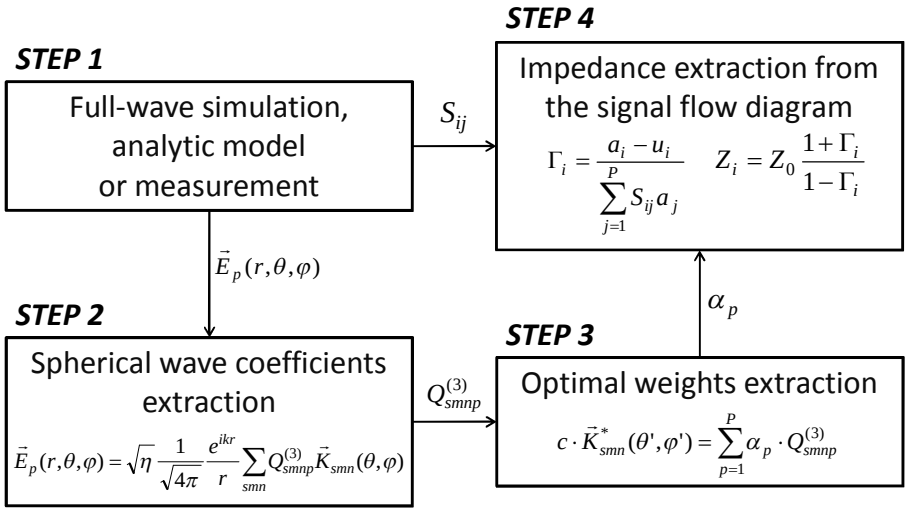

Figure 14 Schematic diagram of the proposed optimization procedure.

2.3.2.1 Spherical wave expansion

The electric field $\vec{E}$ at large distance ($kr \to \infty$) outside an enclosing spherical surface including all the field sources can be represented as a linear combination of far-field spherical wave pattern functions $\vec{K}_{smn}(\theta,\varphi)$ defined in [20]

$$\vec{E}(r,\theta,\varphi) = \sqrt{\eta}\frac{k}{\sqrt{4\pi}}\frac{e^{ikr}}{kr}\sum_{s=1}^{2}\sum_{n=1}^{N}\sum_{m=-n}^{n} Q_{smn}\vec{K}_{smn}(\theta,\varphi), \qquad (2.3)$$

where η is the specific impedance of the medium assumed complex, k is the wavenumber, and Q_{smn} are the spherical wave coefficients. The wave pattern functions $\vec{K}_{smn}(\theta,\varphi)$ are dimensionless and are solution of the Helmholtz wave equation. They are function of three indexes s,m and n. The degree n is equal to 1,2,…,N and the order is limited by $|m| \le n$. The index s = 1,2 indicates a coefficient to a TE- and a TM-mode wave, respectively. The wave pattern functions are defined as:

$$\vec{K}_{1mn}(\theta,\varphi) = \sqrt{\frac{2}{n(n+1)}}\left(-\frac{m}{|m|}\right)^{m} e^{jm\varphi}(-j)^{n+1}\left\{\frac{jm\bar{P}_n^{|m|}(\cos\theta)}{\sin\theta}\vec{e}_\theta - \frac{d\bar{P}_n^{|m|}(\cos\theta)}{d\theta}\vec{e}_\varphi\right\}, \qquad (2.4)$$

$$\vec{K}_{2mn}(\theta,\varphi)=\sqrt{\frac{2}{n(n+1)}}(-\frac{m}{|m|})^m e^{jm\varphi}(-j)^n\left\{\frac{d\overline{P}_n^{|m|}(\cos\theta)}{d\theta}\vec{e}_\theta+\frac{jm\overline{P}_n^{|m|}(\cos\theta)}{\sin\theta}\vec{e}_\varphi\right\}, \quad (2.5)$$

where $\overline{P}_n^m(\cos\theta)$ is the normalized associated Legendre function.

The spherical wave expansion of the radiated field can in practice truncated at some $n = N$ [20], with $N = kr + n_1$. The value n_1 depends on the desired accuracy and on the definition of the coordinate system. In the proposed optimization process, the truncation criterion is fixed making considerations on the radiated power (100%) and on the maximum directivity convergence.

2.3.2.2 Optimal modal weights extraction

In the case of electric field expressed as linear combination of spherical modes, the antenna directivity $D(\theta,\phi)$ can be calculated as [20]

$$D(\theta,\phi)=\frac{\left|\sum_{smn}Q_{smn}^{(3)}\vec{K}_{smn}(\theta,\phi)\right|^2}{\sum_{smn}\left|Q_{smn}^{(3)}\right|^2}, \quad (2.6)$$

where $Q_{smn}^{(3)}$ are the outgoing spherical wave coefficients.

Starting from the (2.6) several authors derived the expression of maximum directivity [20], [22], [23], calculated in a generic direction (θ_0,ϕ_0) as a function of the number of spherical modes (*N*) associated to the antenna radiation.

$$\begin{aligned}D_{\max}(\theta_0,\phi_0)&=\sum_{smn}\left|\vec{K}_{smn}(\theta_0,\phi_0)\cdot\hat{i}^*\right|^2\\&=\sum_{n=1}^{N}(2n+1)=N^2+2N\end{aligned}, \quad (2.7)$$

where $\hat{i}$ represents the reference polarization and the symbol * indicates the complex conjugate operation. The maximum directivity is independent of the direction and the chosen polarization.

In the case of antenna arrays composed of *P* elements, each array element presents a fixed number *smn* = 2*N*(*N* + 1) of spherical wave modes which cannot be independently excited and a modal weight can be applied on a mode series associated to the radiation of a single array element

$$\begin{aligned}Q_{smn}^{(3),\max}&=c\cdot\vec{K}_{smn}^{*}(\theta_0,\phi_0)\\&=\sum_{p=1}^{P}\alpha_p\cdot Q_{smnp}^{(3)}\end{aligned} \quad (2.8)$$

where α_p is the weight applied on each mode series associated to a single array element, *c* is a generic constant and $Q_{smnp}^{(3)}$ are the spherical wave coefficients

associated to the *p* element. The symbol * stay for the complex and conjugate operation.

2.3.2.3 Complex loads extraction

Using the array scattering parameters, the reflection coefficient (*Γ*) definition, and including the excitation vector $\bar{u}$ (equal 1 if the *i* element is fed, 0 also), a generic *p* port network at a given frequency is described by the equations

$$a_i = \Gamma_i b_i + u_i \tag{2.9}$$

$$b_i = \sum_{j=1}^{P} S_{ij} a_j \tag{2.10}$$

where b_i is the output wave of the $i = 1,..P$ port, S_{ij} are the *S* parameters, Γ_i is the reflection coefficient of the *i* port and u_i is the excitation term equal to 1 if the feed is located on the port *i* and equal to 0 in the other cases.

Combining the equations (2.9) and (2.10), we can calculated the reflection coefficient associated to each port (element) of the array as

$$\Gamma_i = \frac{a_i - u_i}{\sum_{j=1}^{P} S_{ij} a_j} \tag{2.11}$$

From (2.11), the impedance (Z_i) on each array element necessary to optimize the directivity can be extracted as

$$Z_i = Z_0 \frac{1+\Gamma_i}{1-\Gamma_i} \tag{2.12}$$

Once the four steps are derived, the super directive array radiated gain pattern is calculated with an EM simulator or assed by measurement of a prototype. The spatial filtering is thus evaluated within a system-level simulation at the small-cell scale which is detailed in the following section.

2.3.2.4 Design, optimization and characterization of compact parasitic array antennas

In order to validate the proposed optimization procedure, two prototypes have been designed, simulated, implemented and experimentally characterized. The first prototype (Figure 15 (a), Figure 15 (c)) is a three elements linear array operated at 868 MHz. The array is printed on the Rogers RO4003 dielectric substrate (ε_r = 3.55 and tanδ = 0.0027) with a thickness equal to 813 µm and is composed of one excited electrical dipole and two parasitic elements. Both fed and parasitic elements are electrical dipoles of length $0.4\lambda_0$. The distance between each dipole has been fixed to $0.1\lambda_0$ (total size including the dielectric substrate equal to $0.45\lambda_0 \times 0.26\lambda_0$ (diameter equal to 0.52 λ_0)). The feed is located on the first dipole. The choice of the feed position is due to the complex load values. In fact, the optimal solution can require the use of negative resistances. The obtained directivity is independent from the choice of the feed position. A commercial surface mounted balun (Anaren

BD0810J50100AHF) has been integrated on the fed-dipole. The *S* matrix of the balun has been taken into account in the electromagnetic simulations.

The second prototype (Figure 15 (b), Figure 15 (d)) is a nine identical elements (monopoles) circular array operating at 1.75 GHz. The nine monopoles are integrated on a circular ground plane of radius 0.6 λ_0. It is important to notify that the ground plane does not contribute to the antenna radiation and is not taken in the account for the definition of the antenna size. In fact, from the image theory, we know a monopole on an infinite ground plane presents the same radiation properties of the electrical dipole with equal arm length. When a finite ground plane is used, the radiation pattern presents its maximum in a plan different of the horizontal one. In view of the realization of the beam-steering, a circular array has been realized. In this prototype, the central monopole is fed and the others are parasitic elements disposed on a circle of radius 0.1λ_0. In this realization, only the optimal weights of the three monopoles disposed along the end-fire direction have been optimized and calculated using the proposed design procedure. The load of the others monopoles is fixed for simplicity to 50 Ω. In this way a beam-steering with an angular step of 45° with directivity similar to the case of the linear array will be obtained by rotating the optimal loads of the parasitic elements of the array. It is important to notice that in theory identical radiation pattern will be obtained as a function of the steering angle. The two arrays have been simulated using CST Microwave studio. The schematic view and the photography of the realized prototypes are presented in Figure 15.

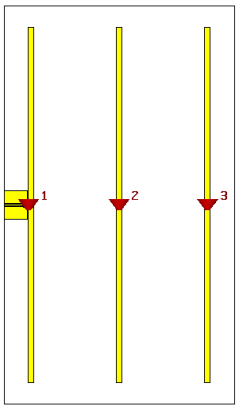

(a)

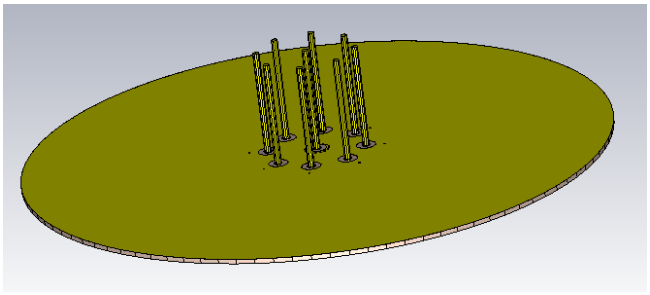

(b)

(c)

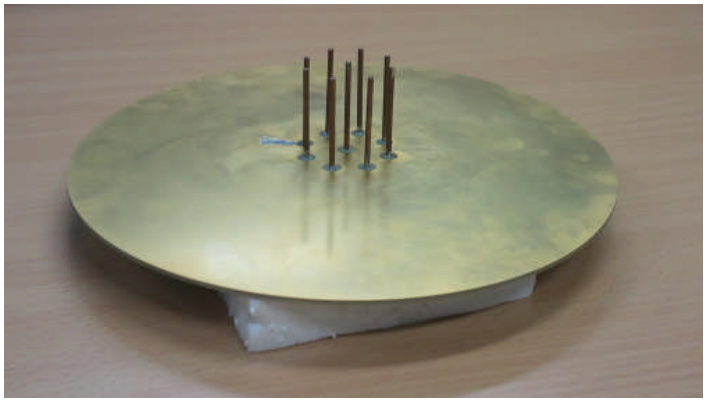

(d)

Figure 15 Realized prototypes. Schematic view of the (a) three element array and the (b) nine element array. Photography of the realized (c) three-element array and the (d) nine-element array.

The electric fields associated to each dipole and the *S* matrix have been calculated by the 3D electromagnetic simulations and exploited as input data of the optimization procedure. The optimal loads calculated with the optimization procedure are calculated using the proposed optimization procedure. In the prototypes, the optimal loads calculated with the procedure are approximated with the commercial load values and the negative resistances are fixed equal to 0 Ω. The values of the complex loads integrated on the prototypes are presented in Table 8. The simulated directivity is equal to 9.02 and 7.90 dBi in the case of the linear and circular array, respectively. It is important to notice, that the approximation of negative resistance equal to 0 Ω produces a directivity reduction. The directivity calculated using the optimal loads is equal to 10.35 and 8.40 dBi, respectively. The theoretical and simulated 3D and 2D radiation patterns obtained in the case of three-element array are presented in Figure 16.

Table 8 Complex load integrated on the realized prototypes. The feed is located in the port 1 and port 2 in the case of linear and circular array, respectively.

	Loads used on the realized prototype			
	Dipole	**Resistance (Ω)**	**Capacitor (pF)**	**Inductance (nH)**
Linear array	1	-	-	-
	2	0	-	0.90
	3	4.99	-	3.40
Circular array	1	2.2	4.7	-
	2	-	-	-
	3	0	5.6	-
	4	50	-	-
	5	50	-	-
	6	50	-	-
	7	50	-	-
	8	50	-	-
	9	50	-	-

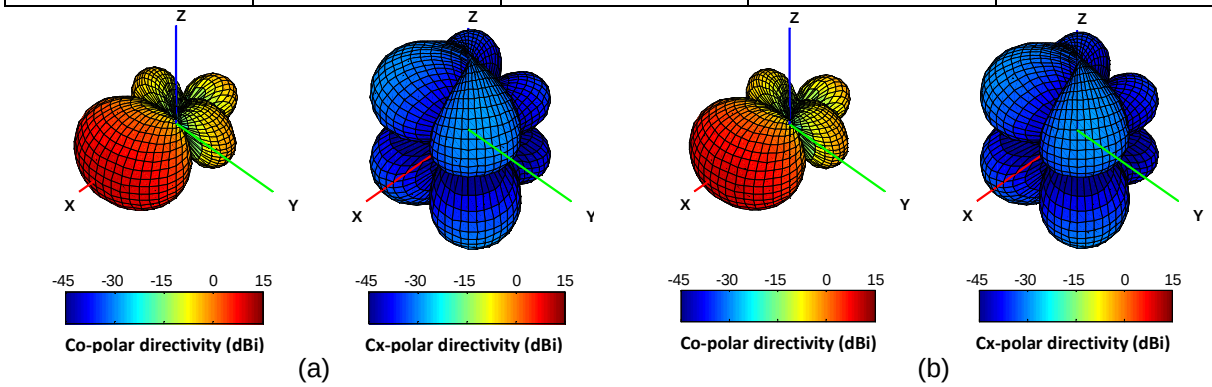

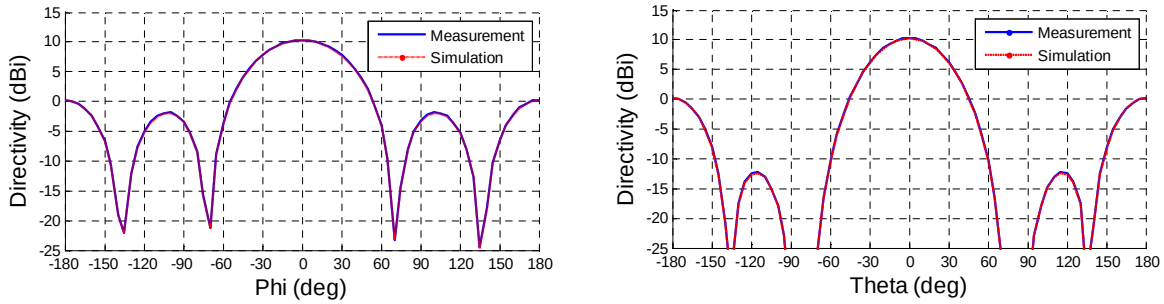

Figure 16 Directivity pattern (Co-polar and Cx-polar components) of the three-element array calculated at 868 MHz. 3D (a) theoretical and (b) simulated results. (c) H- and (d) E-plane.

In the case of the circular array, due to the finite size of the ground plane, the maximum directivity has been obtained on the elevation plan 25°. The theoretical radiation patterns of the circular array computed on two different steering angles are presented in Figure 17.

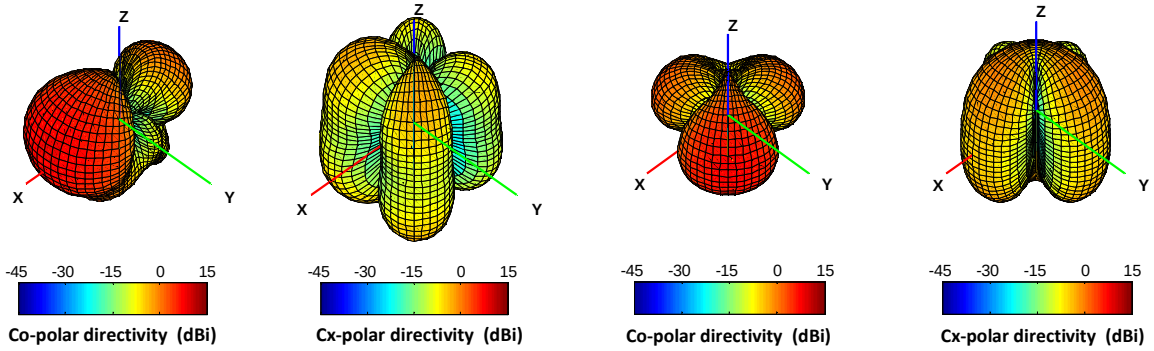

Figure 17 Directivity pattern (Co-polar and Cx-polar components) of the circular array calculated at 1.75 GHz. 3D theoretical results (a) for the end-fire and (b) 45°-steered configurations.

The two prototypes have been characterized in the CEA-Leti UHF anechoic chamber. An optical link connection has been used in order to limit the effect of the RF cable parasitic radiation on the compact antennas radiation. In the case of the linear array, the directivity has been estimated using its definition (ratio of the radiation intensity in a given direction from the antenna to the radiation intensity averaged over all directions (Radiated power/4π)) and starting from the radiation pattern measurement on two orthogonal planes. The radiated power has been calculated by integration of the measured patterns. This approximation does not produce an important error on the directivity estimation due to the symmetry of the radiation pattern. The simulated and measured maximum directivity of the linear array as function of the frequency is plotted in Figure 18. A maximum measured maximum directivity equal to 8 dBi has been obtained at 872 MHz. The frequency shift is probably dues to the real load tolerances and dielectric properties of the substrate. The directivity reduction is probably due to the back radiation increasing (Figure 19).

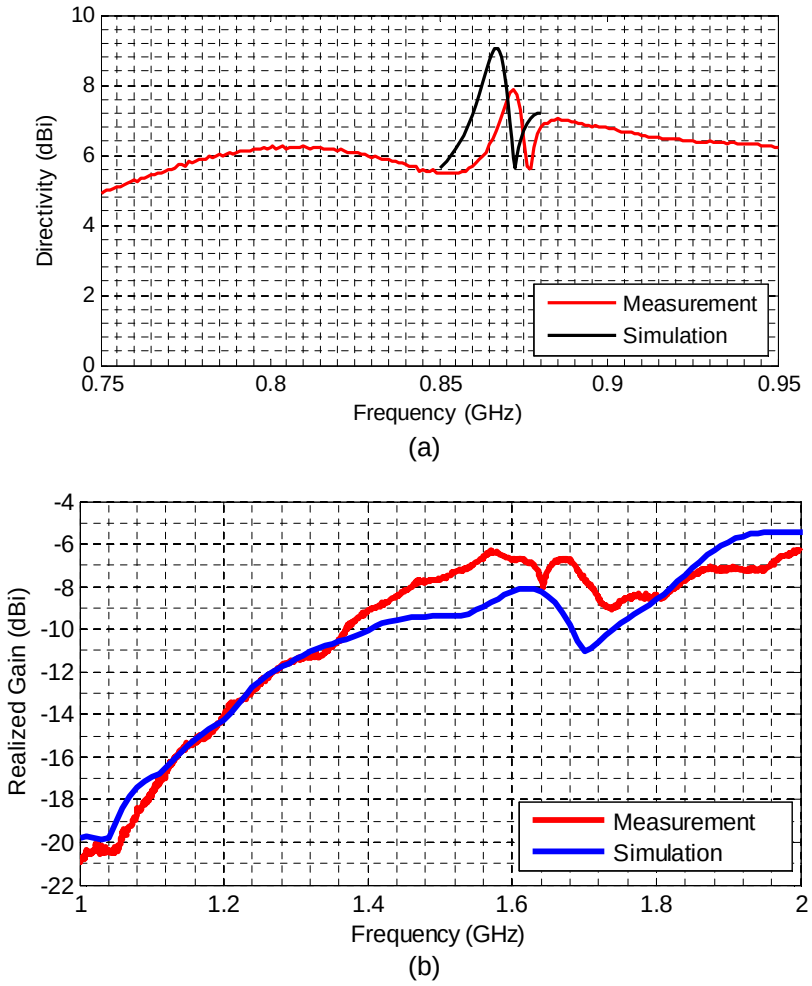

Figure 18 Measured and simulated maximum directivity as function of the frequency in the case of (a) three-element and (b) four-element array

The simulated directivity pattern of the linear array computed on the E- and H-planes at frequency 868 MHz are compared in Figure 19 with the measured pattern at the frequency 872 MHz. In this picture we can observe the increasing of the measured back radiation as compared to the simulated pattern. The simulated 3-dB beam aperture is equal to 62.0° and 50.2° on the H- and E-plane, respectively. Instead, the measured 3-dB beam aperture is equal to 66° and 54° on the H- and E-plane, respectively.

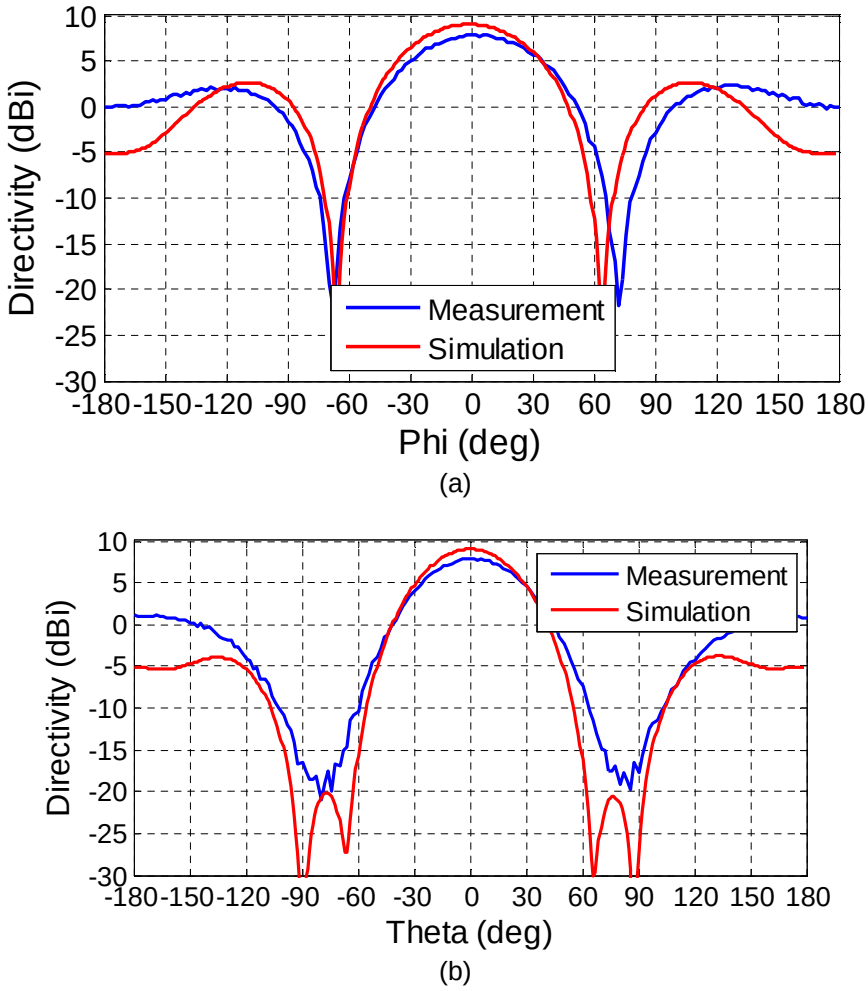

Figure 19 Measured and simulated directivity radiation pattern (simulation frequency 868 MHz, measurement frequency 872) of the three-element computed on the (a) H- and (b) E-plane.

The simulated realized gain pattern of the four-element array computed on the E- and H-planes at frequency 1.75 MHz are compared in Figure 19 with the measured pattern at the frequency 1.72 MHz. Due to the impedance mismatch, the realized gain is about -10 dBi. This impedance mismatch is caused by the parasitic load. In order to obtain the impedance matching a matching network will be integrated in the final demonstrator. Using this circuit a gain of about -2.6 dBi has been obtained in the electromagnetic simulation. The simulated 3-dB beam aperture is equal to 74.0° and 72° on the H- and E-plane, respectively. Instead, the measured 3-dB beam aperture is equal to 68° and 75° on the H- and E-plane, respectively.

In conclusion, two prototypes have been realized in order to validate the design and optimization procedure based on the spherical wave expansion. The measured results are in good agreement with the theoretical and simulated results. In view of the realization of the antenna that will be integrated on the final demonstrator, a preliminary circular array has been realized. This array is composed of nine monopole integrated on a ground plane. The presence of the ground does not contribute to the antenna radiation and could play a key role in view of the implementation of the electronically beam- steering and the integration of the

antenna on the small cells. In fact, the ground plane can electrically isolate the steering logic and the transceiver device from the radiating element.

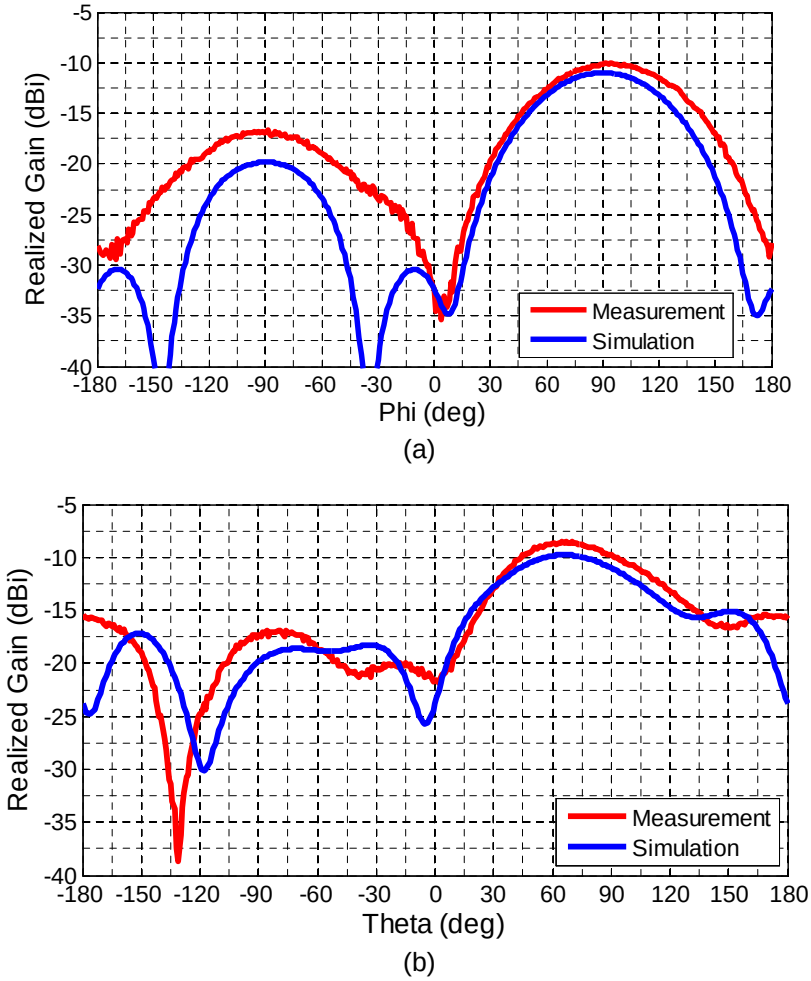

Figure 20 Measured and simulated directivity radiation pattern (simulation frequency 868 MHz, measurement frequency 881) of the three-element computed on the (a) H- and (b) E-plane.

2.3.3 Evaluation methodology

2.3.3.1 Sub-scenario description

Here we investigate Heterogeneous Network (HetNet) operating at 2 GHz [24], [25], and we propose the use of super directive [19] compact parasitic antenna array with real-time beam-steering capability for SC sub-scenario to enable low EMF wireless communications. Notice that this antenna solution could eventually be envisaged for Wi-Fi & WSN sub-scenario on the gateway module but not for MC sub-scenario due to the high level of transmitted power.

In this HetNet architecture, classical macro base stations (MeNBs) are complemented with low-power low-cost Small Cell eNBs (SCeNBs) to extend the cellular network coverage (both in indoor and outdoor environment) and improve performance experienced at end users by shortening the distance between mobile terminals and access nodes.

In our analysis four different antenna radiation patterns (Figure 21) have been considered: i) the omnidirectional pattern with 5 dBi of directivity, ii) the 10 dBi directivity ideal pattern with 100% of efficiency (G_{max} = 10 dBi), iii) the 10 dBi directivity ideal pattern with 15% of efficiency (G_{max} = 2 dBi), and iv) the radiation pattern obtained by full-wave electromagnetic simulation of a three-dipole super directive compact antenna arrays optimized at 2 GHz. The ideal patterns have been calculated considering the equation:

$$D(\theta,\phi) = 2(n+1)\cos^{n}(\theta), \tag{2.13}$$

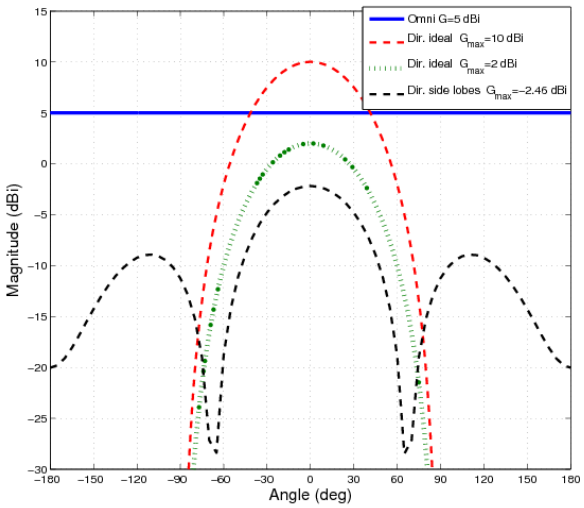

Figure 21. Gain radiation patterns of the antenna models used in the numerical analysis.

In (2.13), it is possible to control the directivity and the angular aperture of the desired synthetic pattern by varying the *n* order,. Imposing *n* = 4, a directivity of 10 dBi and an angular aperture of 65.5° are obtained. The three-dipole compact parasitic array has been optimized using the proposed design procedure based on spherical wave expansion, and simulated using CST microwave studio (3D EM simulator). The antenna is composed of three electrical dipoles of length $\lambda_0/2$ and inter-element distance of $\lambda_0/10$ (total size $0.2\lambda_0 \times 0.5\lambda_0$, 30 × 75 mm² at 2 GHz). A directivity of 9.1 dBi, a gain of -2.46 dBi (total efficiency 7%) and an angular aperture of 62.2° have been obtained.

It is important to notice that in this preliminary investigation, we have considered an ideal beam-steering. In fact, we have assumed that with our antennas it is possible to steer the beam in any possible direction with the same maximum gain.

Coherently with the 3GPP study on small cell enhancement [24], our research focuses on HetNets where small cells are densely deployed. We consider in this study an equivalent full data rate situation. We consider a tri-sectorial macro cell (MC) and we assume that the SCs form a 3 × 3 cluster located inside each MC sector. In each MC sector, 30 UEs are dropped in the MC area: following the 3GPP guidelines [24], 2/3 of the overall UEs are distributed inside the SC cluster and the remaining UEs are uniformly located in the macro cell area. Moreover, 80% of the UEs are deployed indoor and 20% outdoor. Relevant key simulation parameters are detailed in Table 9. The results are averaged over 10^3 independent runs. At the beginning of each run, the clusters of SCs and UEs are randomly deployed in the

macrocell area. The association between the UEs and eNBs is based on the DL reference signal received power (RSRP) [26]. Let $RSRP_i$ be the RSRP of the eNB *i* (in dBm) observed at a certain UE *j*, we may formulate the cell-selection process at the UE *j* as

$$i^* = \arg\max_{i \in e\overline{NB}_j} \{RSRP_i + REB_i\}, \tag{2.14}$$

where $\overline{eNB}_j$ is the set of eNBs located nearby the UEs *j* and REB_i is the range expansion bias [1] associated to the eNB *i*

$$REB_i = \begin{cases} 0 \ \ if \ \ i \ is \ a \ macrocell \\ \geq 0 \ if \ \ i \ is \ a \ smallcell \end{cases}, \tag{2.15}$$

Table 9 Main Simulation Parameters

Parameter	Value	Parameter	Value
Cellular layout	Hexagonal grid	Carrier frequency	2.0 GHz
Macro sector/site	3	MeNB Tx power	46 dBm
SCeNBs/macro sector	9	MeNB max. antenna gain	13 dB
UE dropping	2/3 UEs within the clusters, 1/3 UEs throughout the macro area. 80% UEs are indoor.	SCeNB Tx power	30 dBm
Min. dist. SC-UE	10 m	SCeNB max. antenna gain	See Figure 21
Min. dist. MeNB-UE	35 m	MeNB antenna pattern	2D Three-sectorized
Min. dist. MeNB-SC	75 m	SC antenna pattern	See Figure 21
Dist. SC-SC	40 m	Shadowing distribution	Log-normal
Macro cell path loss	ITU UMa (Table B.1.2.1-1 [3GPP TSG RAN 2010])	Macro/SC LOS Prob.	See Table A.2.1.1.2-3 [3GPP TSG RAN 2010]
Small cell path loss	ITU Umi (Table B.1.2.1-1 [3GPP TSG RAN 2010])	Thermal noise density	*N*0=-174 dBm/Hz

2.3.3.2 Detailed description of your Exposure and your QoS metrics

The average power ($\overline{P}_{TX}$) emitted by the mobile terminal is selected as the exposure metric. To evaluate the QoS metric of our network we initially evaluate the average UL Signal to Noise plus Interference Ratio (SINR) associated to the UE transmissions.

In order to assess the impact of the EMF radiation in HetNets, we use a simplified version of the Exposure Index (EI) [27]. Here, we only focus in the UL of cellular network, and we only consider adult users. With these assumptions, the EI can be computed as the sum of the contributions due to different usages (i.e., data and voice) in the considered time periods (day and night)

$$EI = \sum_{t}^{Nt} \sum_{u}^{Nu} d_{t,u}^{UL} \overline{P}_{TX} \quad \left[\frac{J}{Kg} \right], \tag{2.16}$$

where $d_{t,u}^{UL}$ is a coefficient associated to the exposure induced by the uplink and expressed as an absorbed dose

$$d_{t,u}^{UL} = \frac{t_{t,u}^{UL} \cdot SAR_{t,u}^{UL}}{P_{TX}^{ref}} \quad \left[\frac{s}{Kg}\right], \tag{2.17}$$

In (2.17), $t_{t,u}^{UL}$ is the time spent in the usage *u* during the time period *t* and the ratio $SAR_{t,u}^{UL} / P_{TX}^{ref}$ represents the whole body averaged SAR that characterizes an adult during the usage *u* and an incident reference power [27].

In 3GPP LTE, fractional power control is used at the UEs in the UL transmissions to mitigate inter-cell interference and increase the battery life-time of the end-terminal, and the average emitted power can be evaluated as [26]

$$\overline{P}_{TX} = \min\left\{P_{\max}, P_0 + 10\log_{10} M + \lambda_{cs} \cdot L\right\}, \tag{2.18}$$

where $P_{\max}$ is the maximum transmission power (23 dBm), P_0 is a UE-specific parameter (-78 dBm), *M* is the average number of assigned physical resource blocks (set here equal to 6) to the UE, λ_{cs} is the cell-specific path-loss compensation factor (0.8), and *L* is the downlink path-loss measured at the UE using the control channel.

2.3.3.3 Results and analysis

Figure 22 shows the cumulative distribution function (CDF) of the average UL SINR measured at the SCs with respect to the antenna patterns presented in Figure 21. A REB equal to 3 dB is considered here, similar results have been observed for other values of REB. Blue solid, black dashed, green dotted, and red dashed-dotted represent the omnidirectional antenna with a gain of 5 dBi, the directional antenna with G_{max} equals to -2.46 dBi, the ideal directional antenna with G_{max} equals to 2 dBi, and the ideal antenna with a G_{max} equals to 10 dBi, respectively. Our results show that the SCs characterized with an omnidirectional antenna experience the worst performance: with this solution the SC does not distinguish amongst interference signals and useful signals. On the contrary, the small cells with ideal directive antennas achieve the best performance since only the signals originated into the same direction of the useful signal are received at the SC, and most of the interference is rejected.

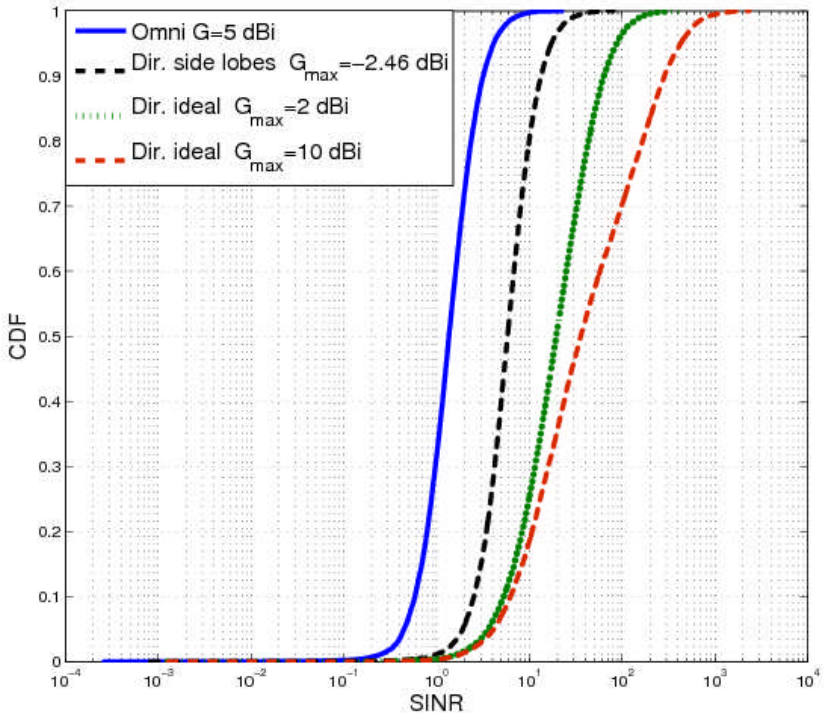

Figure 22 Cumulative distribution functions of the average uplink SINR at SCs with respect to different antenna patterns and a REB equals to 3 dB.

Our simulations show that the small cells achieve a 25x gain factor and 13x gain factor with respect to the standard omnidirectional antennas when using ideal directive antennas with G_{max} equals to 10dBi and 2dBi, respectively.

Finally, when considering realistic directive antennas, most of the interference is only mitigated and not completely cancelled at the receiver. However, this solution achieves notable improvements with respect to the classic omnidirectional antenna and leads to a 3.3 times factor gain (equivalent to 5.2 dB improvement).

It is important to note that the investigated antenna patterns do not directly reduce the EMF exposure at the end user. Strictly speaking the QoS is increased by reducing the interference level and so the SINR in a dense SC test case. Regarding the common evaluation step-4 (section 1.4), this gain should be converted in term of exposure reduction.

2.3.3.4 EI ratio evaluation (or Capacity/QoS improvements converting into EI reduction)

The improvements in terms of SINR may enable a straightforward reduction of the UL power required to operate at the initial target QoS which corresponds to the QoS level using the standard omnidirectional antenna. Therefore by deploying such a miniature and directive antenna, a 5.2 dB average transmitted power reduction can be reached in the dense SC sub-scenario by maintaining constant the QoS level obtained with a standard omnidirectional antenna.

2.3.3.5 Towards the global EI reduction assessment

At the current progress of the project, no global EI is assessed yet. Nevertheless the calculation of absolute IE for the specific case of LTE (2 GHz frequency band) within

dense SC sub-scenario is proposed in the following. The users' activities are taken from initial WP2 data (that will be updated at the end of the 2nd year of the project) and are described in Table 10.

Table 10 Users' activities in a Small Cell dense scenario

	Voice		Data	
	Indoor	Outdoor	Indoor	Outdoor
t=Day	4', 2''	4', 2''	22', 50''	8', 44''
t=Night	2', 1''	2', 1''	38', 55''	5', 6''
$\frac{SAR_{TAU}^{UL}}{P_{TX}^{ref}}\left[\frac{1}{Kg}\right]$	3.95e-06		4.14e-06	

In the following the impact of the cell-selection process at the UE is analysed on absolute EI. Figure 23 shows the cumulative distribution function (CDF) of the measured UL EI at UEs for different REB at the small cells. The black solid, blue dashed, red dotted, and green dashed-dotted lines correspond to a REB equals 0, 3, 6, and 9 dB, respectively.

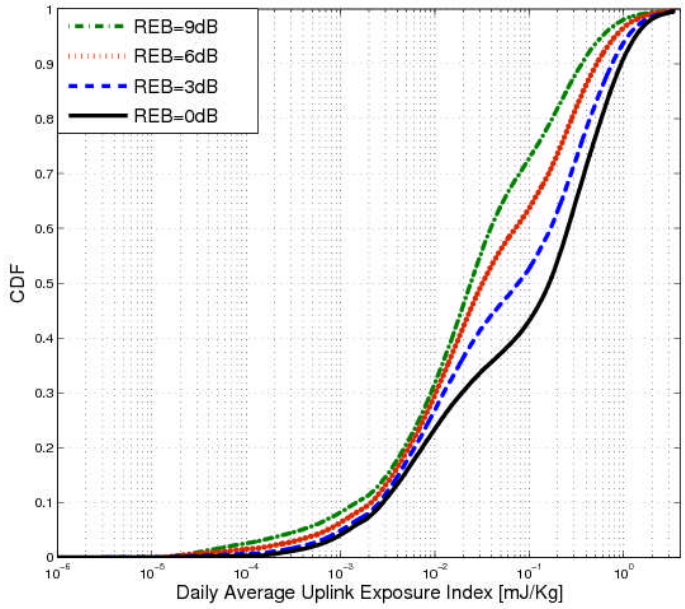

Figure 23 Cumulative distribution functions of the daily average UL EI at UEs for different REB values.

Larger value of the EI (in the right side of the figure) are associated to indoor UEs, which are characterized by high propagation and penetration losses and make large use of wireless data connections [26]. On the other hand, outdoor UEs located close to small cells are characterized by a limited uplink power, which in turns reduces the EI. Due to the power unbalance between the SCeNB and MeNBs, there is a large number of UEs that are prevented to be served by the closest eNB. When the range expansion technique is used, a positive bias is added to the strength of measured signals associated to SCs and part of the UEs is shifted from the MeNBs to the SCs, which results in reduced UL power and limited EMF exposure.

Accordingly, our simulations show that the median values of the experienced EI are $24x10^{-3}$, $32x10^{-3}$, $80x10^{-3}$, and $163x10^{-3}$ mJ/Kg when using a REB equals to 9, 6, 3, and 0 dB, respectively.

2.3.4 Intermediate conclusion & future works

In this section, an innovative miniature and directive antenna design methodology is proposed to reduce the EM exposure. The distance between elements of the antenna array is divided by a factor 5 which allows the implementation of beamforming feature at 800 MHz in a dot radio form factor module. Experimental performances have shown about 60° beamwidth while the radiation efficiency is severely degraded (below 10 % compared to 90% for omnidirectional antenna).

The common EI evaluation methodology has been followed step by step. By deploying such a miniature and directive antenna, a 5.2 dB average transmitted power reduction can be reached in the dense SC sub-scenario by maintaining constant the QoS level obtained with a standard omnidirectional antenna.

Future work will focus on the implementation of the beam-steering feature on the super directive nine-element compact array (in WP6 T6.1 task). At last, the last step of the common methodology will addressed and the global impact of our solution on a global daily basis will be carried on.

2.4 Low noise receiver architecture

2.4.1 Remind on the concept

Currently, multi-band receivers are demanded to fulfil the requirements of next generation wireless technologies. Therefore innovative solutions are essential to develop compact designs avoiding multiple RF chains working in different operating bands. Reconfigurability could be applied using tunable components in different receiver stages. Furthermore, this feature could be combined with innovate low noise receiver architectures to reduce EI. This study proposes a reconfigurable low noise receiver architecture to improve receiver sensitivity while keeping, or even improving, specific requirements such as intermodulation, spurious rejection, channel selectivity or blocking response. By improving the receiver noise figure (NF), lower power will be required at receiver input to ensure a given SNR. Therefore if lower received power should be at BS, the required transmit power at UE will be reduced, improving EI.

Typical multi-band receivers are based on direct conversion receiver (DCR) architecture, where a switch at input selects the operating band, enabling the RF chain composed by a specific bandpass filter (BPF) and a narrowband low noise amplifier (LNA) for each frequency band. Afterwards, a down conversion to baseband (BB) is performed using an I/Q demodulator.

The scope of this study is to develop innovative reconfigurable receiver architectures for LTE femtocell BS applications improving receiver sensitivity to reduce EI. The proposed block diagram is shown in Figure 24. A wideband LNA (or reconfigurable

LNA if it is possible) and a reconfigurable BPF are previous to an intermediate frequency (IF) stage to fulfil receiver requirements in terms of adjacent channel selectivity and blocking. The IF stage provides additional rejection and relaxes the power requirements in the I/Q demodulator, working at fixed frequency. Finally, an I/Q demodulator converts to BB.

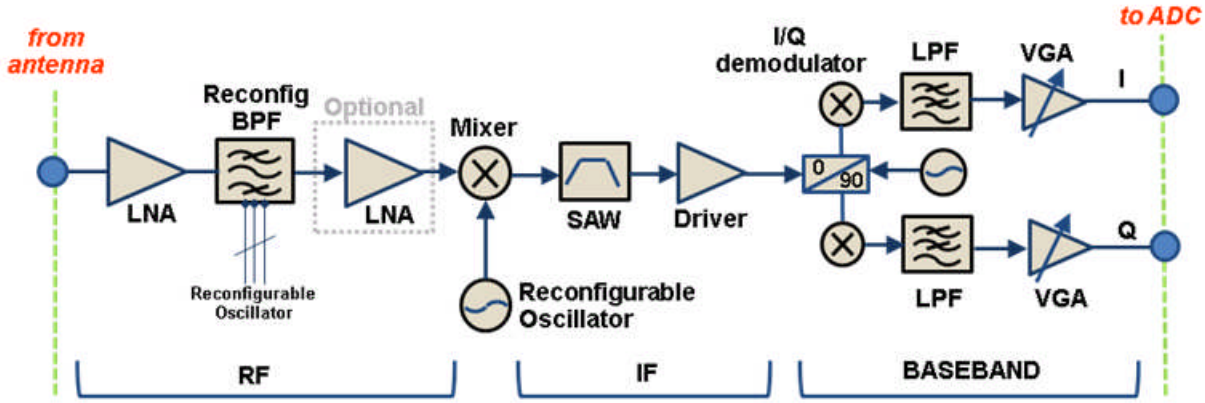

Figure 24 Proposed block diagram for reconfigurable low noise receiver

In this architecture, the LNA (wideband or reconfigurable) is the first block, ensuring a good noise figure (NF) performance. The antenna is assumed to have two different ports for transmission and reception. Nowadays, this configuration is spread due to MIMO.

Reconfigurable BPF design is one of most challenging blocks in this architecture. Later on, more details about its design will be presented.

2.4.2 Evaluation methodology

"Low noise receiver architecture" targets the small cell sub-scenario established in WP4.

2.4.2.1 Sub-scenario description

The scenario in which the proposed reconfigurable receiver will be evaluated is a femto cell. Possible deployment scenarios are residential solutions up to 8 concurrent users or enterprise solutions up to 16 concurrent users. The coverage area is usually limited to few tens of meters. The channel bandwidth for these applications is typically 10 MHz.

Table 11 Sub-scenario Description, [28]

Inputs	Description	Values (or range)
Environment	Spatial deployment (ISD…)	250 m radius for the MC
EU or sources density	EMF sources number	90 active EU in the MC +27 SC BS (9/MC sector)
	Max. Tx Power at MC	46 dBm (13 dBi ant. gain)
	Max. Tx Power at SC	30 dBm (5 dBi ant. gain)
Standard (freq. and BW)	Central frequency bandwidth	800 MHz (10 MHz) 1.7 GHz (10 MHz)
Signal duration	Typical duration (duty cycle)	LTE Frame:10us
Traffic load	Throughput (low, medium, high)	Medium to high (UL:0.1-1 Mbps TBD)

2.4.2.2 Exposure and QoS metrics identification

The evaluation methodology consists on the assessment of a typical multi-band receiver compared to the proposed reconfigurable receiver in Figure 24. Their performance will be evaluated basically in terms of NF, which mainly determines the receiver sensitivity. Nevertheless, other parameters such as receiver spurious, intermodulation products or interfering signals have been considered to check that the receiver requirements are fulfilled.

The EI evaluation focuses on the transmit power reduction at UE due to receiver sensitivity improvement at BS. Some statements and expressions are shown to relate the transmit power at UE with the expected receiver NF improvement. The received signal at BS is the transmit signal at UE adding the antenna gain and subtracting the radio link loss.

The minimum received power ensuring a given QoS can be defined as follows:

$$P_{sens} = KT.B.F_{sys}.P_G.\frac{E_b}{N_o} \quad (2.19)$$

where K is Boltzmann's constant, T is the device temperature in Kelvin, B is the signal bandwidth in MHz, F_{sys} is the system noise factor (NF is expressed in linear

units), P_G is the processing gain (linear), and $^{E_b}/_{N_o}$ is the bit energy to noise energy ratio. These last two parameters are commonly expressed as the receiver SNR, which depends on the modulation (QPSK, 16-QAM, 64-QAM) and codification.

The receiver sensitivity will be evaluated in the typical and the proposed architecture, assessing NF. If receiver sensitivity is improved at BS, the required transmit power at UE will decrease, reducing EI. Furthermore, the interfering signals at neighbouring receivers will decrease due to the transmit power reduction.

Some other important parameters to take into account in the receiver architecture design are defined in 3GPP standard [64]. The receiver sensitivity for a femto cell scenario is -93.5 dBm. The adjacent channel selectivity is evaluated with -28 dBm interfering signal power when the receiver signal is -71.5 dBm. In case of blocking performance, a -15 dBm interfering signal power using continuous wave (CW) or a -27 dBm using E-UTRA signal can be applied, while keeping the receiver wanted signal in -79.5 dBm.

2.4.2.3 EI ratio evaluation (or Capacity/QoS improvements converting into EI reduction)

Considering the same QoS (SNR), the same channel bandwidth and the same processing gain in both architectures, F_{sys} is the only parameter to be improved related to P_{sens}, which is the target of this study.

In a typical femto cell scenario, it can be assumed an antenna gain at UE of 5 dBi and 13 dBi in case of the BS. To simplify calculations, the radio link path loss will be supposed to be two-ray ground-reflection model, and both architectures will be compared under the same radio link conditions.

The received power could be defined as:

$$Pr = \frac{Pt*G*ht^2*hr^2}{d^4} \quad (2.20)$$

Therefore, if the antenna gain, the antennas height and the distance between the transmitter and the receiver are maintained, there is a clear 1-to-1 relation between P_{sens} and P_{TX}. Furthermore, looking at (2.19) there is also a 1-to-1 relation between P_{sens} and NF, assuming the same bandwidth and SNR. As a result, the EI evaluation is based on a 1-to-1 relation between NF, P_{sens}andP_{TX}.
To sum up, the EI improvement is expressed as:

$$Ratio_{EI-Reconfigurable\ receiver}(\%) = \frac{NF_{Typical}(linear) - NF_{Reconfigurable}\ (linear)}{NF_{Typical}\ (linear)} \times 100 \quad (2.21)$$

The following evaluation has been done using datasheets of commercial components. Most relevant parameters will be mentioned to clarify the expected results.

In a typical multi-band receiver, narrowband LNAs are used for each frequency band with NF around 0.7 dB and 20 dB gain. In this architecture, a RF switch is required to

select among RF chains and insertion loss could be approximately 0.5-0.7 dB. Moreover specific LTE band BPFs have around 2-3 dB insertion loss. Therefore, the expected receiver NF is in the range of 3.5-5 dB, because at least 2.5 dB insertion loss is preceding narrowband LNAs.

Whereas in the reconfigurable receiver, a wideband LNA is proposed at first stage with NF about 1dB and up to 20 dB gain. In this architecture, a reconfigurable BPF, which is the critical block, presents higher insertion loss than commercial BPFs. If the insertion loss at the reconfigurable BPF is in the range of 4-7 dB, the expected receiver NF would be about 2-3 dB. Further details about the reconfigurable BPF design will be presented.

Based on this analysis, some calculations have been done to evaluate the potential EI improvement with the proposed reconfigurable architecture. EI improvement is calculated as function of receiver NF in both architectures. This evaluation uses previous details to assess the EI enhancement ratio presented in (2.21). Table 12 summarizes the potential EI improvement:

Table 12 Potential EI improvement as function of the receiver NF reduction

EI improvement as function of NF (%)		**Typical multi-band receiver NF (dB)**			
		3.5	***4***	***4.5***	***5***
Reconfigurable receiver NF (dB)	***2***	29.2	36.9	43.8	49.9
	2.5	20.6	29.2	36.9	43.8
	3	10.9	20.6	29.2	36.9

The maximum expected enhancement comparing both architectures is as high as 49.9%, when the receiver NF improvement is 3 dB. If only 0.5 dB receiver NF improvement is obtained, the EI improvement will be 10.9%. Table 12 summarizes the potential EI enhancement which could vary from 10.9% to 49.9%.

Some hardware developments have been done to assess the EI enhancement, complementing the specifications from datasheets. Furthermore, in WP6 a hardware demonstrator will be developed to compare both architectures. Two different LTE bands were selected for developing hardware prototypes in WP6. These frequency bands are LTE band 20 (832 – 862 MHz) and LTE band 3 (1710 – 1785 MHz). Nevertheless, the proposed reconfigurable architecture could be applied to different frequency bands. Moreover, the proposed solution is more promising compared with the typical solution in terms of size and cost, when large number of frequency bands is considered.

Reconfigurable BPF design is the most challenging block in the proposed architecture and several solutions based on tunable elements have appeared [29], [30], [31], [32] and [33].These solutions present constraints in terms of insertion loss,

wideband operation, high frequency operation range or manufacturing integration. However, into this study some solutions have been revisited, evaluating the filter topologies and tunable components.

The study has focused on lumped elements, and two different solutions of tunable capacitances were evaluated: digitally controlled capacitors (DTC) and varactors. DTCs present limited tuning ratios (up to 10:1) with discrete capacitance steps depending on the number of bits. Varactors could achieve tuning ratios higher than 30:1 and the capacitance values are not discrete. However, their control is a challenging issue because high tuning ratios are related to high reverse voltages, presenting sensibility constraints. Furthermore, their capacitive response depends on the frequency. Anyway, varactors were selected as the most promising solution due to their advantages in terms of tuning ratio to provide wideband performance. Among varactor solutions, SMV1247 from Skyworks was selected as the most suitable one due to its convenient features, such as a 14:1 tuning ratio and 8V maximum control voltage, [34]. Moreover its capacitance values between 0.64 pF and 8.86 pF are appropriate to implement a reconfigurable BPF from LTE band 20 to LTE band 3.

Firstly, typical filter topologies (Butterworth, Chebyshev, Elliptic...) were studied using this varactor (SMV1247). LPF and HPF topologies were simulated to check the varactor suitability and some prototypes were implemented showing good performance but high insertion loss. Afterwards, a reconfigurable BPF has been designed based on 7-section Chebyshev LPF and 7-section Chebyshev HPF. The electrical diagram of the mentioned topology and the manufactured prototype are shown in Figure 25.

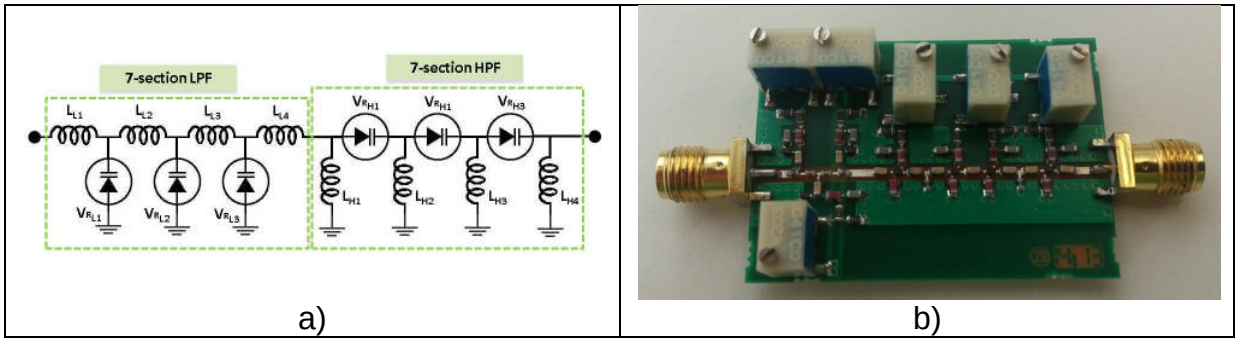

Figure 25 a) Electrical diagram of reconfigurable BPF (7-section LPF and 7-section HPF) based on varactors and b) Manufactured prototype

The design requires 6 varactors using 6 different control voltages (Vr_{L1}, Vr_{L2}, Vr_{L3}, Vr_{H1}, Vr_{H2} and Vr_{H3}) to adjust its filtering performance. Figure 26 shows some measurements results from LTE band 20 to LTE band 3.

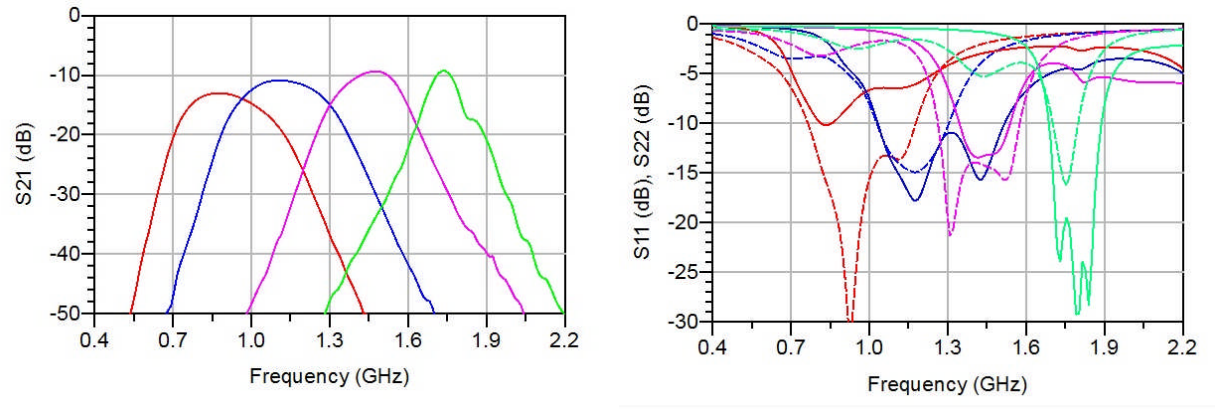

a) b)

Figure 26 a) Measured insertion loss and b) Measured return losses of reconfigurable BPF (7-section LPF and 7-section HPF) based on varactors

The measured insertion loss is as high as 13 dB at LTE band 20. Therefore this design is not suitable for the proposed architecture, because the BPF insertion loss should be lower than 7 dB to achieve 3 dB receiver NF. A trade-off between frequency selectivity and insertion loss should be reached. However, the greater is the order of the filter, the higher would be the selectivity, but more insertion loss would be achieved.

Another filter topology, the stepped impedance resonator (SIR)[35], has been considered in order to reduce the insertion loss while showing wideband performance. Figure 27 depicts the block diagram of the varactor-tunable SIR and the manufactured prototype.

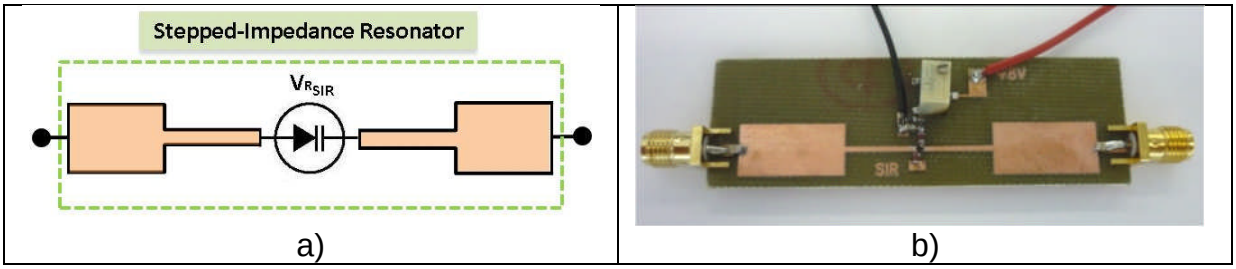

a) b)

Figure 27 a) Block diagram of the varactor-tunable SIR and b) Manufactured varactor-tunable SIR

In this configuration a single varactor is implemented, and its operating band can be set adjusting its reverse voltage. Figure 28 presents the measured insertion loss of the varactor-tunable SIR from LTE band 20 to LTE band 7.

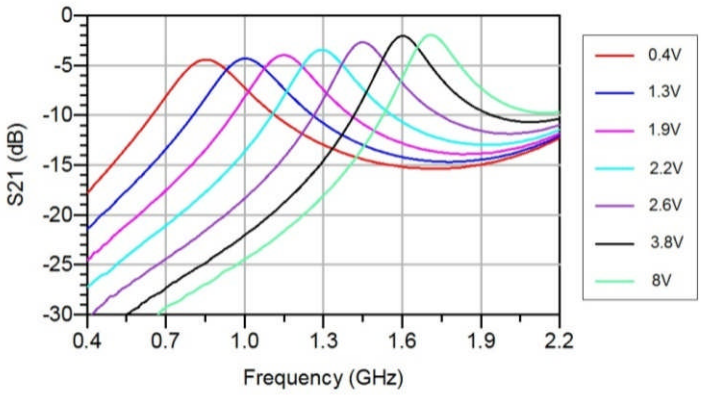

Figure 28 a) Measured insertion loss of the varactor-tunable SIR

Using this solution, the insertion loss is lower than 5 dB. However, the frequency selectivity is poor in order to fulfil the blocking specifications defined in 3GPP for LTE reception. In next steps this configuration could be modified to improve the frequency selectivity and out-of-band rejection.

2.4.2.4 Global EI reduction assessment

Up to now the EI evaluation has been carried out comparing a typical architecture with the proposed architecture for a femto cell scenario. Finally, the EI evaluation will be quantified on the exposure of global population. In WP2, statistical information about the usages, the locations, etc., will be analysed to provide a weighted coefficient to determine the effective impact of this technique on the global EI.

2.5 Cell DTX amplifier deactivation

2.5.1 Remind on the concept

Since 3GPP release 7, the UE can shut down the transmitter completely when there is no data channel transmission. This could provide significant power savings and obviously reduce EI. In the case of downlink (DL) communication, the transmitter at base station (BS) could also shut down leading to reduce EI. This technique is named cell DTX (Discontinuous Transmission).

This study has focused on DL because it presents more challenging requirements, especially in the high power amplifier (HPA) design, due to the high power level that it handles. LTE macro cell HPAs could deliver up to 46 dBm and to enable cell DTX, the HPA should have fast transition times in order to deactivate and reactivate itself following traffic demand. In HPAs, transition times are higher because of the intrinsic parasites and the inherent higher capacitance discharges due to the relatively high voltage supplies used in these amplifiers. Two different transistor technologies were considered: LDMOS (Laterally Diffused Metal Oxide Semiconductor) and GaN (Gallium Nitride). Furthermore, different biasing circuits such as gate pulsing and drain pulsing were studied to obtain the optimal configuration to implement cell DTX.

Cell DTX technique presents upper enhancement in low load traffic scenarios where there are higher periods of time with no data. Therefore the potential improvement due to this technique increases, reducing EI and providing significant power savings.

2.5.2 Evaluation methodology

"Cell DTX amplifier deactivation" targets the macro cell sub-scenario established in WP4.

2.5.2.1 Sub-scenario description

Table 13 Sub-Scenario Description, [36]

Inputs	Description	Values (or range)
Environment	Spatial deployment, such as the inter-site distance (ISD)	250 meters radius for the Macro Cell
UE or source density	Max. Tx Power at MC	46 dBm (15 dBi ant. gain)
Frequency	Central frequency (bandwidth)	2.6 GHz (20MHz)
Signal duration	Typical duration (duty cycle)	LTE Frame:10us
Traffic load	Throughput (low, medium, high)	Low

Cell DTX technique could be applied in different frequency bands and bandwidths. Nevertheless during the design phase, it should select the suitable transistor to work on these frequencies.

2.5.2.2 Exposure and QoS metrics identification

The evaluation methodology consists on the assessment of the average transmit power reduction when cell DTX is applied. During a day, the traffic load in a cellular network presents high variability as it is shown in Figure 29. BSs are only running under the full load for which they were designed during few hours per day. Therefore there is most likely a considerable amount of periods when no users are active. This means that cell DTX would be beneficial since there are empty symbols where it can be enabled.

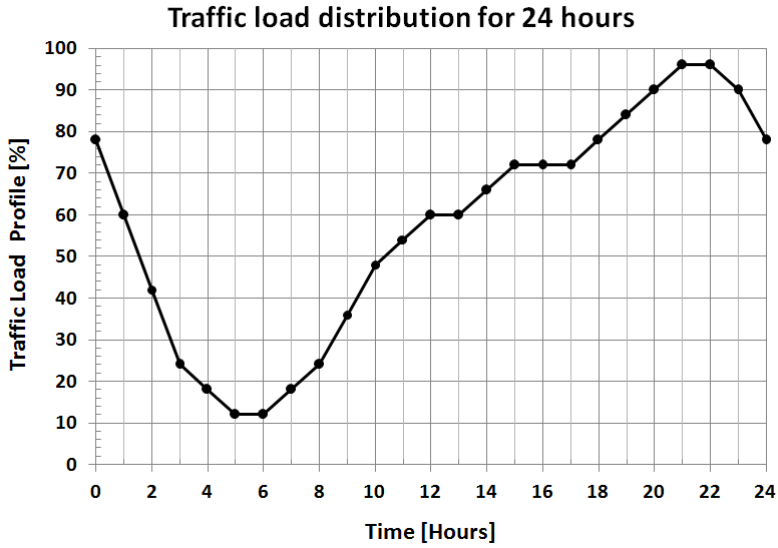

Figure 29 24 hours traffic load profile – Urban area during a day [38]

Even when no user data is transmitted by a BS, LTE standard stipulates that certain control signals must be transmitted. Examples of such signals are reference signals, synchronization signals and broadcast information. Different signals are used for many reasons: UE synchronization, mobility cell search, data reception, initial cell search or channel state information feedback. These signals are well justified when the traffic load is high into the cell. However, when there is low traffic load, they could be reduced. Due to that, cell DTX appears as a promising solution.

LTE standard defines two different states depending on the information transmitted: active mode or idle mode. In active mode, the user data information is mainly transmitted together with control signals (reference signals, synchronization signals and broadcast information). Meanwhile in idle mode, only control signals are transmitted to handle the communication.

The power level of the transmitted signal is associated with the LTE state: active mode or idle mode. In active mode, the signal power level is higher because resource elements (RE) allocated to user data will be partially or completely occupied depending on the traffic load, and resource elements allocated to control signals will be occupied. On the other hand, working in idle mode only the resource elements allocated to control signals will be occupied. Therefore there will be more empty symbols in the LTE frame.

To assess the impact on EI, the average transmit power at BS should be evaluated with and without applying cell DTX. And particularly in this study, the influence on specific HPAs to implement cell DTX is studied.

Cell DTX technique enables lower number of control signals and therefore more empty symbols in LTE frame. Note that the most significant impact on EI comes at low traffic load, since here the probability of having empty subframes is higher, while at high traffic load there are basically no empty subframes left where cell DTX can be enabled. Different LTE frame distributions can be appreciated in Figure 30.

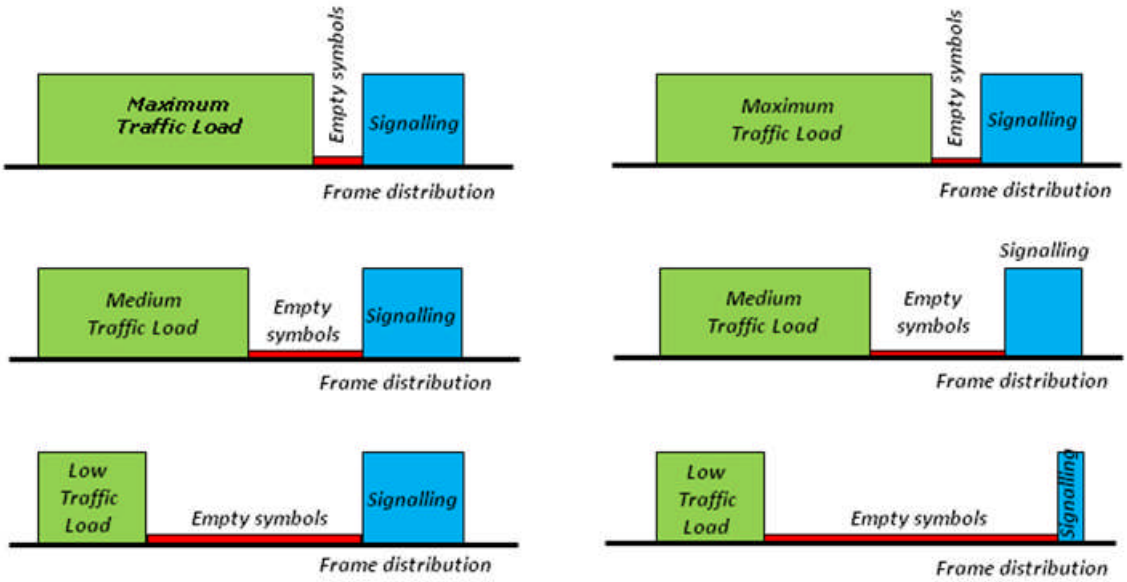

Figure 30 Different LTE frame distributions according to the traffic load a) without cell DTX and b) with cell DTX

Without applying cell DTX, signalling could be assumed as constant and the average transmit power will vary due to traffic load, as shown in Figure 30 a). At high traffic load, the average transmit power is high because there are few empty symbols. Most of REs allocated to user data will be occupied. At medium traffic load, the number of empty symbols increases and therefore the average transmit power decreases. And finally at low traffic load, the average transmit power will be the lowest because there is a large number of empty symbols.

When cell DTX is applied, the signalling could be modified according to the traffic load. At maximum load, when there are active users, the cost of transmitting the control signals is justified. However, when there are no active users, there is little or no need for these signals most of the time, suggesting that there are possibilities for cell DTX. At low traffic load, the signalling could be reduced appearing even more empty symbols, as it is shown in Figure 30 b).

Table 14 Exposure KPIs identification in the WP4 solution evaluation

WP4 solution title	UL/DL	Exposure KPIs			QoS KPI
		SAR	Mean Tx power	Mean Tx duration	
Cell DTX amplifier deactivation	DL	×	√	√	

HPAs should be designed specifically to support cell DTX. This technique will manage the duration of power transmission in order to decrease it. Applying cell DTX, the amount of required control signals decreases reducing the duration of power transmission. Due to that, the average transmit power at BS will decrease. And these enhancements in DL will reduce the average received power at UE, improving EI.

The most relevant parameter in the scenario is the traffic load. At low traffic load scenarios, the improvement will be higher because the probability of having empty symbols is higher.

2.5.2.3 EI ratio evaluation (or Capacity/QoS improvements converting into EI reduction)

The specific EI enhancement is evaluated comparing the transmit power during empty symbols when a specific HPA is developed for cell DTX or not. Cell DTX has been clearly probed as an energy efficiency enabler [38]. Nevertheless, from HPA point of view, if it is not turned off when cell DTX feature is applied there will be noise power radiated by the antenna.

For a typical transmitter, the noise figure could be around 15-20 dB, with gain of about 60-70 dB. A specific duplexer for each LTE band is commonly implemented with bandwidths up to 100 MHz. By calculating the noise power density and integrating it over 100 MHz, a total noise power of -4 dBm results. Without a specific HPA design to implement cell DTX, the noise power is ever presented in both active and idle modes. Developing a specific HPA, it will turn off during empty symbols and the noise power will decrease drastically. Therefore the radiated transmit power will decrease, decreasing the average transmit power.

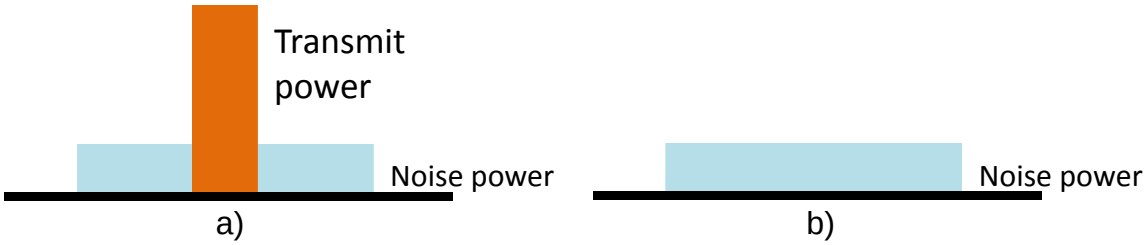

Figure 31 RF spectrum for a) non empty symbols and b) empty symbols without a specific HPA to implement cell DTX

Figure 31 represents RF spectrum when there is not a specific HPA to implement cell DTX. Even when there are empty symbols, the noise power will be radiated by the antenna.

Based on the previous analysis, the transmit power (P_{TX}) will be evaluated during empty symbols in case that a specific HPA is performed or not. The enhancement is related to the noise power radiation if no data or signalling is been transmitted.

$$Ratio_{EI-HPA\_Cell\ DTX}(\%) = \frac{P_{TX}\ (w/o\ HPA\_Cell\_DTX) - P_{TX}\ (w/\ HPA\_Cell\_DTX)}{P_{TX}\ (w/o\ HPA\_Cell\_DTX)} \times 100 \qquad (2.22)$$

When there is not a specific HPA the noise power could be as high as -4 dBm, as it was previously calculated, while if a specific HPA is developed the noise will

decrease close to noise floor that it can be estimated in -74 dBm. Then the power improvement ratio is:

$$Ratio_{EI-HPA\_Cell\ DTX}(\%) = \frac{[-4dBm]linear - [-74dBm]linear}{[-4dBm]linear} \times 100 \approx 100\% \qquad (2.23)$$

The relative improvement in the transmit power during empty symbols is remarkable. However, this improvement should be referred to the average transmit power. The most significant impact on EI comes at low traffic load, therefore the evaluation will be done in this scenario. For this evaluation, Figure 30 could be used as reference. Without applying cell DTX, it can be assumed that 10% of time is allocated to traffic load (user data), 20% of time is allocated to signalling and 70% of time is allocated to empty symbols. If cell DTX technique is applied, the LTE frame distribution could change to 10% of time allocated to traffic load (user data), 10% of time allocated to signalling and 80% of time allocated to empty symbols. Therefore a reduction in signalling around 10% is assumed using cell DTX in a low traffic scenario which is performed at network level.

In order to assess the average transmit power, firstly it should be evaluated for each type of signal: traffic load, signalling and empty symbols. In a macro cell BS, 46 dBm is defined for maximum traffic load. Therefore at low traffic load without applying cell DTX, 30% of time is used for traffic load and signalling (46 dBm) and 70% of time for empty symbols (-4 dBm // noise power). The average transmit power could be estimated in 40.8 dBm. However when cell DTX is applied, only 20% of time is used for traffic load and signalling (46 dBm) and 80% of time for empty symbols (-4 dBm // noise power), then the average transmit power is estimated in 39 dBm. The average power reduction at BS will be 33% at network level when there is low traffic load. This technique is really relevant and the enhancement will decrease when user data increase.

If this EI evaluation takes into account the development of a specific HPA to implement cell DTX, the power level presents a remarkable improvement in terms of noise power. A specific HPA will provide a reduction in the average transmit power during empty symbols from -4 dBm to around -74 dBm. However, the noise power level is not significant compared to the average transmit power (around 40 dBm). Using (2.23) to assess the average transmit power, the power reduction at BS could be estimated about 0.004%. From an energy efficiency point of view, a specific HPA has been proved as an energy efficiency enabler [37]. However, it is not a significant solution in terms of EI reduction.

2.5.2.4 Global EI reduction assessment

Additionally, EI evaluation should be carried out in terms of a global metric that aims to quantify the exposure of a population within its diversity of usages, environments, etc. The statistical information about the usages, the activities, the locations and so on is analysed in WP2. WP2 will provide a weighting coefficient to apply to this technique to obtain the effective impact on the global EI. Anyway, the expected global impact in terms of EI reduction is not significant.

2.6 Sleep/idle mode in a mesh gateway deployment

2.6.1 Remind on the concept

Wi-Fi access point (AP) in commercial gateways usually supports only two modes of operation: ON or OFF. More advanced state machines may be found in the client device or station (STA) especially for battery saving reasons. However, these refinements are usually discarded for commercial APs since battery saving is not really an issue.

Switching-off one radio (sleep mode) means that services through this radio cannot be offered anymore. If this mode clearly produces no EMF exposition at all, it is only suitable for periods of time where services are not needed. Typically, in an enterprise environment, this mode can “safely” be used outside the working hours. Such “scheduled sleep mode” will be implemented and evaluated within a wireless mesh network context (WMN) in WP6 [39].

To reduce the exposure during the classical “ON” time, the first idea can be the introduction of a new state in the two-state machine of the gateway as shown in Figure 32. In **this “idle mode”,** the radio is not be completely shut down, but operates in a “degraded” mode, where (to summarize) the transmit power is going to be reduced.

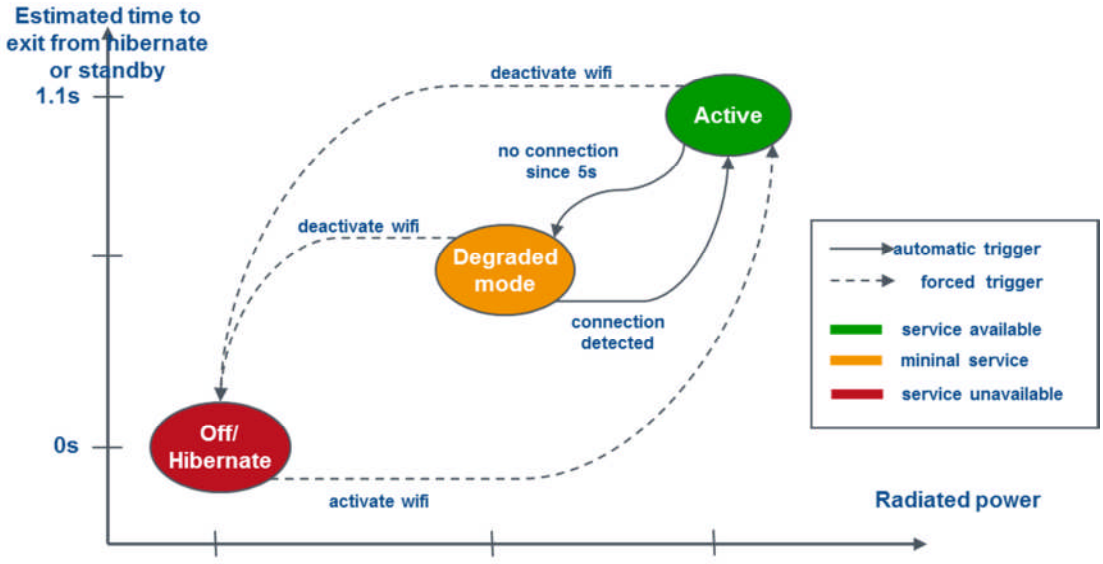

Figure 32 Idle-enabled State-Machine of a WLAN Access Point

By being able to broadcast the Wi-Fi beacons, the services provided by the AP are still available to STAs which are in the AP’s range. The triggers between all the states will be investigated in this study. At a first glance, one can think of a simple trigger, which could be applied to both standalone and WMN deployment of Wi-Fi gateways, where the number of associated STAs is considered. For instance, Figure 32 shows the advanced state machine where a timer of 5s is set after the last connection detected to decide to go to idle mode. Once expired and if no connection is

requested, the radio goes to the idle mode. If a connection is attempted, then the radio switches back to its normal state.

Of course such trigger essentially reduces the EMF produced by the beacon transmission only, which in itself does not participate a lot in the exposure due to the short beacon transmission time. The main benefit of such idle mode should be investigated when ongoing traffic is happening with a trade-off between QoS and EMF reduction to be evaluated. The WMN nature of the deployment brings also additional degree of freedom to be exploited.

2.6.2 Evaluation methodology

To assess the performance of idle algorithms in standalone and mesh network deployment, system-level simulations will be performed. The idea behind such methodology is to be able to “quickly” evaluate different idle algorithms without the burden of deploying a real testbed and with a reproducibility of the scenarios much more controlled.

In system-level simulations, a Monte-Carlo approach is used to drop (randomly or not) APs/STAs and to simulate the propagation conditions. Once a drop is performed, a first stage consists of the determination of the “static” parameters such as shadowing and path-loss (i.e., large-scale parameters) for each communication link. A second stage consists of the simulation of the “dynamic” behaviour of the system, i.e., the modelling of the fast fading (large scale parameters), of the media access (CSMA/CA in the Wi-Fi case), of the traffic pattern ... The dynamic evolution is handled on per frame basis. Finally, a third stage consists of the gathering of relevant statistics (both static and dynamic) for this run.

System-level simulations are commonly used in the cellular space (for large scale evaluation), while Wi-Fi technology generally relies on real testbed evaluations and/or event-driven network simulators such as ns-3, [40]. By using the same approach, various idle algorithms can be stochastically evaluated before being implemented in real products, i.e., evaluated on different environment conditions which would be quite difficult to reproduce in a real testbed.

2.6.2.1 Sub-scenario description

The sleep/idle mode propagation in a mesh gateway deployment addresses the Wi-Fi & WSN sub scenario. The method could be applied to small cell scenario if cellular accesses are collocated with Wi-Fi accesses by an Operator for instance.

In particular, an enterprise environment is targeted, where it is more likely to deploy gateways providing user services (such as Internet access) using a mesh configuration as opposed to standalone deployment in a residential scenario.

In the wireless community, different layouts have been proposed to capture such hot-spot scenarios. In particular, two layouts can be considered for further investigations:

- The first layout is the Indoor / Hotspot (InH) layout from the ITU-R [41]. The 3GPP extended the original layout from the ITU-R in [42] by doubling the number of hotspots deployed (4 instead of 2) as shown in Figure 33. It extends the ITU-R. Such layout may have up to 2 floors. One floor has 16 blocks separated by a hallway and one block's area is 15m x 15m. The position of the hotspots per floor is fixed.

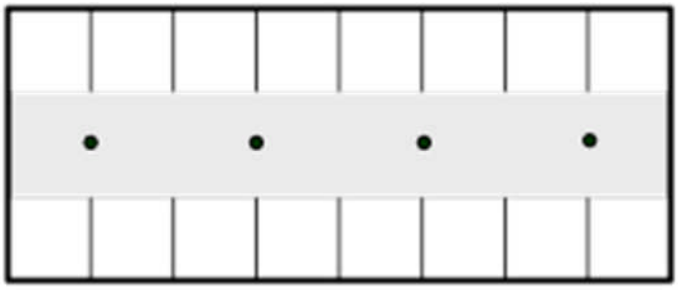

Figure 33 ITU-R InH-based layout [42]

- The second layout comes from the IEEE 802.11 group [43]. It captures several offices (2 rows of 4 offices). The layout of one office with a single basic service set (BSS) is given in Figure 34. One office is a 20x20 block where 4 APs are deployed in fixed positions.

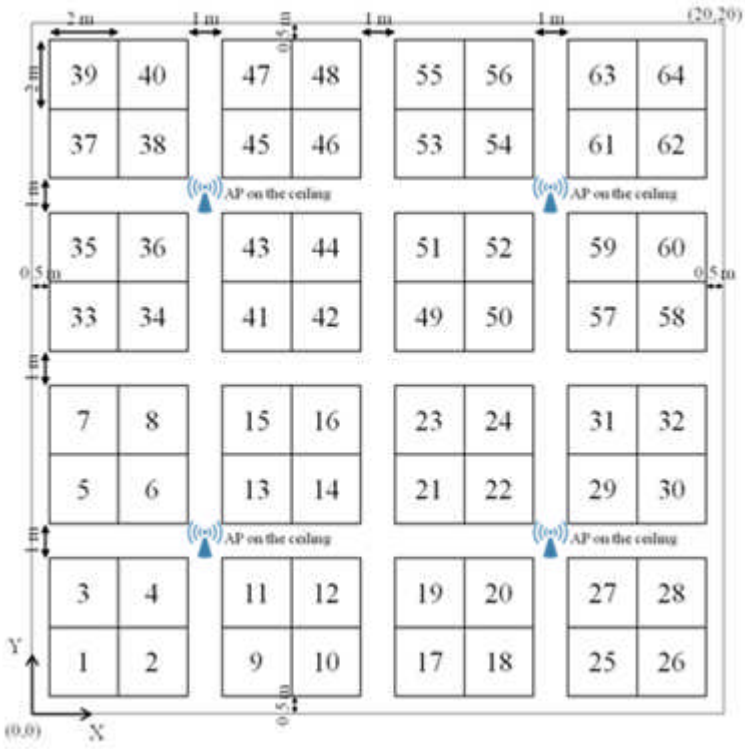

Figure 34 IEEE 802.11 enterprise layout for a single BSS [43]

To reflect an office deployment with a wireless mesh network deployed, the previous layouts may need to be a bit refined.

The system parameters are chosen to reflect the IEEE 802.11n amendment, known as high throughput (HT) in the IEEE 802.11 standard of 2012 [44], which can operate in both the 2.4GHz ISM band and the 5GHz ISM band. When a dual-band AP is used as a standalone AP, we assume that both radios can work concurrently.

In the deployment scenario envisaged, the 2.4GHz band is used by an AP for local connection of STAs while the 5GHz is dedicated to the backbone transmission (mesh). One STA can be connected to any AP. By default, the best received power is the criterion chosen for connection (no load balancing / QoS constraints).

The IEEE 802.11n amendment supports 20 and 40MHz bandwidth transmission [44]. When 40MHz bandwidth is used, this bandwidth is divided into a primary channel and an adjacent (upper/lower) secondary channel. The primary channel is used for frame management, while both 20MHz channels are used for data transmission.

In the 2.4GHz ISM band, it is only possible to fit 4 non-overlapping 20MHz-large channels as shown in Figure 35. In practice, IEEE 802.11b STAs need also to be supported by the AP, leading to only 3 non adjacent 22MHz-large channels: channel 1 (2412MHz), 6 (2437MHz) and 11 (2462MHz). Due to the high level of interference in the 2.4GHz ISM band, we will assume first that we will only use 20MHz transmission mode of 802.11n on the channels 1, 6 and 11. In this band, the maximum radiated power is 20dBm/100mW in Europe (including antenna gain).

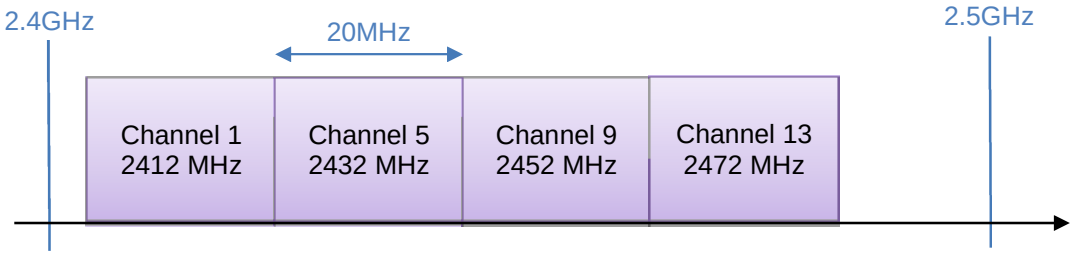

Figure 35 IEEE 802.11n adjacent channels in the 2.4GHz ISM band

Regarding the 5GHz ISM band, we assume that we can use the 40MHz transmission mode of IEEE 802.11n, since interference and available spectrum are less an issue. The same 5GHz channel is chosen for all APs within the Wireless Mesh Network (WNM), where the maximum transmit power can go up to 30dBm/1W (in the 5470 – 5725MHz frequency range).

While the IEEE 802.11n amendment supports up to four antennas [44], we will assume that the 2.4GHz radio has two antennas, while the 5GHz radio has three antennas. Those values are chosen to reflect the antenna configurations of the residential Gateways (APs) which will be used in the scheduled on/off activity in WP6 [39].

Table 15 summarizes the common parameters used.

Table 15 – Inputs description for the InH-based layout

Inputs	Description	Values (or range)	Reference
Environment	Spatial deployment (ISD…)	AP in fixed positions based on the layout	[42], [43]
Frequency	Central frequency (bandwidth)	2.4GHz (20 MHz) 5 GHz (40 MHz)	
Power	Maximum Tx	20dBm @2.4GHz 30dBm @2.4GHz	
Path loss model, indoor/outdoor	Channel Model (path-loss, shadowing, fast fading)	TGn D	[43]
Protocols	Any process managing Ptx, transmit duration or SAR	Association: Best received power (same BSS is broadcasted by all the APs)	

2.6.2.2 Exposure and QoS metrics identification

Through system-level simulations, the following key performance indicators (KPIs) can be evaluated:

- For Access Points:
  - **Transmit Power**: setting and evolution during the time;
  - **Idle Mode Usage**: percentage of time when idle mode is engaged;
  - **Throughput**: average uplink throughput (based on traffic pattern).

- For Stations:
  - **Throughput**: average downlink throughput (based on traffic pattern);
  - **Failure Rate**: if idle mode is engaged, the rate of transmission failure.

- For any Probe (i.e. a point dropped in the layout):
  - **Received Power**: evolution of the received power over the time
  - **Outage**: if the signal of all (authenticated) APs is below a given threshold (sensitivity), then no coverage can be provided at the probe's position

Most of these KPIs can be evaluated only when dynamic system-level simulations are possible (stage 2 in the previous description). If only the static part is available (stage 1), KPIs such as receive power or coverage can still be computed but using long-term parameters: neither fast fading, nor medium access impact can be taken into account for instance.

With respect to the exposure assessment, it is quite clear that only the mean transmit power of an AP and the associated mean Tx duration are going to be impacted, while the coverage will be the main Quality of Service metric as it defines when an AP is in idle mode if a STA is able to detect the AP's signal (e.g., beacon).

2.6.2.3 EI ratio evaluation (or Capacity/QoS improvements converting into EI reduction)

So far, only the InH layout is supported, with a static behaviour. We have updated the model to deploy 3 APs (similar to the number of APs involved in the scheduling on/off activity in WP6 [39] as shown in Figure 36.

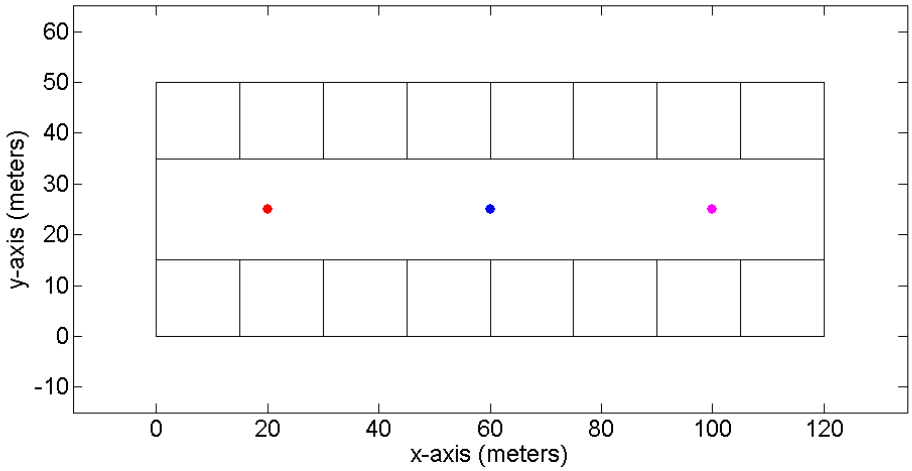

Figure 36 ITU-R InH-based layout with 3 APs

The main parameters of the layout are given in Table 16. Only static simulations have been performed, but they are sufficient to deduce some preliminary results from any idle algorithm in terms of received power and coverage, both KPIs associated to a Probe point.

Table 16 – Main simulation parameters

Propagation		
Layout		ITU-R Indoor Hotspot
Channel model		D
Shadowing		Disabled
Separating wall modelling		Enabled
Separating wall attenuation	2.4GHz 5GHz	10dB 15dB
Parameters		
Number of APs		3
2.4GHz radio	Enabled Bandwidth Maximum Tx power Antenna Number Gain	Yes 20MHz 20dBm 2 0dBi (omni)
5GHz radio	Enabled Bandwidth Maximum Tx power Antenna Number Gain	No 40MHz 30dBm 3 0dBi (omni)

Since the 5GHz radio is used for the backbone of the WMN and therefore, is not modified yet, we did not simulate the associated propagation. We use the channel 'D' variant for the large scale parameters modelling which are given in Table 17.

Table 17 – Channel D large scale parameters

Large scale parameters: d in meter, f_c in GHz		
Channel model		D
d_{BP} (break point distance)		10m
$d \leq d_{BP}$	Path-loss (dB)	$L(d) = L_{FSL}(d) = 38.46 + 20\log_{10}(d) + 20\log10(f_c/2)$
	Shadowing	3dB (standard deviation)
	Line of Sight	Yes
$d > d_{BP}$	Path-loss (dB)	$L_{FSL}(d) = 38.46 + 20\log_{10}(d) + 20\log10(f_c/2)$
	Shadowing	5dB (standard deviation)
	Line of Sight	No

In the following simulations, we have disabled the shadowing. We also added to the previous propagation equations the explicit computation of the exact number of separating walls crossed, separating walls are represented by the black lines in Figure 36.

The degraded mode of the idle algorithm as described in Figure 32 will consist for the simulation to switch-off one RF chain of the 2.4GHz radio, leading to a SISO transmission. By doing so, the maximum transmit power (used for the beacon transmission for instance) is divided by 2.

To assess the idle algorithm impact on any point of the layout (or probe), we compute the receive power from the APs as well as the coverage in a static way. Since we are assuming a WMN based on Wi-Fi technology, the Carrier Sense Multiple Access with Collision Avoidance (CSMA-CA) mechanism controlling the medium access will try to avoid transmission collision, meaning that at the probe location the best received signal from one of the deployed AP will most likely represent the worst case scenario in terms of received power originating from the APs (no STA are deployed yet). We should normally observe a -3dB reduction as the transmit power is divided by 2 for all APs. Idle mode for specific AP will be investigated at a later stage, when STA will be dropped in the layout as well.

More importantly, the coverage provided by the APs will also be evaluated at the probe location, i.e., the capability of a STA located at the probe position to detect one AP's signal at a given packet error frame (PER). As a reminder, we assume that a STA can be connected to any deployed AP. According to the IEEE 802.11n specifications [44], the minimum sensitivity required at the receiver side to detect the most robust modulation and coding scheme (MCS) with a PER of 10% is -82dBm on a 20MHz channel, see Table 18. If the best received signal from one of the deployed

AP is below this value at one's probe position, then we can assume that this position is out of coverage.

Table 18 – Receiver minimum input sensitivity (see Table 20-23 [44])

Modulation	Rate (R)	Adjacent channel rejection (dB)	Nonadjacent channel rejection (dB)	Minimum sensitivity (20 MHz channel spacing) (dBm)	Minimum sensitivity (40 MHz channel spacing) (dBm)
BPSK	1/2	16	32	–82	–79
QPSK	1/2	13	29	–79	–76
QPSK	3/4	11	27	–77	–74
16-QAM	1/2	8	24	–74	–71
16-QAM	3/4	4	20	–70	–67
64-QAM	2/3	0	16	–66	–63
64-QAM	3/4	–1	15	–65	–62
64-QAM	5/6	–2	14	–64	–61

We evaluate the two previous KPIs with no idle mode algorithm running. Figure 37 shows the received power map due to the 2.4GHz radio in the worst case scenario (without collision). The separating walls can be well identified from the map, indicating that their explicit counting is well implemented. Indeed, the received signal received by a probe when only one wall has to be crossed (e.g. directly above and below the middle AP) is greater than when more than one wall have to be crossed.

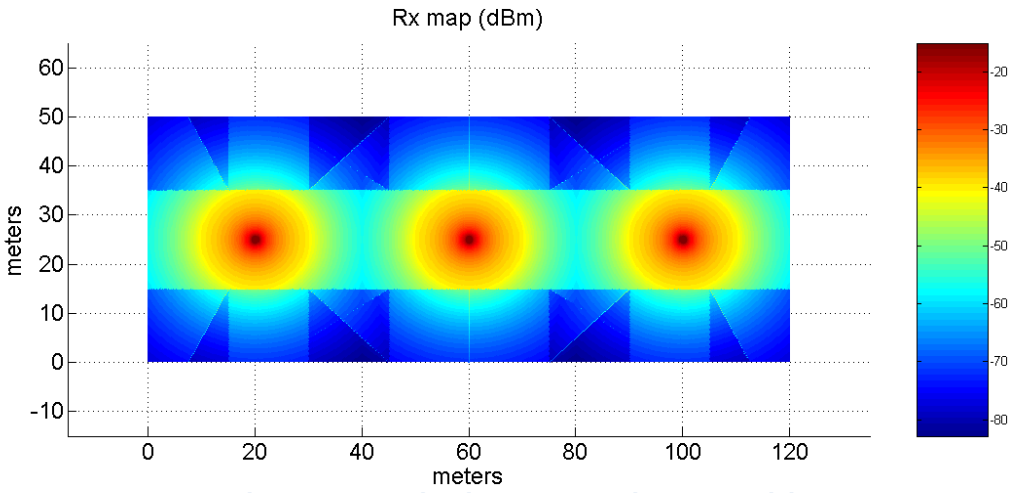

Figure 37 Received power map (2.4GHz only)

Figure 38 illustrates the coverage estimation in the layout: an area in blue is covered by an AP (i.e., the received power is above the sensitivity of -82dBm), while an area in red shows that no Wi-Fi access is possible in the 2.4GHz band. Without any idle algorithm, the outage areas are quite small and perfectly identified in the geometry. Since no shadowing is modelled, only the geographical elements are considered for the path-loss computation. Such map indicates that with our deployment, any STA in

the layout can most likely detect the presence of an AP in the 2.4GHz band, thus, be able to access the service.

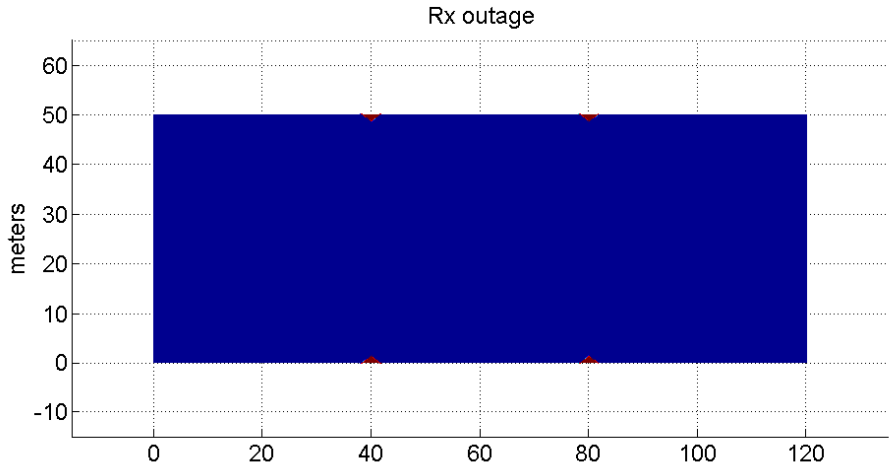

Figure 38 Outage map (red area, 2.4GHz)

We re-run the same simulations but with the idle algorithm enabled for all AP. The idea is to be able to evaluate the loss in coverage when the idle mode consists of using entering a SISO configuration instead of a MIMO one, meaning in our setup a division of the transmit power by a factor 2. Figure 39 shows the received power map in the 2.4GHz band and compared to Figure 37, we measure an expected reduction of 3dB which will be translated to the EMF exposure.

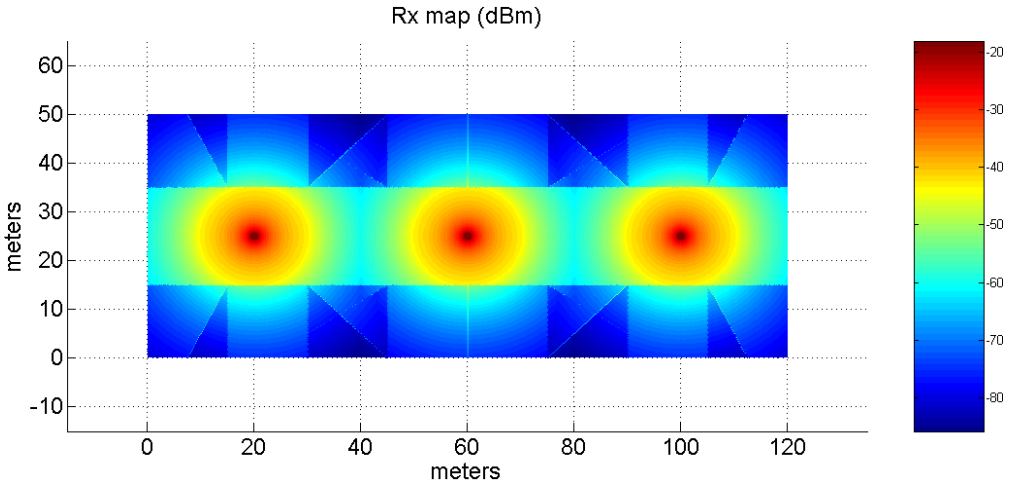

Figure 39 Received power map with all APs running in SISO idle mode (2.4GHz only)

Figure 40 shows in red the outage areas, which are places where no coverage can be provided. Compared to the previous case, the idle mode clearly has an impact on the coverage by increasing the areas where a STA cannot correctly detect an AP. The idea of the idle mode described in Figure 32 is that once a STA detects an AP and requests an association, the AP will exit the idle mode. Since the outage area is increased, we may have cases where the STA will not be able to detect any AP in idle mode and it will have to move to a coverage area while it would have been able to connect without moving in the normal case.

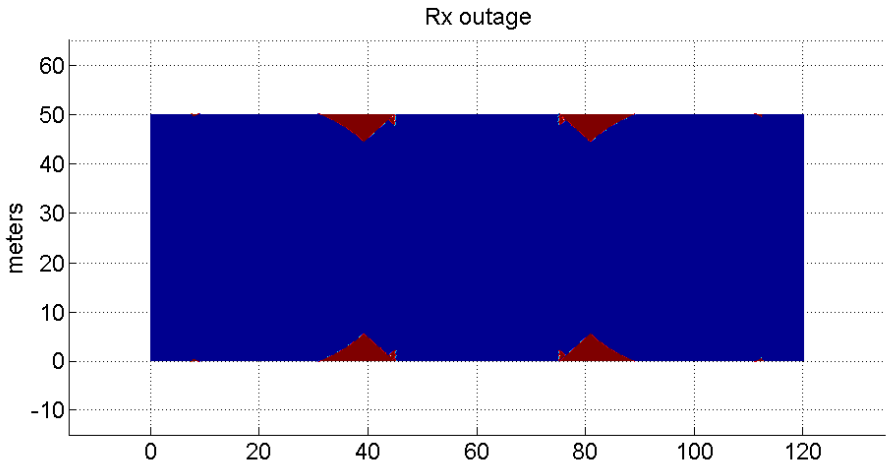

Figure 40 Outage map with all APs running in SISO idle mode (red area, 2.4GHz)

However, despite an increase of the outage area, this zone remains quite constrained. Indeed, the outage area is equal to only 2.67% of the total area when all APs enter in idle mode (0.2% without idle mode).

The parameters of the idle mode (or degraded state) will be refined in the next studies. So far, it was only consisting in switching off one RF chain leading to a SISO configuration, without balancing the transmit power. This means that in our case, the transmitted power is basically divided by two. Therefore, $\mathrm{PTX}_{\mathrm{partial}}(\mathrm{w\ LEX}) = 0.5\mathrm{PTX}_{\mathrm{partial}}(\mathrm{wo\ LEX})$ leading to a -50% reduction ($\mathrm{Ratio}_{\mathrm{EI}}(\%) = -50\%$). This value needs to be correlated to the time duration when the idle mode is engaged and which will be studied as a next step.

2.6.2.4 Future work

The previous evaluations have also assumed that all APs enter in idle mode for a worst case scenario evaluation over the whole layout. With addition of explicit stations drop and the exploitation of the mesh capabilities, smarter policies could be deployed to trigger the idle mode, including AP-AP cooperation.

As a future work, we will implement the shadowing and the station drop model to be able to run more advanced Monte-Carlo simulations and gather more precise statistics (such as supported throughput, …) when idle mode is triggered or not. As mentioned previously, we will also refine our idle mode triggers and take benefit from the mesh network availability.

In terms of modelling, we may also consider the channel model being currently discussed in the IEEE community [43]. Those channels are usually optimistic in terms of propagation.

Finally, we are going to develop the dynamic part of the system-level simulator, which means the ability to analyse idle algorithms with ongoing stations/traffics for instance, instead of relying only on static parameters (coverage …)..

3 PERFORMANCE EVALUATION OF LOW EXPOSURE RADIO TECHNIQUES

3.1 Enhanced efficiency in reference symbols usage

3.1.1 The Concept Overview

The evolution of the wireless networks such as the LTE-A constantly involves increasing data throughput to meet the ever-increasing traffic demand, and at the same time aims for reduction of transmission power for green and low EMF radios. Among a number of reference symbols (RS) in the LTE systems, such as the common reference symbol (CRS), demodulation reference signals (DMRS), channel state information (CSI) RSs. The solution we envisaged is to reduce the "transmission overhead" for a specific amount of data, therefore to reduce to the overall data transmission time. The reduction of RSs may be commonly perceived as associated with the loss of performance and therefore it is necessary to find some specific scenarios such as the small cells environment so that such losses are negligible.

3.1.2 Evaluation methodology

Previously, within the context of WP4, a definition to the EI is developed to help better interpret the context of how radio transmission techniques will impact the value of the EI. The EI is therefore defined as follows with the inclusion of the total number of periods, individuals, locations and radio access technologies (RATs), as in equation (1.1).

The impact of the more efficient reference symbol usage on EI is mainly reflected through the reduction of downlink transmission time, $t_{i,j,k}^{\mathrm{DL}}$ in equation (1.1). Such reduction in transmission time can be possible when more data OFDM symbols, in the form of a Resource Element in LTE, can be conveyed per LTE DL frame (with duration of 10ms) or sub-frame (with duration of 1ms). In order to allow for more data RE in a frame, some of the non-data related REs will need to be removed and then replaced with data REs. As mentioned previously in [1], the non-data REs investigated in this study is the DMRS and CRS. If designed properly, a new DMRS/CRS pattern will allow a reduced number of DMRS and CRS RE to be used a LTE frame and cause no apparent QoS loss.

There are two approaches to evaluate the effectiveness of the proposal. The first on is on the basis of theoretical/numerical analysis, and by counting the number of REs of a LTE system's resource block (RB) being made available by using a newly designed RS patterns. With consideration to REs occupied by other RSs and control signalling employed in a LTE system, comparisons in number of data REs available per sub-frame with or without the new RS pattern can be carried out. Subsequently, assuming the amount of data OFDM symbols for the transmission remain the same, a transmission time reduction can then be calculated.

The second approach is through a simulation justification. This is a phase of evaluation that has been developed intensively and has generated a number of preliminary results. However these results in the 2nd phase evaluation is not included in this deliverable as some calibration of the simulator itself is currently been carried out. The following is an outline of the simulation set-up.

1. Reference Measurement Channel (RMC) - 3GPP 36.101 Compatible[13];
2. Transmission simulated using extended pedestrian propagation channel model.
3. Channel noise is added to the received waveform which is then OFDM demodulated, resulting in a received resource grid
4. Calculate average frame throughput on various transmission configuration
5. Channel estimation is performed to determine the channel between the transmit/receive antenna pairs.
6. The PDSCH (Physical Downlink Shared Channel) data is then extracted and decoded from the received resource grid.
7. Using the result of the block CRC the throughput performance of the transmit/receive chain is determined.

The solution “Enhanced Efficiency in Reference Symbol Usage” is applicable to LTE DL and mainly designed for the Mean Tx duration reduction (see Table 1 and Table 3).

3.1.2.1 Sub-scenario description

The solution of “Enhanced Efficiency in Reference Symbol Usage” is envisaged to be mainly applicable to the scenario of “small cell” and to some extent also for the “Macro cell”.

Table 19 Sub-Scenario Description

Inputs	Description	Values (or range)	Reference
Environment	Spatial deployment, such as the inter-site distance (ISD)	250 meters radius for the Macro Cell	[14]
EU or source density	EMF sources number	90 active UEs in the MC	[14]
	Antenna gain	27 SC BS (9/MC sector)	[14]
	Max. Tx Power at MC	46 dBm (13 dBi ant. gain)	[14]
	Max. Tx Power at SC	30 dBm (5 dBi ant. gain)	[14]
Frequency	Central frequency (bandwidth)	800 MHz (5 MHz) 2 GHz (10 MHz)	[14]
Signal duration	Typical duration (duty cycle)	LTE Frame:10us	[14]

Traffic load	Throughput (low, medium, high)	Medium to high (UL:0.1-1 Mbps)	[14]
Path loss model, indoor/outdoor	Fast fading model Shadowing model Directional model	Winner phase 2 Winner phase 2 Winner phase 2	[15]
Protocols	Any process managing Ptx, transmit duration or SAR	-Association: Best SINR+CRE* (CRE={0,3,6}) -Uplink Power Control -retransmission	[14]

3.1.2.2 Exposure and QoS metrics identification

Exposure and QoS metrics for the considered solution are given in Table 3.

3.1.2.3 EI ratio evaluation (or Capacity/QoS improvements converting into EI reduction)

In this section, details of the numerical analysis will be given. As previously introduced in [1], a new DMRS pattern will be designed to reuse part of the CRS REs. There are several ways of configuring the new DMRS patterns.

It is assumed in the small cell environment that, from the REs that may be reserved for the configuration of 4 CRS ports, a significant amount of these REs can be saved from being used by CRS, and instead to be used by the transmission of the DMRS. This is because the configuration of CRS does not always need to cover four antenna ports (In LTE, one antenna port correspond to one radio channel) is in the small cells environment. This is as with small cells, it is likely that the channel conditions between the antenna ports may exhibit strong correlation, due to the fact that the antennas are closed placed together and exhibits very similar fading patterns. The layer 1 transmission is likely to be always or at least frequently used with high order modulation such as the 256 QAM.

Now we refer to (1.3), replacing KPI_{partial} with t_{partial} in (1.3), we get the formula as:

$$\text{Ratio}_{\text{EI}}(\%) = \frac{t_{\text{partial}}(\text{w LEX}) - t_{\text{partial}}(\text{wo LEX})}{t_{\text{partial}}(\text{wo LEX})} \times 100 \qquad (3.1)$$

where $\text{EI}_{\text{partial}}$ is the Exposure Index for a specific sub-scenario, t_{partial} is the identified metric (time reduction) among the three details in section 1.2. The subscript ‘w LEX’ correspond to the LEXNET solution implementation, and the subscript ‘wo LEX’ correspond to the SotA or baseline (without the solution implementation).

The arrangement of reusing the CRS resources for the new DMRS pattern will offer ample possibilities for the configuration of the new DMRS pattern. Depending on the number of cells will be considered for DMRS multiplexing, and the number of DMRS

REs desired in a RB, there are a number of possibilities available for the configuration of the new DMRS, which will be introduced as following.

Starting from the 2 CRS ports configuration case, the antenna port 0 will remain to be used by CRS, which is essential to maintain backward capability. Then the remaining antenna port 1 will be used by the DMRS as drawn in Figure 41. The shaded "R_0" is the CRS port 0 and the shaded "D_0" is the first DMRS port.

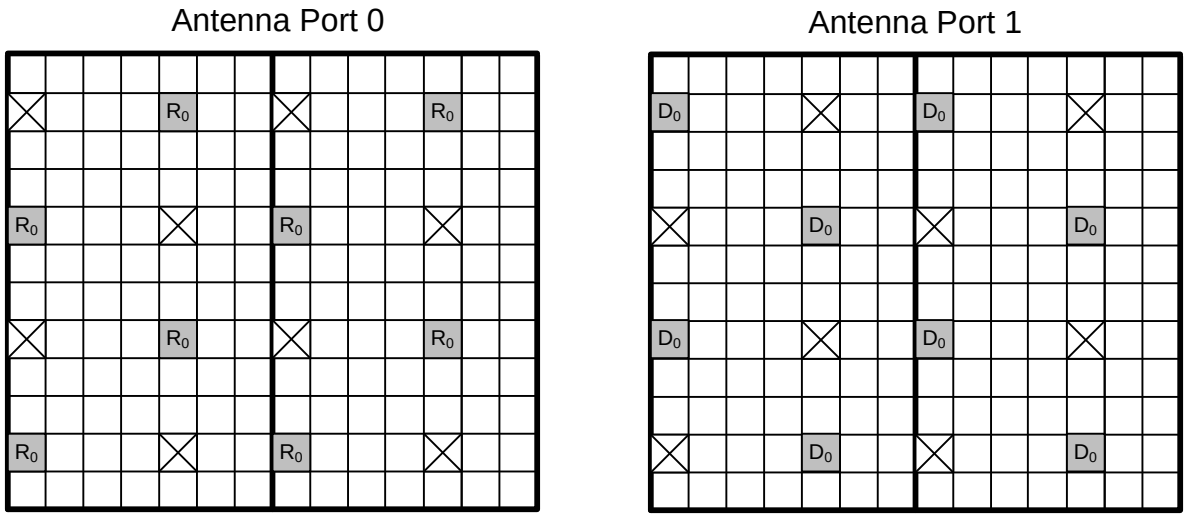

Figure 41: Antenna Port 1 configured for DMRS in the 2 CRS ports case

During the case of 4 CRS ports being available, similar to the 2 CRS ports case, the configuration of Antenna Port 0 CRS is essential to be reserved, and assuming only 1 CRS port is required, the other 3 CRS ports REs can be configured as DMRS. If assuming 4 REs required for rank 1 DMRS in two of the neighbouring cells and 2 REs required for the rest of cells, the re-used REs from CRS port 1-3 will be to able host 6 orthogonal new DMRS patterns, as depicted in Figure 42.

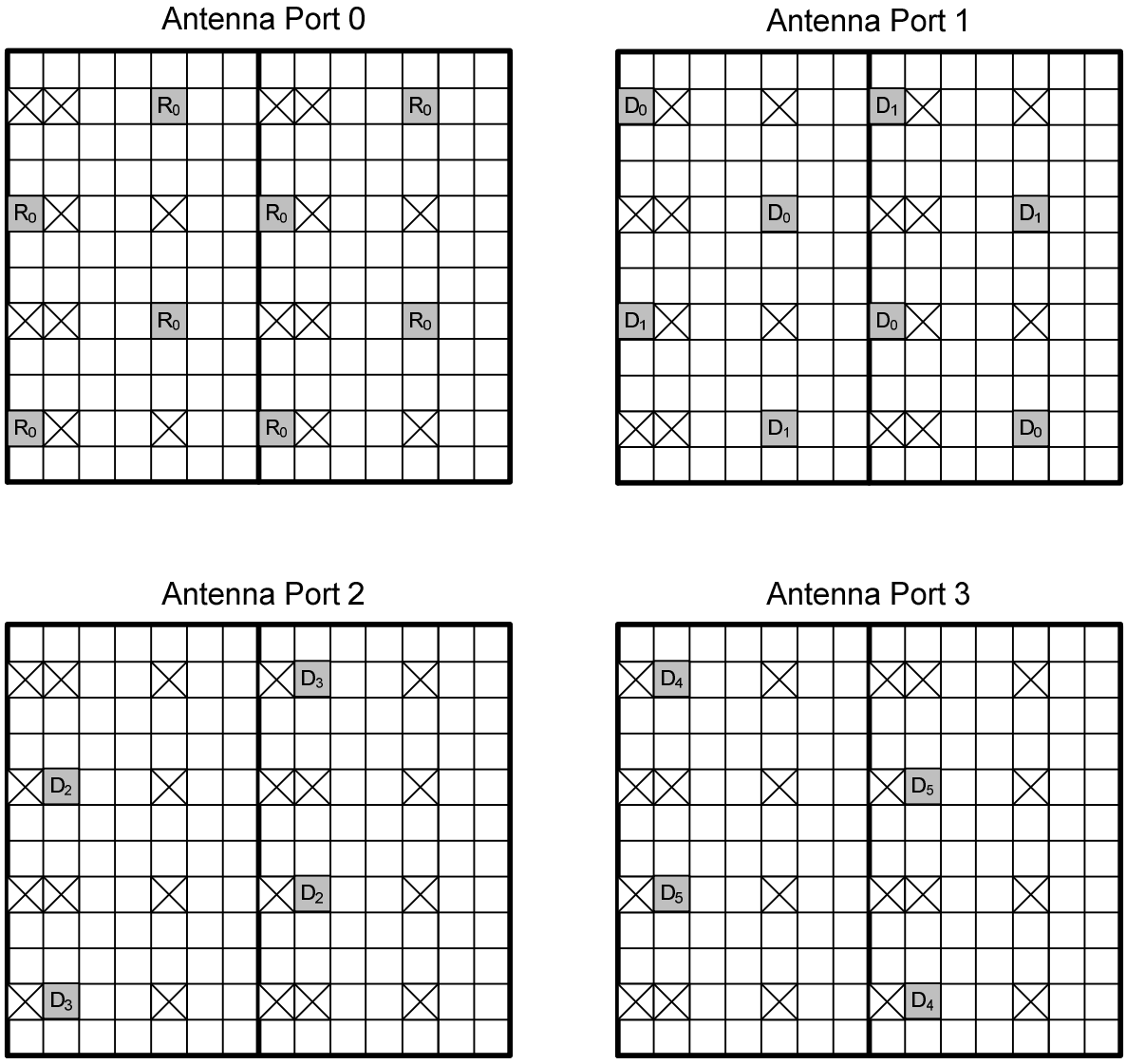

Figure 42 DMRS configured on 3 CRS antenna ports in the 4 CRS ports case in LTE RBs

This is only an example of the possible configuration of the DMRS use of the CRS ports. Depending the scenario, there may be more or less REs required for a reduced DMRS pattern in a cell therefore the total number of REs saved from the CRS ports 1 – 3 will be able to host the orthogonal new DMRS pattern for a different number of cells, depending on configuration. In the any of the configurations, to ensure a good spread of time and frequency, the DMRS REs for the same cell is likely to be located on different frequency and/or different time, but they do not have to be exactly as in Figure 43.

As in the case where 2 CRS ports are required to be configured, assuming those are the ports 0 and 1 as indicated by areas labelled "R_0" and "R_1", CRS port 2 and 3 may be reconfigured as DMRS. Figure 43 illustrates an example. In this example, both CRS port 2 and port 3 are configured for the DMRS for one spatial layer in the same cell. This configuration will boost the total DMRS energy for that cell. The shaded areas indicated by "D_0" represent these DMRS symbols.

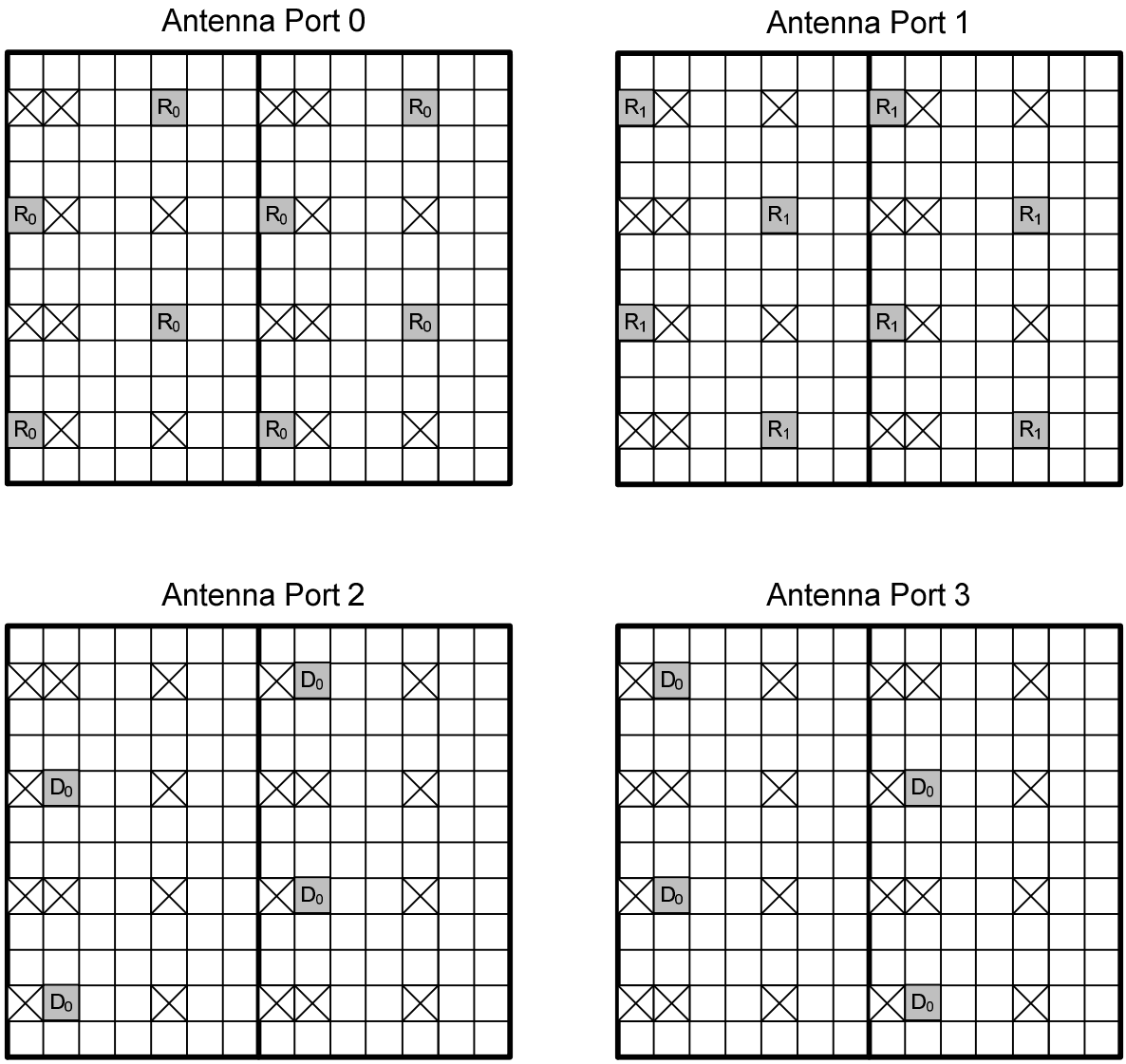

Figure 43 A new DMRS pattern configured on 2 CRS antenna ports in the 4 CRS ports case

The following is the numerical analysis on the performance improvement. Table 20 introduces the comparison between 2 cases. The 1st is the baseline case where 2 CRS ports and 1 DMRS ports are configured. The 2nd case is when 2 CRS ports are configured and a third CRS port is being used a DMRS port. The results show when comparing the peak rate, the number of REs may be available for PDSCH transmission will be increased from 128 to 136 for a pair of LTE RBs, which is a 6% increase in available resources. This translates into a 5.7% reduction in number of sub-frames required for the same amount of OFDM symbols.

Table 20 Number of REs Analysis on Proposed Schemes on 2 CRS ports configuration

Comparison Items	Total Number. of REs in a pair of LTE RB(normal CP)	Taken by CRS	Taken by Rel 9 DMRS	Taken by control channel (PDCCH)	Taken by CRS used for new DMRS	Remaining REs possible for PDSCH transmission
2CRS ports + 1 DMRS port	168	16	12	12	0	128
2 CRS port + 1 CRS port used for new DMRS	168	16	0	12	4	136

Table 21 compares two configurations. The first is the baseline case where all 4 CRS ports plus 1 DMRS ports are configured. The second case is when a reduced DMRS pattern is applied and thus result in 3 CRS ports configured and the 4th CRS port is used by the new DMRS pattern. When comparing the peak average data rate, the number of REs may be available for PDSCH transmission will be increased from 120 to 132 for a pair of LTE RBs, which is a 10% increase in available resources. This translates into a 9.1% reduction in number of sub-frames required for the same amount of data symbols.

Table 21 Number of REs Analysis on Proposed Schemes on 4 CRS ports configuration

Comparison Items	Total Number. of REs in a pair of LTE RB(normal CP)	Taken by CRS	Taken by Rel 9 DMRS	Taken by control channel (PDCCH)	Taken by CRS used for new DMRS	Remaining REs possible for PDSCH transmission
4CRS ports + 1 DMRS port	168	24	12	12	0	120
3CRS port + 1 CRS port used for new DMRS	168	20	0	12	4	132

The above two cases are the examples where the transmission time for a fixed amount of data can be achieved by using a more efficient RS design, under radio conditions which allow the new pattern to be deployed.

3.1.2.4 Global EI reduction assessment

To evaluate the effectiveness of developed technique, it is crucial to understand the conditions where the technique is applicable, i.e., under what percentage of time and for what percentage of traffic the reduced reference symbol patterns can be used. On the other hand, the loss of performance incurred from increased channel estimation error from the reduced use of CRS will be investigated, in order to understand trade-off.

3.2 Interference mitigation in Zigbee & WiFi

3.2.1 Remind on the concept

We consider interactions between Wi-Fi traffic and 802.15.4 (WSN) traffic. Since they operate in the same frequency band, these two RATs interfere with one another. WiFi is not traditionally considered to be affected by WSN traffic, because of great differences in transmission power. This is disproved both by previously referenced state of the art and by the following tests. Interference between these two technologies causes loss of packets (decrease of Packet Reception Rate – PRR). We argue that this decrease in PRR can be seen either as a decrease in QoS with unnecessary EI increase or as an increase in EI in an effort to maintain QoS. The former can be seen in a UDP-like stream where lost packets are not retransmitted, while the latter can be seen in TCP (Transmission Control Protocol) traffic, where lost packets have to be retransmitted, causing an increase in EI. Our goal is to detect the PRR decrease both in Wi-Fi networks and in WSN networks, to quantify it in terms of EI and then to find methods to maintain a high PRR even in high traffic conditions for both Wi-Fi and WSN networks.

3.2.2 Evaluation methodology

A series of tests were conducted to assess the degree of interference between Wi-Fi and ZigBee networks. These tests show several characteristics concerning the quality and quantity of interference between the two types of networks. Packet Reception Rate (PRR) can be reduced in both networks in some conditions. PRR could also be reduced to 0 in some tests. The key points are:

- Wi-Fi can be seen backing-off after "silent" collisions;
- WSNs can detect most Wi-Fi traffic when on a close channel, selectively less when channels further away are selected:
- Wi-Fi can be brought to a halt (even losing association) with WSN frames transmitted in close proximity;
- PRR for Wi-Fi can be anywhere from 0-100%, depending on WSN configuration.

A ratio of EI versus EI without any collisions will be calculated with theoretical data, as well the data from these tests. Maintaining a calculated PRR and considering a TCP flow with retransmissions, we will calculate the benefits of eliminating interference. QoS is also significant in our study, as a TCP stream over Wi-Fi with all packets lost is an example of extreme low QoS. UDP streams over Wi-Fi with conditions favorizing low PRR will also relate to low QoS.

3.2.2.1 Sub-scenario description

“Interference Mitigation on ZigBee and Wi-Fi” targets the WiFi & WSN sub-scenario established in WP4.

The sub-scenario has the following inputs:

Table 22 Sub-Scenario Description

Inputs	Description	Values (or range)	Reference
Environment	Spatial deployment, inter-node distance	User home with installed WSN, 10m typical inter-node distance, Wi-Fi Access Point and Wi-Fi enabled device	[46], [47]
EU or source density	Antenna gain	802.15.4 device -1..3 dBi Wi-Fi 2 dBi	[48]
	Max. Tx Power	WSN 2 mW Wi-Fi max 93mW	[48]
Frequency	Central frequency (bandwidth)	WSN 2.4 GHz (80 MHz) Wi-Fi 2.4GHz (20 MHz)	[46], [50]
Signal duration	Typical duration (duty cycle)	WSN 1-6% Wi-Fi varies with traffic	[46], [50]
Traffic load	Throughput (low, medium, high)	WSN Low Wi-Fi Medium to High (2-54Mbps)	[46], [50]
Protocols	Communication stack	IEEE 802.15.4 compatible IEEE 802.11g	[46], [50]

3.2.2.2 *Exposure and QoSmetrics identification*

Exposure KPI for Interference management is mean Tx duration, or duration of exposure ($t_{i,j,k}^{\mathrm{UL}}$). Reducing interference will reduce the number of retransmissions necessary to maintain a level of QoS (e.g. TCP retransmitting lost packets over WiFi), which in turn means less duration of exposure from the user. For exposure, mean transmitter power is considered a secondary KPI for the case in which transmitted power can be safely reduced (i.e. not affecting QoS adversely) to reduce interference between Wi-Fi and ZigBee. QoS KPI is identified as PRR (Packet Reception Rate).

3.2.2.3 *EI ratio evaluation (or Capacity/QoS improvements converting into EI reduction)*

EI improvements will be calculated with respect to the modification of the time spent transmitting. In the case of UDP (User Datagram Protocol) packets, the time spent transmitting is proportional to the number of packets sent, we will use PRR as a metric.

$$PRR = \frac{Nr_{packets} - Nr_{lost}}{Nr_{packets}} \tag{3.2}$$

Assuming an environment which attempts to preserve QoS:

$NR_{lost,0} = Nr_{packets}(1 - PRR)$ and $NR_{retransmissions,0} = Nr_{lost,0}$, where $NR_{lost,0}$is the number of packets lost and $NR_{retransmissions,0}$ is the number of packets initially retransmitted. Because these are also subject to a fractional PRR, some of the packets that have been retransmitted once will require another retransmission:

$$Nr_{retransmissions,1} = Nr_{retransmissions,0}(1 - PRR)$$

The total number of retransmissions will be:

$$\begin{aligned} \mathrm{Nr}_{\mathrm{retransmissions,total}} &= \sum_{\mathrm{i=0}}^{\mathrm{n}} \mathrm{Nr}_{\mathrm{retransmissions,i}} = \mathrm{Nr}_{\mathrm{packets}} \sum_{\mathrm{i=0}}^{\mathrm{n}} (1-\mathrm{PRR})^{\mathrm{i}} \\ &= \mathrm{Nr}_{\mathrm{packets}} \frac{1-(1-\mathrm{PRR})^{\mathrm{n+1}}}{1-(1-\mathrm{PRR})} \sim \frac{\mathrm{Nr}_{\mathrm{packets}}}{\mathrm{PRR}} \end{aligned} \quad (3.3)$$

The transmission time is directly proportional to the number of packets, which will now be $\frac{Nr_{packets}}{PRR}$.

$$Ratio_{EI}[\%] = \frac{EI_{\text{int erference}} - EI_{IM}}{EI_{\text{int erference}}} \times 100 = \frac{t_{transmission,\text{int erference}} - t_{transmission,IM}}{t_{transmission,\text{int erference}}} \times 100$$

$$= \frac{\frac{Nr_{packets}}{PRR_{interference}} - \frac{Nr_{packets}}{PRR_{IM}}}{\frac{Nr_{packets}}{PRR_{interference}}} \times 100 = \frac{PRR_{IM} - PRR_{interference}}{PRR_{interference}} \times 100 \quad (3.4)$$

where …

PRR_{IM} denotes PRR when using Interference Mitigation module.

$PRR_{interference}$ denotes PRR under interference conditions.

$t_{transmissions,interference}$ is the time needed to transmit Nr packets under interference.

$t_{transmissions,IM}$ is the time needed for Nr packets when using IM.

Tests show a PRR of 0.1 to 0.9 for WSN (ZigBee) nodes, which would lead to 10-90% EI reduction. For Wi-Fi, common PRRs of 0.4 to 0.9 lead to 10-60% EI reduction with the Interference Mitigation module.

There are also cases in which PRR is effectively zero, due to the networks interfering. In this case, while IM does not offer direct EI improvements, there are substantial QoS benefits from using Interference Mitigation

Interference between ZigBee and WiFi depends heavily on relative positioning, transmit power for both RATs and on transmission environment. Due to these factors interference is asymmetrical, so we can expect any range of values for PRR for the two networks, independent of each other. This covers a lot of possible cases:

- Wireless Sensor Networks on ZigBee cannot talk to each other due to interference, but Wi-Fi networks are unaffected;
- ZigBee networks affecting Wi-Fi traffic without being affected themselves (less likely, yet still possible);
- Both types of networks being affected, down to 0 PRR each;

- No network is affected (PRR=1 for both networks).

Table 23 EI reduction with theoretical PRRs

EI Reduction (%)		PRR_{WiFi}				
		0	0.25	0.5	0.75	1
PRR_{WSN}	0	100% WiFi 100% WSN	75% WiFi 100% WSN	50% WiFi 100% WSN	25% WiFi 100% WSN	100% WSN
	0.25	100% WiFi 75%WSN	75% WiFi 75% WSN	50% WiFi 75% WSN	25% WiFi 75% WSN	0
	0.5	100% WiFi 50% WSN	75% WiFi 50% WSN	50% WiFi 50% WSN	25% WiFi 50% WSN	0
	0.75	100% WiFi 25% WSN	75% WiFi 25% WSN	50% WiFi 33% WSN	25% WiFi 25% WSN	0
	1	100% WiFi	75% WiFi	50% WiFi	33% WiFi	0

We will now describe our test-bed for measuring interference. We will begin by describing the test scenario, since this is vital to the study. Not all scenarios will produce interference. Our test-bed includes Sparrow v3.2 nodes, shown in Figure 44, and commodity hardware with Wi-Fi transmission capabilities [52].

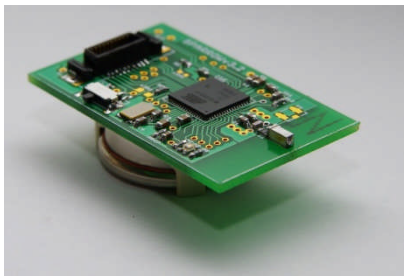

Figure 44 our test-bed consists of these Sparrow v3 nodes

In the case of interference, it is very important to take into consideration the fact that certain scenarios will be more affected than others. There is an asymmetric radio link between a WiFi device and a WSN node, caused by the fact that there is at least an order of magnitude more transmission power (at least) in a Wi-Fi device. Wi-Fi access points will have variable transmission power, from 1 to 10 dBm or more, while WSN nodes may have only up to 3.5 dBm (such as the ones we use in our test-bed).

This means that there is a distance between a Wi-Fi device A and a WSN node B where B detects an occupied channel when A is transmitting but A can never detect when B transmits. This means that there are a lot of scenarios in which Wi-Fi devices will hinder the transmission of packets in the WSN network but will not detect this

fact. WSNs can also interfere with WSN traffic when the opposite is true: A and B are close, Wi-Fi device A can detect that B is transmitting and its SNR is close to the SNR coming from its Wi-Fi peers. In this case interference that affects both networks becomes possible, and this is the type of scenario of most interest to this study.

Another condition for interference is one of duty-cycle and actual traffic. Many WSN protocols are based on periodic data updates which generate only a few bytes of traffic on every period, which is typically a few seconds long. In this case interference is less probable since transmissions are less likely to align in the time domain.

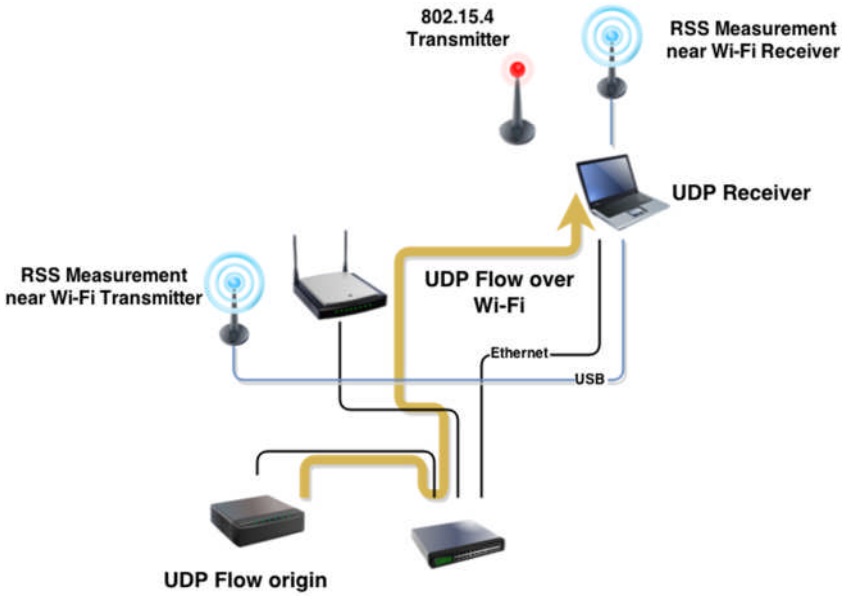

Figure 45: Testbed arrangement for RSS (Received Signal Strength) measurements of Wi-Fi traffic

The real-life scenario where these conditions are met can be the following: A person is fit with a Body Sensor Network, a network of WSN nodes close to the body that transmit different parameters. This is mapped within the Wi-Fi & WSN sub-scenario. If there are health parameters present, WSN nodes may transmit several packets per second. For example, if we consider measuring a heart rate signal at 50Hz and 32 bytes per packet WSNs would have 6% channel occupation at a standard bit rate of 250 kbps. A high rate of channel occupancy greatly increases the chances of collisions. The user also has a smartphone with a Wi-Fi connection with a Wi-Fi AP that is further away. In this scenario, having the AP further away means that WSN packets have the same SNR ratio as Wi-Fi packets, which will cause interference on both sides as mentioned.

The test scenario for our experiment is loosely based on the real-life scenario described previously, and can be observed in Figure 45. It is composed of a laptop, a Wi-Fi AP and an embedded network device capable of generating a UDP stream of data. The embedded device generates a stream of fixed-length UDP packets that have to arrive to the laptop over the wireless interface. UDP was chosen because it's easier to calculate how many packets were lost. UDP packets can either be lost by being dropped by a router or lost due to a collision.

Instead of positioning the Wi-Fi Access Point further away from the laptop, we chose to decrease its transmission power instead to 7mW, due to space constraints. The effect is equivalent to having a more powerful transmitter further away. The important condition is that that the Wi-Fi Access Point does not detect any WSN transmission, and this will be apparent in the results section.

The parameters of the experiment are the following:

- Wi-Fi:
  - Transmitter power 7mW
  - Bandwidth: Automatic, defaults to 54Mbps
  - Channel 1 – 2.412MHz
  - Transmitter-Receiver distance: 2m
- WSN:
  - Transmitter power 2.23mW
  - RSS sampling speed 200kHz, limited by serial connection (radio samples at 500kHz)
  - Channel 11 – 2.405MHz

The scenario consists of sending fixed-length UDP packets (1000 bytes long) over Wi-Fi and determining on the receiving end how many packets were lost. We generated graphs with 3 data sets: The number of packets lost, deduced from a sequence number assigned at an application level in the UDP packets, the RSS indicator measured by the WSN node near the laptop (receiver) and near the Wi-Fi AP (transmitter). These are provided for reference in IR4.2. An excerpt is shown in Figure 46 and Figure 47. In Figure 46, Wi-Fi traffic can be seen from the left (green bars close together), high-throughput transfer is stopped once a WSN node is placed near the receiver, denying correct transmission of ACK packets. We have tested several of the asymmetric interference cases, and all can be shown to be possible in certain circumstances of transmitter positions and strengths.

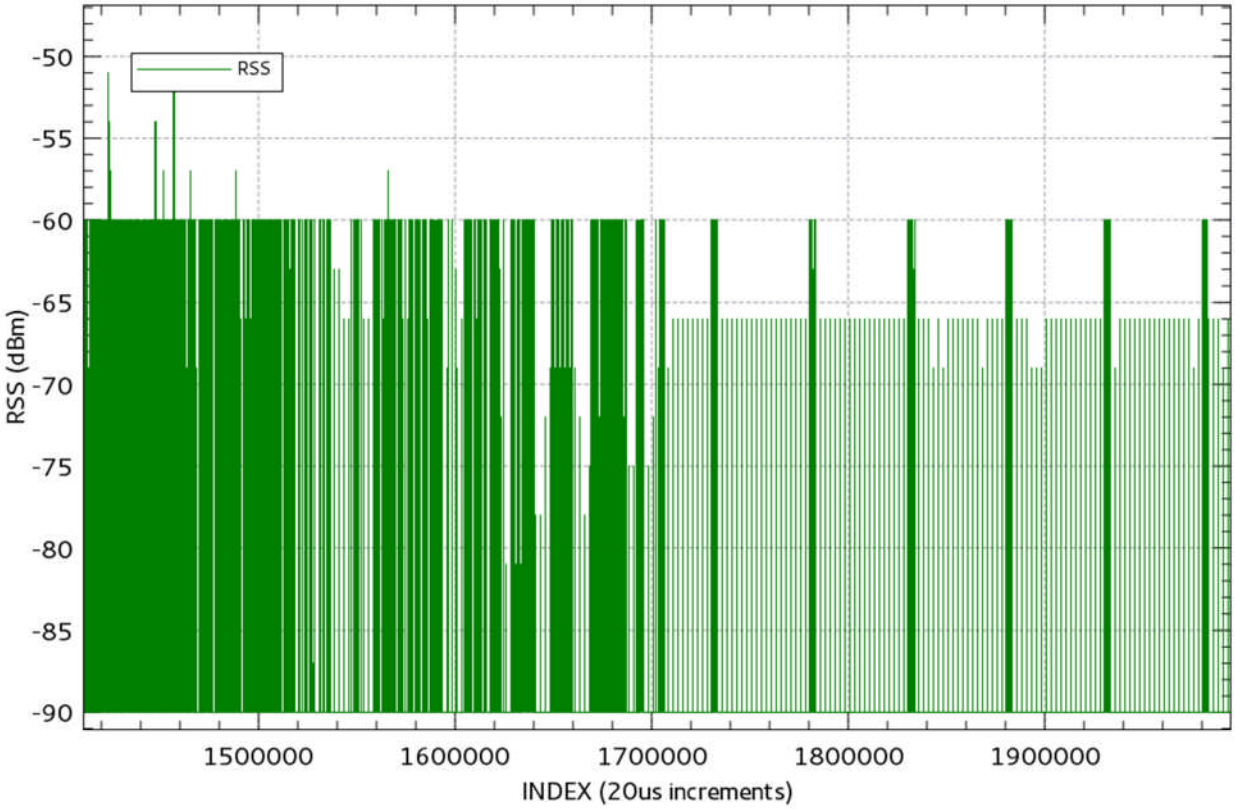

Figure 46 Moment of interference between ZigBee and Wi-Fi

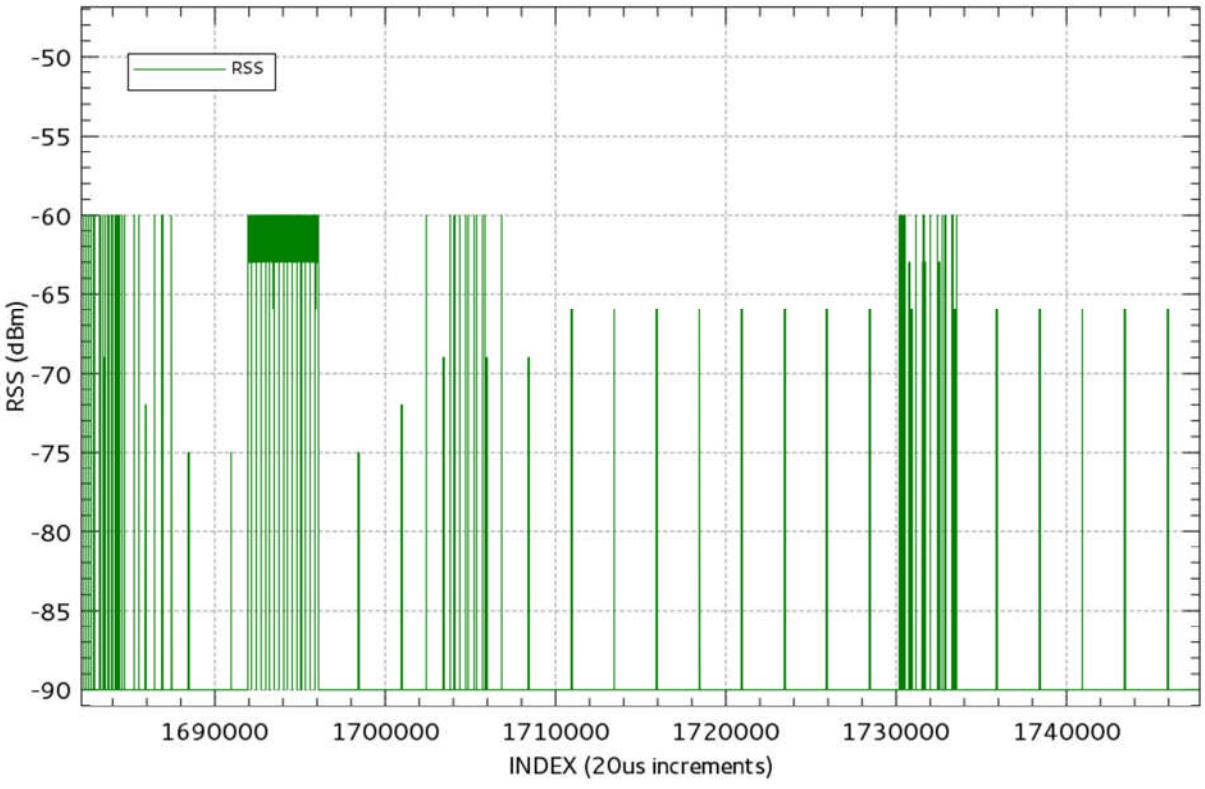

Figure 47 The same sequence with a higher resolution timescale show individual Wi-Fi packets failing and the router backing off, slowing down throughput.

3.2.2.4 Global EI reduction assessment

To assess the global EI reduction given by this solution, we require weighting coefficient to apply to the EI reduction calculation, which takes into account daily (24h) usage patterns, number of users concerned etc. This weighting coefficient will be evaluated in WP2. For this section, a weighting coefficient is required both for ZigBee traffic and for Wi-Fi traffic.

3.3 Radio link allocation in WSNs

3.3.1 Remind on the concept

Typical deployments of wireless sensor networks in a Smart Home application exhibit special communication patterns that differentiate them from normal data-carrying wireless networks. An important difference between WSNs and data-carrying wireless networks is that most WSN applications use a single-sink model where data is gathered from a multitude of sensor nodes and must be sent to a special node called the sink (or coordinator). In this model, transmission is usually done in a tree fashion with intermediate nodes gathering data from leafs and forwarding it towards the sink [47]. Another difference between WSNs and traditional networks is that, in most WSN applications, delays in data transmission are tolerated.

Considering that real-time delivery of data is not critical in most WSN scenarios we can schedule node transmissions at appropriate times, by locally buffering data, in order to reduce user exposure to EMF radiation. This can be achieved for example by limiting the transmit power of sensor nodes to a single room and scheduling data transmission when no users are detected in the room, using presence sensors or static and/or dynamic schedules.

3.3.2 Evaluation methodology

Assessing the impact of the proposed solution on the EI requires determining the average received power. This can be done by measuring the power at which a node's transceiver is transmitting and the time it is in the transmit state. These metrics must be correlated with the time of day at which the transmission occurred and its location. Using this data an EI can be derived based on the formulas developed by WP2.

A QoS metric that must be maintained by the solution is to have an equivalent PRR with the baseline network stack. At a high level this mean that an environment monitoring application running on top of the improved network stack can transmit the same number of environment data updates to the central server in a given time interval (e.g. 24h) as the baseline. The EI will be improved though because the proposed solution will buffer and schedule packet transmission at appropriate times to reduce user exposure.

3.3.2.1 Sub-scenario description

"Radio link allocation in WSNs" targets the WiFi & WSN sub-scenario established in WP4.

Specifically, it considers an indoor deployment of a WSN that is used for environment monitoring inside an office building or a smart home. Multiple network nodes are distributed around a room and communicate with a gateway that is connected to a wired network node and that forwards packets from the WSN to a server. The nodes operate in the 2.4GHz ISM band and use a communication stack based on the IEEE 802.15.4 MAC layer, Table 24.

Table 24 - Sub-Scenario Description

Inputs	Description	Values (or range)	Reference
Environment	Spatial deployment, inter-node distance	Building with installed WSN, 10m typical inter-node distance	[47]
EU or source density	Antenna gain	-1..3 dBi	[51]
	Max. Tx Power	2 mW	[51]
Frequency	Central frequency (bandwidth)	2.4 GHz (80 MHz)	[52]
Signal duration	Typical duration (duty cycle)	less than 1%	[52]
Traffic load	Throughput (low, medium, high)	Low	[52]
Protocols	Communication stack	IEEE 802.15.4 compatible	[52]

3.3.2.2 Exposure and QoS metrics identification

The purpose of the proposed technique is to minimize the average received power ($P_{RX\ avg}$) to which people are exposed from an environment monitoring WSN. This network can be part of an office building's Heating, Ventilation, and Air Conditioning (HVAC) system or it can be part of a smart-home deployment. As the nodes of the network are usually placed at a distance from users, usually high on the walls of a room or on the ceiling, and because user do not directly interact with the network, we consider the nodes as being mini-base stations and use the DL parameters for EI calculations. Of the 3 main parameters defined in WP2 for the global EI formula calculation, the ones that are optimized by this technique are the Mean Tx power and Mean Tx duration (Table 3).

We use the following formula to relate the average received power ($P_{RX\ avg}$) with the Mean TX duration (t_{TX}) and Mean RX power (P_{RX}, which for the purpose of simplifying calculations we assume is related to the Mean TX power by a constant factor):

$$P_{RX\ avg} = \frac{\sum_{T\in(0h,24h)} P_{RX} \cdot t_{TX}}{T} \quad (3.5)$$

In order to evaluate the impact on QoS of the proposed technique we use PRR that takes into consideration the service requested by applications running on the WSN. The technique works by letting each application specify the delay which is acceptable for delivering sensor data to the WSN gateway. Thus, in evaluating the PRR we consider the packets that are correctly delivered to the application's server within the delay specified by each application.

3.3.2.3 EI ratio evaluation (or Capacity/QoS improvements converting into EI reduction)

Theoretical evaluation

In order to evaluate the EI reduction of the proposed technique, we consider the simplified form of the EI ratio formula, which uses the average received power ($P_{RX\ avg}$) as a KPI:

$$Ratio_{EI-link\ allocation}(\%) = \frac{P_{RX\ avg}(w\ LEX) - P_{RX\ avg}\ (wo\ LEX)}{P_{RX\ avg}\ (wo\ LEX)} \times 100 \quad (3.6)$$

Expanding the average received power for the baseline solution (without LEXNET) and considering the number of bytes transferred by the network during a day we obtain ($P_{RX\ byte}$ is the mean power received when transmitting a byte and $t_{TX\ byte}$ is the time required to transmit one byte):

$$P_{RX\ avg} = \frac{\sum_{T\in(0h,24h)}^{nr\_bytes} P_{RX\ byte} \cdot t_{TX\ byte}}{T} \quad (3.7)$$

When the network is in normal operation an environment monitoring application will transfer sensor data at a constant rate (r) using packets of a constant length (len_p). We can further assume that the transmission power of the nodes has settled to the minimum required for a successful transmission ($P_{RX\ min}$) and remains constant during the operation of the network. For a WSN deployed inside an office building, this small transmit power translates into an exposure which is limited to the occupants of each room and to almost zero exposure outside office hours. The averaged received power for the baseline solution thus becomes ($t_{TX\ packet}$ is the time required to transmit one packet of length len_p):

$$P_{RX\ avg} = \frac{\sum_{T\in(0h,24h)}^{nr_{packets}} P_{RX\ min} \cdot t_{TX\ packet}}{T} = \frac{\sum_{T\in(8h,18h)}^{nr_{packets}} P_{RX\ min} \cdot t_{TX\ packet} + \sum_{T\notin(8h,18h)}^{nr_{packets}} 0 \cdot t_{TX\ packet}}{T} = \frac{r \cdot T' \cdot P_{RX\ min} \cdot t_{TX\ packet}}{T} \quad (3.8)$$

When we expand the averaged received power for the proposed solution, part of the transmissions, depending on the available buffer size (len_B) and the delay requested by each application, will be scheduled during times of zero exposure. The average received power for the proposed solution thus becomes:

$$P_{RX\ avg} = \frac{max(0, r\cdot T' - \frac{len_B}{len_p})\cdot P_{RX\ min}\cdot t_{TX\ packet} + min(\frac{len_B}{len_p}, r\cdot T')\cdot 0\cdot t_{TX\ packet}}{T} = \frac{max(0, r\cdot T' - \frac{len_B}{len_p})\cdot P_{RX\ min}\cdot t_{TX\ packet}}{T} \quad (3.9)$$

The term $r \cdot T'$ represents the number of packets that are sent during the fraction of the time when users are exposed (T') and $\frac{len_B}{len_p}$ represents the maximum number of packets that can be buffered by one node. This result assumes that sensor nodes send data to a gateway located in each room. The delay requested by an application can be modelled by a smaller buffer size.

From the previous two equations the formula for the expected EI ratio can be summarized as:

$$Ratio_{EI-link\ allocation}(\%) = \frac{\max\left(0, r\cdot T' - \frac{len_B}{len_p}\right) - r\cdot T'}{r\cdot T'} \times 100 = -\min(1, \frac{len_B}{len_p}\cdot\frac{1}{r\cdot T'}) \times 100 \quad (3.10)$$

To calculate the potential EI reduction we consider that packets are transmitted using an IEEE802.15.4 MAC frame (with a typical overhead of 19 bytes) [52] and have a payload of 5 sensors readings and 1 timestamp each occupying 4 bytes. This gives us a total of 43 bytes per packet. We also consider an exposure of 10h/day for a typical office building. The improvement is calculated with respect to the available buffer space for scheduling (from 1KB to 64KB) and to the sensor update rates (from 0.1 to 10 packets/min), Table 25.

Table 25 - Potential EI improvement as a function of buffer size and update rate

$Ratio_{EI-link\ allocation}$ (%)		Update rate (packets/min)						
		0.1	0.2	0.5	1	2	5	10
Buffer size (bytes)	1024	-39.68	-19.84	-7.93	-3.96	-1.98	-0.79	-0.39
	2048	-79.37	-39.68	-15.87	-7.93	-3.96	-1.58	-0.79
	4096	-100	-79.37	-31.75	-15.87	-7.93	-3.17	-1.58
	8192	-100	-100	-63.50	-31.75	-15.87	-6.35	-3.17
	16384	-100	-100	-100	-63.50	-31.75	-12.70	-6.35
	32768	-100	-100	-100	-100	-63.50	-25.40	-12.70
	65536	-100	-100	-100	-100	-100	-50.80	-25.40

Practical evaluation

In order to validate the theoretical results a practical measurement of the average received power of a WSN deployment is being pursued. The simplest way to do this is to record the transmit power and the transmit time of each node for each packet.
There are multiple ways in which the transmit time ($TX_{on\ time}$) and transmit power (TX_{power}) can be measured in order to compute the relevant KPIs. The most accurate solutions required specialized RF sensing hardware, are expensive and cumbersome to deploy and cannot be easily deployed in the field.

The next paragraphs describe the methodology used by this study to derive those metrics. Even though the proposed EI improvement method is general enough for any IEEE802.15.4 compatible network stack and can be equally applied to different hardware platforms a concrete implementation based on Atmel transceivers is used to measure the necessary metrics.

A simple approach to the problem of evaluating the identified metrics is to log the number of transmitted bytes on the node and calculate the $TX_{on\ time}$ and TX_{power} based on the transceiver's characteristics. For example, on the Atmel ATmega128RFA1 and ATmega256RFR2 chips sending a byte of data requires 32us. Frame synchronization and PHY header adds an additional 192us of $TX_{on\ time}$ overhead. By logging the number of transmitted packets and bytes, the total time the transceiver was in the transmit state can be easily calculated. The other parameter required for EI evaluation, the transmit power, is also easily available as a configuration register of the transceiver. This register can be read by software and the TX_{power} at which a packet was sent can be recorded. If the network stack does not do any dynamic power adjustments, this can be done a single time, at node initialization.

This approach can be implemented as an additional exposure logging software module for the network stack that intercepts the number of packets and bytes per packet that are sent to the transceiver. However, because WSN network stacks do not generally provide a standardized interface, adding an additional software module will necessarily be stacked dependent. If we take into consideration the fact that transceiver characteristics differ from model to model, the required software module will also be transceiver dependent.

For the Atmel ATmega128RFA1 and ATmega256RFR2 [48], [49] the implementation of the exposure logging is further complicated by the fact that it provides an extended operation mode, for efficiency reasons, in which part of the MAC layer operations (frame acknowledgment and retransmission) are handled by a hardware accelerator module. Implementing the exposure logging software module for these Atmel transceivers requires re-implementing the hardware accelerated parts in software in order to correctly account for all transmitted packets (ACKs and retransmissions).
An alternative solution for implementing exposure logging in the software stack of a WSN is measuring the actual time the transceiver is in the transmit state, as opposed to indirectly determining the transmission time by measuring the number of packets and bytes sent per packet. This solution requires some sort of hardware support from the transceiver which needs to report the state of its power amplifier. The advantage

of measuring the state of the transceiver at such a low level is that no knowledge of the network stack is required and a transceiver dependent implementation is sufficient and can be used with any network stack.

The Atmel ATmega128RFA1 and ATmega256RFR2 transceivers used in a number of sensor node implementations from Dresden Elektronik (e.g. deRFmega128, deRFmega256) and the sensor platform developed at University Politehnica of Bucharest (Sparrow v3.2) provide a hardware feature for connecting an external RF front-end [48], [49]. This feature includes 2 digital pins (DIG3 and DIG4), for connecting an external power amplifier, that are activated whenever the transceiver is transmitting data. The architecture of Atmel microcontrollers allows reading of external pins even when they are controlled by other peripheries (i.e. transceiver) thus providing a way of sampling the state of the transceiver at a very low level.
The proposed evaluation method is to measure the time a sensor node's transceiver is in the transmit state together with the power setting of the transceiver. This is done on the previously mentioned hardware. A software module running alongside the measured network stack is periodically sampling the external power amplifier pins to determine the time the transceiver is transmitting and logging the data together with the power setting of the transceiver.

An important characteristic of the evaluation method is the tradeoff between accuracy and sampling period. Because the state of the transceiver is sampled and the transmission time is derived from the time difference of the transmitter activation and deactivation a high sampling frequency is desired for high accuracy. A high sampling frequency will however consume more CPU time and interfere with the normal functioning of the measured network stack. Considering that the transceivers transmit with the IEEE 802.15.4 compliant data rate of 250kbps transmission time for each packet will be a multiple of 32us, thus a sampling period of 32us was chosen in order to accurately account the time required for each packet.
Instructions are available for executing both the sampling code and the normal network stack operation. In these circumstances a few optimizations are required for the exposure measuring software module. The first of these is that transmission times and power are accumulated over a period of time and logged to an external device less often than packets are transmitted (1 sec in the current implementation). A second optimization is represented by reducing the number of instructions in the sampling code (the part of code run every 32us) to a minimum. In the current implementation this is achieved by writing the relevant portion of code in AVR assembly language. The proposed evaluation method was used to measure the metrics of a baseline scenario comprised of 3 transmitting nodes and a gateway all based on the Atmel ATmega128RFA1 and ATmega256RFR2 microcontroller/transceiver combination. The scenario used the Dresden Elektronik multihop network stack, which is based on the Atmel IEEE 802.15.4 compliant MAC implementation. The three nodes were configured as one router and two end nodes, simulating a small home environment monitoring application, measuring temperature and brightness at every 10 seconds and forwarding the data to a PC connected to the gateway. One of the end nodes (*E2*) was connected to the network via de router (*R*), while the other node (*E1*) was directly connected to the gateway. As the network stack does not support dynamic TX power management, during the experiment the transmission power of all nodes was constant at a value of 3.5dBm.

Figure 48 presents an average transmitter duty cycle, calculated as the ratio between $TX_{on\ time}$ is active *vs* time of the measured period at different times of day, for the 3 nodes in the baseline scenario. As expected, the router node *R* has a double duty cycle compared to the other nodes, as it must also transmit the messages received from node *E2*. The graph also shows an increase in the duty cycle during some hours of daytime, caused by more packet retransmissions attributed to an increase in LoS obstruction between end nodes and router/gateway.

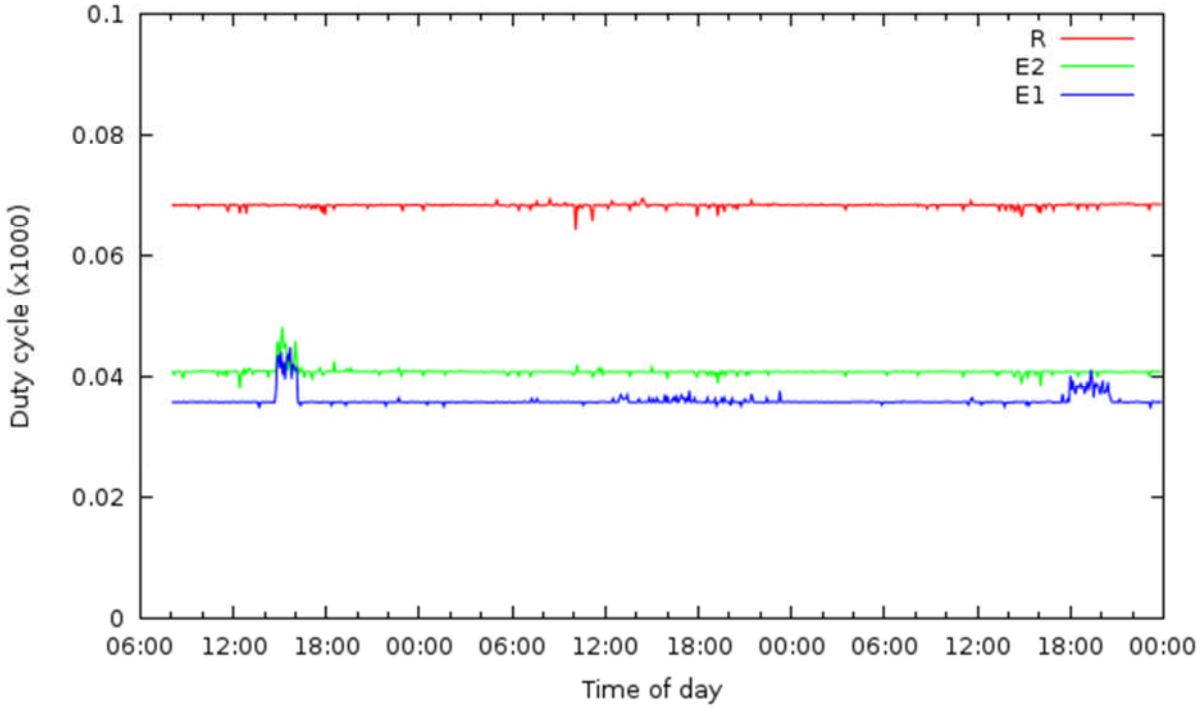

Figure 48 - Transmitter duty cycle in baseline scenario

Figure 49 presents how transmission scheduling can shift a node's transmission to a later time compared to the baseline scenario. In this graph node *E2* was configured to delay its transmission from night time to day time. If *E2* is a node deployed to monitor the environment parameters in the bedroom of a smart home, this can effectively reduce exposure by avoiding the transmission of packets in the presence of users.

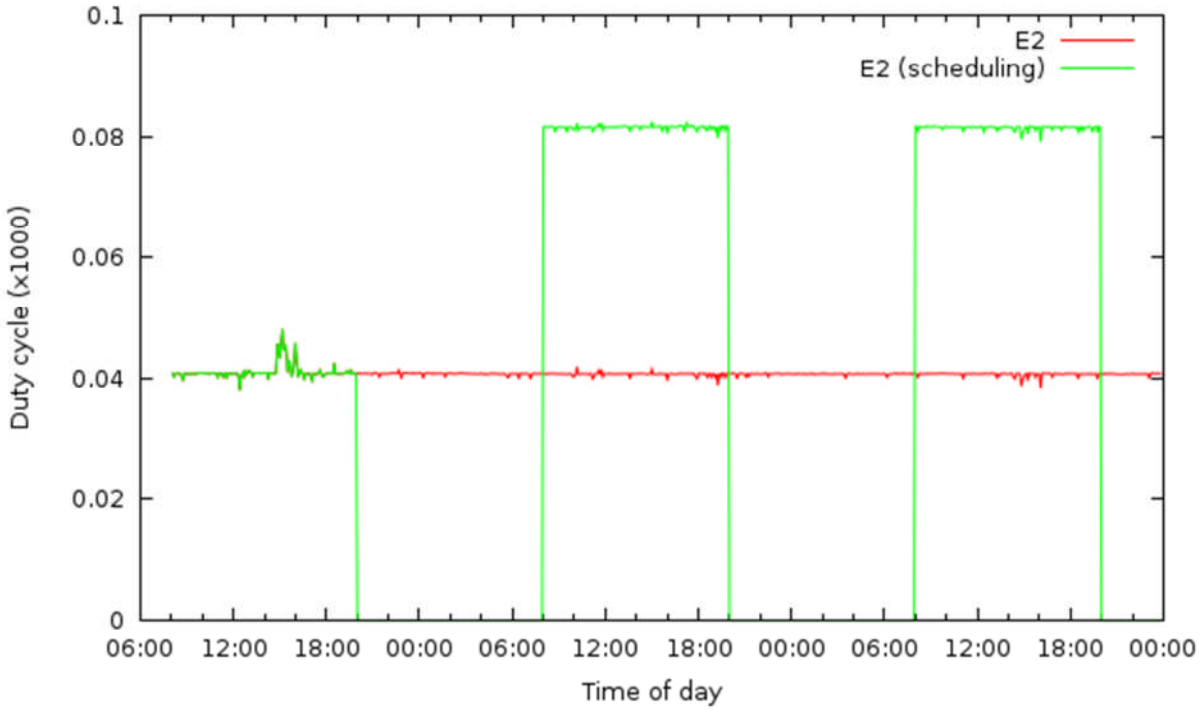

Figure 49 - Transmitter duty cycle with static scheduling

Further work is required on implementing the mechanisms which will be used by applications to specify their tolerance to transmission delay and on assessing the PRR of the solution. This work will then be integrated with the practical EI evaluation method presented above.

3.3.2.4 Global EI reduction assessment

The potential EI reduction was calculated for the proposed solution, in isolation, when compared to an unmodified IEEE 802.15.4 protocol stack. This improvement will be validated with a real deployment of a WSN, which will run a modified network stack, using the practical methodology described previously.

Furthermore, the contribution to the global EI reduction will be determined based on the statistical parameters determined by WP2 for the indoor scenario. A weighting factor for this solution remains to be computed to assess the impact on the final EI.

3.4 Low exposure cooperative communication techniques

Implementation of relay (R) stations in LTE-A systems will cause decrease in the mean transmitted power (P_{Tx}) in UL communication process, due to a shorter distance between the UE and R station comparing with the distance between the end-user and a macro BS. This will result in significant EI reduction, as the same QoS level will be achieved in UL transmission, with much lower power transmitted by end-user device. However, on the other side, closer position of R stations to end-users will cause a certain level of EI increase on DL, compared to the scenario with

no relays. Therefore, we have been working on a solution for reducing of EI that originates from R station in DL communication process.

3.4.1 Remind on the concept

We consider DL communication in dual-hop OFDM based relay system implementing decode-and-forward (DF) relaying, which corresponds with the relay solution adopted in LTE-A standard. Relay station (R) in LTE-A system will primarily serve for BS coverage extension, assuming that the complete communication process between BS (source of information – S) and end-user (destination terminal – D) is performed through the R station. For such LTE-A relay system, we propose a solution for EI reduction on DL, which is based on the implementation of the ordered subcarrier mapping (SCM) at the R station, assuming that the subcarriers from the first hop (S-R link) are mapped to corresponding subcarriers on the second hop (R-D link), all in accordance to their instantaneous signal-to-noise ratios (SNRs) [53]. This solution, denoted as best-to-best SCM (BTB SCM),actually enables to reduce the power transmitted from both R station and BS, while it keeps the system capacity at the same level capacity [54], [55]. In the analysis we assumed that adjacent subcarriers, having similar transfer functions, are grouped in “chunks”, and that mapping at R station is performed on chunk basis.

3.4.2 Evaluation methodology

In our research work we examined through simulations the level of power decrease, radiated from R station, which can be attained through implementation of ordered SCM, while keeping the same ergodic capacity. In that way, the level of received power reduction is determined, and this directly relates to EI reduction.

3.4.2.1 Sub-scenario description

The proposed solution for reducing EI in OFDM based relay systems can be used in both Macro Cell and Rural sub-scenarios, but in this research we put focus only on the Rural sub-scenario. Using the reference scenarios corresponding to relay implementation for the coverage of rural area in LTE-A system and appropriate system parameters given in [56], we develop a simulation model for evaluating average ergodic capacity per subcarrier of the OFDM DF relay system with BTB SCM, as well as of the same system when no SCM is applied. Through this simulation model we manage to perform fair comparisons of average ergodic capacities per subcarrier of the two mentioned systems.

In order to make tractable the obtained results, in the next part we provide details of the parameters used in the presented simulations. Most of the simulation parameters are taken from [10], while few of them are from practice and from [57].

- Bandwidth: 5 MHz (25 resource blocks x 12 subcarriers = 300 subcarriers).
- Subcarrier spacing: 15 kHz.
- Guard interval: 17μs.
- Carrier frequency:2 GHz
- 14 OFDM symbols create a frame.
- S (BS) transmit power is 43 dBm. R station transmit power is 30 dBm.
- Feeder loss at S station is 3 dB. Feeder loss at R station is 1 dB.

- S antenna gain is 17dBi. R station antenna gain is 15 dBi. D antenna gain is 0 dBi.
- Additive white Gaussian Noise (AWGN)$10\log_{10}(kTB)$=-137.45 dB (both at R and D).
- Noise figures of D and R stations are 7 dB.
- Interference margin is 4 dB.
- S-R distance is taken to be greater than 3km.
- Doppler shift for S-R link is 0Hz.
- Doppler shift for R-D link is 10Hz for the scenario with slow mobile user (pedestrian) and 100Hz for the scenario with the medium mobile user (vehicular).

Path loss models, defined as the reference ones for LTE-A relay systems, are taken from [56]. We assumed that both R and D stations are placed outdoor, while for the scenario with indoor D terminal, additional path loss due to wall penetrations should be taken into account. We assumed that R station is placed with site planning, [56]. Multipath propagation fading models for both S-R and R-D links are also taken from [56]. We have considered two possible scenarios for the S-R link, i.e. a NLOS scenario and LOS scenario with medium dominant component.

The two scenarios considered for the multipath propagation fading on the R-D link are Extended Pedestrian A (EPA) model and Extended Vehicular A (EVA) model, both given in [56]. The Doppler shift of 10 Hz for EPA model is taken, which corresponds to user mobility of ~5 km/h, while Doppler shift of 100 Hz for EVA model corresponds to user mobility of ~50 km/h at 2GHz.

In these analyses we have assumed that the R station has perfect channel knowledge of both S-R and R-D links, so channel estimation is not included in the simulation model.

3.4.2.2 Exposure and QoS metrics identification

The considered solution for EI reduction in LTE-A relay systems, assuming SCM implementation at R station, does not change the nature of DL communication process, so the transmission time can be considered to remain unaffected compared to the case with no SCM implemented (actually, the only minor change is in the preamble, as the implemented SCM scheme should be sent from R station to end-user). The SCM employment provides the possibility for reduction of power transmitted from R and from base station, while keeping the same capacity performance as the QoS metric. Thus, when observing relation (1.1) for EI, we can say that P_{Rx} i.e. the power that end-user receives is the parameter affected with the proposed solution. On the other side, this actually means that Mean Tx power on DL is exposure KPI for the considered relay system.

On the other hand, this solution does not affect the UL communications. Namely, it uses freedom that OFDM provides through its transmission over orthogonal subcarriers in DL communications of dual-hop LTE-A relay systems, while it has no influence on transmission power, nor ergodic capacity of single-carrier FDMA transmission on UL.

3.4.2.3 EI ratio evaluation

Using the approach described by (1.3), and having defined P_{tx} on DL as the exposure KPI, we can evaluate EI ratio for the considered solution as:

$$\text{Ratio}_{\text{EI}}(\%) = \frac{P_{tx\_partial}\left(\text{wo LEX}\right) - P_{tx\_partial}\left(\text{w LEX}\right)}{P_{tx\_partial}\left(\text{wo LEX}\right)} \times 100 \tag{3.11}$$

3.4.2.4 Capacity improvements converting into EI reduction

In the simulations we calculate capacity of each subcarrier at D terminal for the both systems analysed, for each S-R and R-D channel realization. The *k*-th subcarrier channel capacity at D in the OFDM DF relay system with BTB SCM, in the *i*-th channel realization, normalized to unit of bandwidth, is obtained through [54]:

$$C_k^{(i)} = 0.5 \cdot \log_2\left(1 + \min\left(SNR_{\nu(n),1}^{(i)}, SNR_{k,2}^{(i)}\right)\right), \tag{3.12}$$

where 0.5 comes from the half-duplex operation of the R station, and min(·,·) denotes minimum of SNRs of the *n*-th subcarrier on the first hop and of the *k*-th subcarrier on the second hop, in the *i*-th channel realization. Here, it is assumed that the SCM function $\nu(\cdot)$ has mapped the *n*-th subcarrier from the first hop to the *k*-th subcarrier on the second hop. In the system with no SCM, the *k*-th subcarrier from the first hop is paired to the *k*-th subcarrier on the second hop. From the given expression it is clear that the subcarrier having a worse SNR, from the two subcarriers mapped to each other at the R station, imposes limit on the capacity that can be achieved on the *k*-th subcarrier at the end user terminal D. Averaging over the total number of OFDM symbols sent through each S-R and R-D channel realization, then over the total number of subcarriers in OFDM symbol, and over total number of simulation repetitions, we obtained average ergodic capacities per subcarrier for the both considered systems (with SCM, $\bar{C}_{BTB\_SCM}$, and with no SCM, $\bar{C}_{no\_SCM}$), for the assumed scenario.

Based on these results, we evaluate the "equivalent SNR" at D for the OFDM DF relay systems with BTB SCM as well as for the OFDM DF relay system with no SCM. The introduced equivalent SNR corresponds to the SNR value which is in the case of AWGN channel necessary for the analysed relay systems to attain the same ergodic capacity per unit of bandwidth like in the assumed multipath fading scenarios. Thus, we have obtained equivalent SNR expressions for the system with BTB SCM (SNR_{BTB_SCM}) and for the system with no SCM (SNR_{no_SCM}) as:

$$SNR_{BTB\_SCM} = 2^{\left(2\cdot\bar{C}_{BTB\_SCM}\right)} - 1 \quad \text{and} \quad SNR_{no\_SCM} = 2^{\left(2\cdot\bar{C}_{no\_SCM}\right)} - 1 \tag{3.13}$$

where $\bar{C}_{BTB\_SCM}$ and $\bar{C}_{no\_SCM}$ denote average ergodic capacity per subcarrier in the system implementing BTB SCM and in the system with no SCM, respectively. Comparison of SNR_{BTB_SCM} and SNR_{no_SCM} gives an insight into the level of equivalent SNR improvement achieved with BTB SCM, for the same conditions in both analysed systems, and for the same transmitted power from both BS and R

stations. Having in mind that our goal is to keep the system capacity at the same level, it is clear that the same equivalent SNR should be achieved in both analysed systems. Thus, the expression:

$$p_{red}[\%] = \left(1 - \frac{SNR_{no\_SCM}}{SNR_{BTB\_SCM}}\right) \cdot 100 \tag{3.14}$$

actually provides information on the percentage of the equivalent SNR reduction at D in the system implementing BTB SCM, necessary to attain the same capacity like the system with no SCM. This equivalent SNR reduction is realized by decreasing the transmitted power from both S and R stations for the calculated percentage p_{red}. The lower transmitted power from the R station by p_{red} per cents means lowering average signal power at D terminal for the same percentage, i.e. EI reduction for p_{red} per cents. Such a direct relation between the transmitted power from R station and EI value at D can be introduced, as the proposed method does not affect the total transmission time compared to the system without BTB SCM.

We will now show that the defined p_{red} actually has the same value like the defined EI ratio from (3.11):

$$\begin{aligned} \text{Ratio}_{\text{EI}}(\%) &= \left(1 - \frac{P_{tx\_partial}(\text{w LEX})}{P_{tx\_partial}(\text{wo LEX})}\right) \times 100 = \\ &= \left(1 - \frac{(1 - 0.01 p_{red}) P_{tx\_partial}(\text{wo LEX})}{P_{tx\_partial}(\text{wo LEX})}\right) \times 100 = p_{red} \end{aligned} \tag{3.15}$$

In the following, we provide simulation results for four different scenarios corresponding to LTE-A relay system implementation in rural areas. In Figure 50 to Figure 52 we give the obtained average ergodic capacity per subcarrier for both OFDM DF relay systems with BTB SCM and with no SCM. The results are presented as the function of distance between R and D terminals, for the fixed S-R distance.
Figure 50 corresponds to the scenario with S-R distance of 10 km and LOS propagation conditions between S and R. For the R-D hop, LOS propagation with EPA multipath fading model is assumed. It is taken that the implementation of R station extends the cell radius up to 40%. The presented results approves that the BTB SCM technique enables a certain level of capacity enhancement in OFDM DF relay systems.

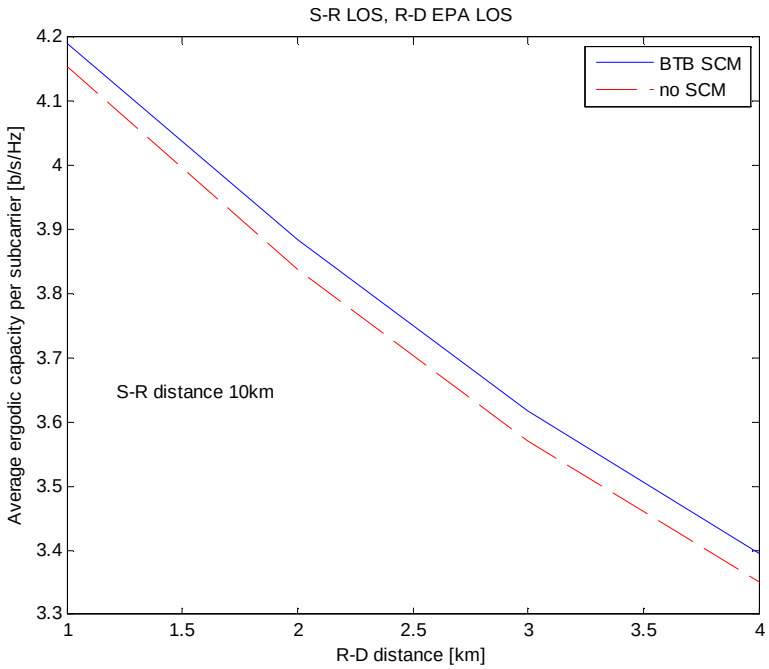

Figure 50 Average ergodic capacity per subcarrier for OFDM DF systems with BTB SCM and no SCM (S-R LOS, R-D EPA LOS scenario)

Table 26 Simulation results for the scenario S-R LOS link on 10km S-R LOS link on 10km, and R-D LOS link with EPA multipath fading

R-D distance [km]	1	2	3	4
$\overline{C}_{BTB\_SCM} / \overline{C}_{no\_SCM}$	1.009	1.013	1.0132	1.0134
$SNR_{no\_SCM} / SNR_{BTB\_SCM}$	0.9473	0.9395	0.9381	0.9381
EI ratio	5.27%	6.05%	6.19%	6.19%

Table 26 gives better insight in the level of capacity enhancement achieved with the BTB SCM technique, as well as in the equivalent SNR increase. It can be seen that ergodic capacity is enhanced at the level of 0.9 to 1.34%, which on the other side enables EI reduction between 5.27 and 6.19% when the same ergodic capacity in both systems is achieved.

Figure 51 also assumes scenario with EPA multipath fading on the R-D channel, but it is taken that no line of sight (LOS) exists on both S-R and R-D links. The S-R distance is equal to 5km, and cases where R station extends cell radius up to 30% are considered. From the Table 27 it can be seen that the capacity enhancement achieved with the BTB SCM ranges from 2.2% to 5.5%, while in the analysed conditions EI can be reduced up to 7.1%.

Figure 52 and Figure 53 assume Extended Vehicular A multipath fading model, where Figure 52 corresponds to LOS-LOS scenario, and Figure 53 corresponds to NLOS-NLOS scenario for S-R and R-D links, respectively.

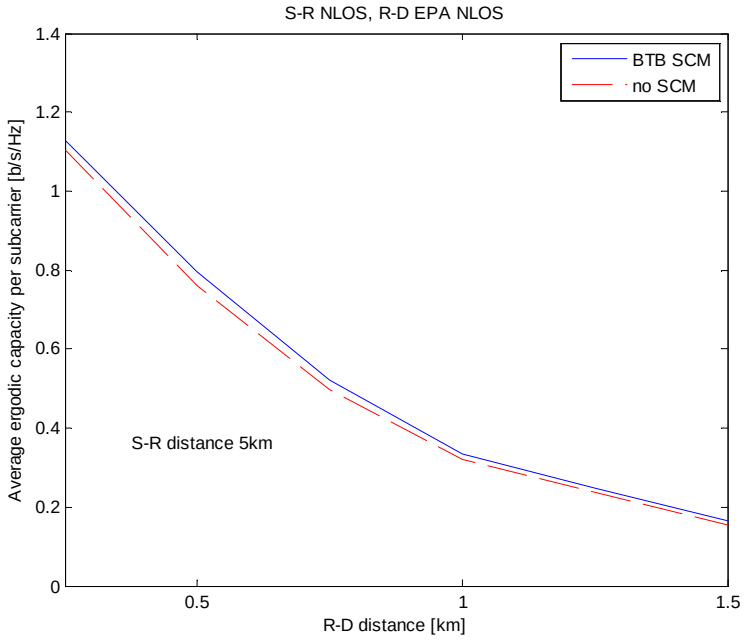

Figure 51 Average ergodic capacity per subcarrier for OFDM DF systems with BTB SCM and no SCM (S-R NLOS, R-D EPA NLOS scenario)

Table 27 Simulation results for the scenario S-R NLOS link on 5km, and R-D NLOS link with EPA multipath fading

R-D distance [km]	0.25	0.5	0.75	1	1.25	1.5
$\bar{C}_{BTB\_SCM} / \bar{C}_{no\_SCM}$	1.023	1.046	1.054	1.053	1.055	1.052
$SNR_{no\_SCM} / SNR_{BTB\_SCM}$	0.956	0.929	0.929	0.937	0.939	0.946
EI ratio	4.4%	7.1%	7.1%	6.3%	6.1%	5.4%

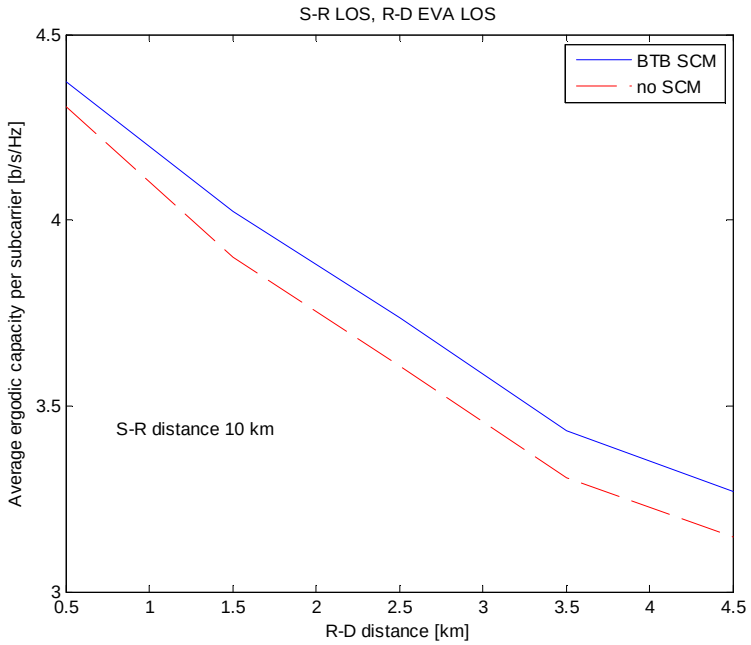

Figure 52 Average ergodic capacity per subcarrier for OFDM DF systems with BTB SCM and no SCM (S-R LOS, R-D EVA LOS scenario)

Table 28 Simulation results for the scenario with S-R LOS link on 10km, and R-D LOS link with EVA multipath fading

R-D distance [km]	0.5	1.5	2.5	3.5	4.5
$\overline{C}_{BTB\_SCM} / \overline{C}_{no\_SCM}$	1.016	1.031	1.036	1.038	1.039
$SNR_{no\_SCM} / SNR_{BTB\_SCM}$	0.909	0.844	0.833	0.838	0.84
EI ratio	9.01%	15.54%	16.67%	16.2%	16%

Simulation results given in Table 28 shows that in LOS-LOS scenario with EVA multipath fading on the R-D link, the ergodic capacity enhancement achieved with SCM goes up to 3.9%, which reflects the potential for EI reduction of up to 16.67%.

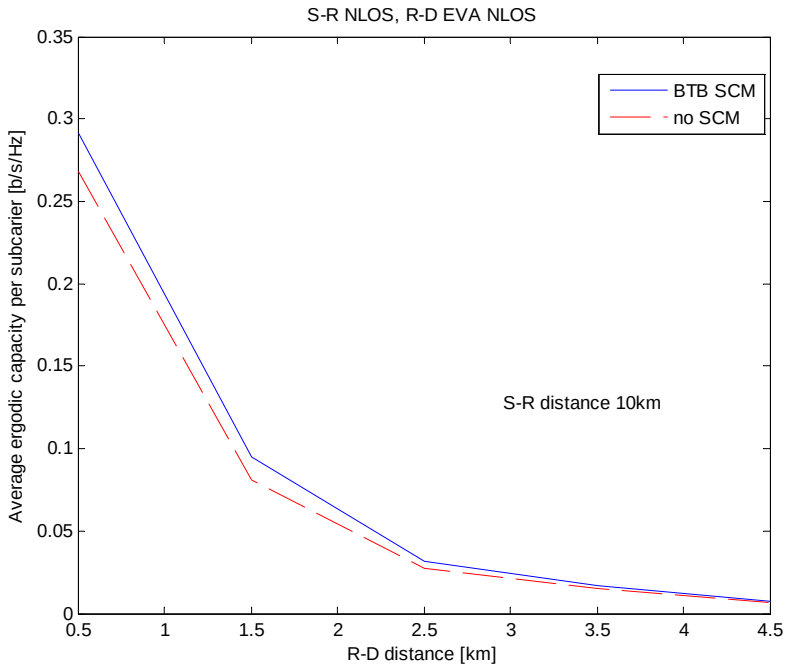

Figure 53 Average ergodic capacity per subcarrier for OFDM DF systems with BTB SCM and no SCM (S-R NLOS, R-D EVA NLOS scenario

Table 29 Simulation results for the scenario with S-R NLOS link on 10km, and R-D NLOS link with EVA multipath fading

R-D distance [km]	0.5	1.5	2.5	3.5	4.5
$\overline{C}_{BTB\_SCM} / \overline{C}_{no\_SCM}$	1.085	1.187	1.185	1.133	1.166
$SNR_{no\_SCM} / SNR_{BTB\_SCM}$	0.905	0.895	0.84	0.881	0.856
EI ratio	9.5%	10.5%	15.97%	11.89%	14.4%

Table 29 shows that for the EVA multipath fading model on the R-D link, and NLOS-NLOS links on S-R and R-D hops, the implementation of the SCM technique enables the ergodic capacity enhancement of up to 18.7%, while in the analysed conditions EI can be reduced up to 15.97%.

Further on, our analyses have shown that the ordered SCM technique can bring even greater capacity enhancement, i.e. greater equivalent SNR increase, if the instantaneous SNRs on both hops do not differ too much. This is certainly expected,

as it is explained earlier that the link with the lower subcarriers SNRs imposes the limit on the achievable ergodic capacity in OFDM DF based relay systems.

3.4.2.5 Future works

The proposed solution assuming implementation of SCM at R station brings EI reduction in DL communications for all the users (both active and passive ones) in the coverage area of a R station, as well as a certain level of EI reduction for passive users in area between base station and R station, which are not in the service zone of R station. This is accomplished as SCM technique enables achievement of the same level of the system capacity in the LTE-A relay systems, but with a lower transmitted power from both BS and R station. In other words, such a solution reduces EI, compared to the R station without SCM, if there is only one active user in the area of R station coverage.

The presented results illustrate the significant potential of the proposed ordered SCM technique for the EI reduction in LTE-A relay systems, taking into account different real-case scenarios. As it is known that combination of the ordered SCM and power allocation schemes may further enhance the capacity of OFDM DF relay systems [57]-[60], it is expected that this kind of solution would enable further EI reduction, while keeping the same level of total system capacity. We are working on simulation models corresponding to real scenarios, which will help to find an optimal combination of ordered SCM technique and appropriate power allocation strategy, all with the goal to achieve the highest EI reduction while keeping the same level of the total OFDM DF system capacity.

3.5 Interference management in heterogeneous network

3.5.1 Remind of the concept

Our objective is to develop powerful physical and MAC layer resource allocation techniques for both ad-hoc and cellular networks adapted to several QoS requirements and to different topological settings e.g., macro, heterogeneous, etc. We consider OFDMA since we mostly focus on LTE. In addition, at MAC layer, retransmission mechanism (such as HARQ) has to be considered. The main interest of this technique is to be versatile and adaptive which enables us to reduce the exposure when it is possible. The goal of our work is to prove that the resource allocation taken into account the MAC layer (so the HARQ) can reduce the EI keeping the QoS constant.

3.5.2 Evaluation methodology

3.5.2.1 Sub –scenarios description

Assume that the considered network comprises *K* active nodes, each of them transmitting on one or more outgoing link. Let I_k be the number of links associated with node *k* ($k \in \{1, \dots, K\}$). In a DL cellular scenario for example, these nodes could be macro BSs, femto base stations, or a mixture of both. In the DL, they could be

user mobile equipments or a micro (pico, femto, etc.) BS connected to the macro BS using an in-band wireless link.

In our simulations, we considered the DL of one sector of a heterogeneous network with *K*=10 active transmitting nodes and 30 UEs). One of these nodes is the macro BS while the other 9 nodes are small-cell BSs.

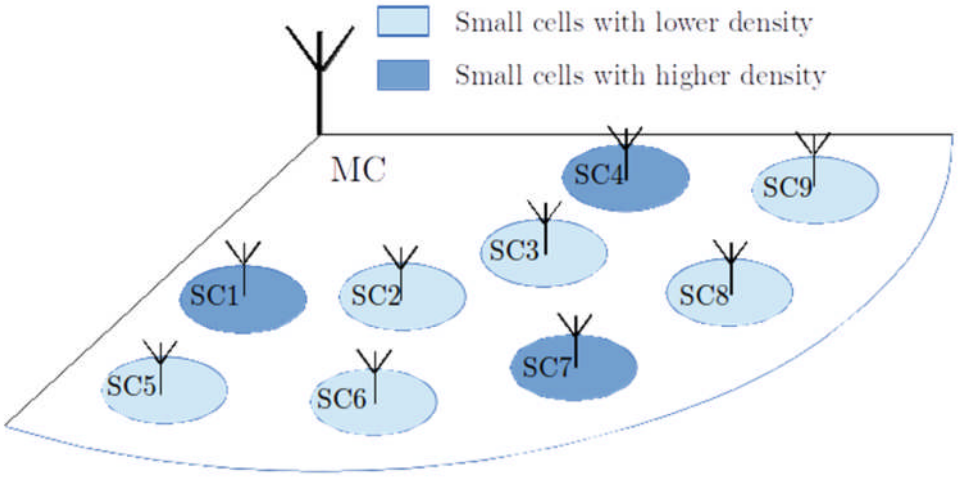

Figure 54 Configuration of the network

We assume a fixed cell association based on distance and that each one of the small-cell BSs with indexes 2,3,5,6,8,9 (in blue on previous Figure) serves 1 UE, that each one of the small-cell BSs with indexes 1,4,7 (in dark blue) serves 2 UEs and that the macro BS serves 18 other UEs. It is worth mentioning that these numbers of links are chosen in accordance with the population's densities given in the next paragraph. The total bandwidth is assumed equal to W=20 MHz centred around the carrier frequency of 2.4 GHz. For macro-cell users, the distance between the transmitter and the receiver is randomly drawn from a uniform distribution between 25m and 250m. As for small-cell users, the range is between 2.5 and 25m. A Winner phase-2 model is considered for the path loss [61]. Note that this model treats differently the propagation in the macro-cell, in the small cells and from the macro-cell base station to the indoor environment of the small cells. For the sake of simplicity, each user has the same target efficiency η so that the required sum rate is equal to 30η. In addition, $Q_k^{(0)}$ is the maximum individual transmit power for node *k* which we assume is divided equally among all the outgoing links of the node. This information is summarized in below Table.

Table 30 Sub-Scenario Description, [62]

Inputs	Description	Values (or range)
Environment	Spatial deployment, such as the inter-site distance (ISD)	250 meters radius for the Macro Cell
EU or source density	EMF sources number	30 active UEs in the MC
	Antenna gain	27 SC BS (9/MC sector)
	Max. Tx Power at MC	46 dBm (13 dBi ant. gain)
	Max. Tx Power at SC	30 dBm (5 dBi ant. gain)
Frequency	Central frequency (bandwidth)	2.4 GHz (20 MHz)
Signal duration	Typical duration (duty cycle)	LTE Frame:10us
Traffic load	Throughput (low, medium, high)	high (5-35 Mbps)
Path loss model, indoor/outdoor	Fast fading model	Winner phase 2
	Shadowing model	Winner phase 2
	Directional model	Winner phase 2

3.5.2.2 Available side information

In addition to the environment setting, it is crucial to describe the information available at the transceivers for performing the resource allocation. We consider only statistical Channel State Information at the Transmitter (CSIT), which is realistic for most practical wireless ad-hoc or infrastructure-based systems. In wireless ad-hoc networks, generally a node, called "resource manager", is elected to perform the resource allocation even if pairwise communications are allowed. The time delay between the initiation of a specific link and the reception by the resource manager of the CSI feedback associated with that link may last several frame periods. As a consequence, the resource manager has only outdated CSI whereas its statistical knowledge of the channel is much more accurate due to its much larger coherence time. In cellular networks, statistical CSIT is always available and is not costly in terms of overhead. Even in infrastructure-based networks, statistical CSI is still a valid assumption in most real-world settings. In LTE for example, there is a trade-off between the frequency of CSI feedback reports and the amount of information contained in them. More precisely, the most frequent CSI reports are only allowed to contain rough CSI estimates that are, for instance, the quantized version of the average over the entire cell bandwidth of the real per-subcarrier CSI values which in fact corresponds to statistical CSI (due to the average). To send more precise CSI

feedback messages (which means these CSI messages contain more information about channel behaviour on each subcarrier), their periodicity must be significantly lowered leading sometimes (when the coherence time is too short) to outdated CSI validating our assumption of statistical CSI. As future work, we would like to incorporate more CSIT (deterministic or almost perfect) in the current problem in order to improve the performance, but at the expense of overhead and information (not data) exchange in the whole network.

3.5.3 Exposure and QoS metrics identification

In order to limit the exposure, we propose to minimize a weighted sum of the transmit powers with respect to the power (per subcarrier) and the subcarriers assignment. Our metric just corresponds to an average of the third metric described in Chapter 2 and thus this objective function has a direct effect on the EI. In addition, we optimize the modulation and coding scheme (MCS) selection jointly with transmit power and subcarriers allocation. This problem has been widely studied when only physical layer has been considered.

Here the main originality is to take into account the presence of the retransmission scheme in our resource allocation algorithms. To do so, even a slight modification of standard algorithms is impossible. Actually all the performance metrics have to be re-defined. As a retransmission scheme, we consider the Type-II HARQ which is much more powerful than the Type-I HARQ. In contrast, the closed-form expressions for the performance metrics of the Type-II HARQ are much more complicated and so we need to work hard to obtain practical algorithms.

As only statistical CSIT is available, there is no obvious way to assign specific subcarriers to the different links since the channels associated with the subcarriers of any given link are statistically identical. Therefore, we will only optimize the proportion of the set of subcarriers, denoted by $\gamma_{k,i}$, that should be assigned to each link (*k*,*i*). The actual assignment of subcarriers can then be done through a frequency-hopping scheme which also handles the diversity issue. As for the power, each link operates with the same transmit power $P_{k,i}$ per subcarrier which will be also optimized. The transmit power on link (*k*,*i*) is thus $\gamma_{k,i}P_{k,i}$. Note that in our model each link can operate with its own level of transmit power. Finally, we let $m_{k,i}$ designate the modulation order on link (*k*,*i*) and $R_{k,i}$ the initial coding rate so that $(m_{k,i}, R_{k,i})$ designates the used Modulation and Coding Scheme (MCS). As a consequence, each node has three parameters to choose on each of its outgoing links: its power, used bandwidth and MCS.

3.5.3.1 KPI definition

Focus for the moment on the DL of the cellular network and let (*x*,*y*) be the position of some person (not necessarily with a mobile equipment) in the Cartesian coordinate system associated with the considered network. Define $G_k(x,y)$ as the propagation fading gain between node *k* and a virtual receiver at position (*x*,*y*). In the following, we use the notation $P_{RX}(x,y)$ to designate the power sensed by a virtual receiver at position (*x*,*y*) due to the *K* nodes of the considered network. This power is given by

$$P_{RX}(x,y) = \sum_{k=1}^{K} G_k(x,y) \sum_{i=1}^{I_k} \gamma_{k,i} P_{k,i}. \quad (3.16)$$

To go from the location-dependent quantity $P_{RX}(x,y)$ to an average indicator of the received exposure, we should model people's positions with a random variable (*X*,*Y*) whose statistical characterization is assumed known (the density of its distribution for example). We then can use this knowledge to compute $E_{X,Y}[P_{RX}(X,Y)]$ the expected value of $P_{RX}(X,Y)$ with respect to the distribution of (*X*,*Y*) (assuming that the expectation exists). Typically, such a distribution should reflect the average density of people at each position in the affected area.

Then we able to define our KPI. By referring to the expression of $P_{RX}(X,Y)$, we can write

$$KPI = E_{X,Y}[P_{RX}(X,Y)] = \sum_{k=1}^{K} E_{X,Y}[G_k(X,Y)] \sum_{i=1}^{I_k} \gamma_{k,i} P_{k,i} = \sum_{k=1}^{K} w_k \sum_{i=1}^{I_k} \gamma_{k,i} P_{k,i}, \quad (3.17)$$

where we defined the weight parameter associated with the transmitter node *k* as $w_k = E_{X,Y}[G_k(X,Y)]$.

By referring to the definition of the exposure index, it becomes clear that the contribution of the *K* nodes of the network in the downlink portion of the exposure index is proportional to

$$\sum_{k=1}^{K} w_k \sum_{i=1}^{I_k} \gamma_{k,i} P_{k,i},. \quad (3.18)$$

Indeed, this weighted sum of transmit powers is proportional to the term $\sum^{N_{locations}} P_{RX}$ which is present in the expression of the EI.

To be more precise, the main motivation behind incorporating the population's positions (*X*,*Y*) distribution into the resource allocation problem via the weights w_k is, as we showed above, to make the objective function of the associated optimization problem relevant from an exposure index perspective. Indeed, by setting $w_k = E_{X,Y}[G_k(X,Y)]$ when minimizing $\sum_{k=1}^{K} w_k \sum_{i=1}^{I_k} \gamma_{k,i} P_{k,i}$, a higher weight is given to nodes *k* that affect a larger portion of the population in the area where the considered network is deployed. Of course, for that to hold true, the weights w_k should adapt to changes in the population distribution during the different periods of the day.

For example, the small-cell BS serving a crowded work place should typically have a higher weight during the work hours *e.g.,* from 8 AM to 6 PM. The emphasis should be shifted accordingly to the femto-cell transmitters in residential homes by assigning them larger weights during the evening hours after 8 PM. The entity performing resource allocation should, therefore, have at its disposal estimates of the population's geographical density during the different periods of the day.

Now that the weights in the weighted sum of transmit powers have been defined, the main challenge is to solve the optimization problem as described below. To overcome the discrete nature of the MCSs, we consider at first that they are fixed in advance. The selection of these MCSs is dealt with later on. The problem that we first solve is thus the minimization of $\sum_{k=1}^{K} w_k \sum_{i=1}^{I_k} \gamma_{k,i} P_{k,i}$ with respect to variables

$\{\gamma_{k,i}, P_{k,i}\}_{k=1\dots K, i=1\dots I_k}$ while respecting a number of practical and some QoS-related constraints.

3.5.3.2 QoS metrics

Now we have to make explicit these QoS metrics constraints. As we consider a heterogeneous network, users may have very different rates. Therefore, we assume that each link should operate under a given data rate (here a throughput since HARQ is used) constraint.
The QoS metric considered in our work is thus the throughput, which is defined as the average number of successfully received bits per second. The throughput on any link (k,i) associated with any of the Type-II HARQ schemes considered in our work is given by the following formula

$$\eta_{k,i} = W m_{k,i} R_{k,i} \gamma_{k,i} \frac{1-q_{k,i,L}(P_{k,i})}{1+\sum_{l=1}^{L-1} q_{k,i,l}(P_{k,i})} \text{ (bps)}, \quad (3.19)$$

Where *W* is the system bandwidth, and $(m_{k,i}, R_{k,i})$, is the MCS on link (k,i). Here, *L* is the maximum number of transmissions and $q_{k,i,l}(P_{k,i})$ is the packet error rate after *l* transmissions ($1 \leq l \leq L$). Last but not the least, we take into account that each transmitting node has a maximum individual transmit power constraint. Such constraints are imposed either *i)* due to limited battery life, *ii)* to respect regulations, *iii)* to avoid nonlinearities of the power amplifiers or even *iv)* to reduce near-field exposure (in UL communications). Finally, MCS is also optimized in a second step jointly with the other resource parameters via a heuristic algorithm.

By using the same approach as adopted in [63], one can prove that the above-mentioned optimization problem is geometric programming and thus can be seen as a convex optimization problem via a change of variable. Consequently standard convex optimization algorithms can be used such as projected gradient descent algorithm, barrier algorithm, interior-point algorithm. But before applying these approximate algorithms, we try to solve our problem in closed-form. Therefore, we derive the Karush-Kuhn Tucker (KKT) conditions and we manage to develop a practical algorithm associated with them.

Now that the optimal solution to the resource allocation problem with predefined MCSs is known, it is proposed to optimize the MCS selection by using a suboptimal (but efficient) greedy scheme. The proposed scheme consists in iteratively changing the MCS of only one link per iteration. The link is chosen as described in [63]. The approach is greedy in the sense that it continues as long as the obtained transmit power decreases.

3.5.4 EI ratio evaluation

Before implementing the algorithm, we need to compute the weights $\{w_k\}_{k=1,\dots,10}$. We assume that the density of the population in each one of the small cells and in the area of the macro cell not covered with these small cells is uniform. However, we allow that this density varies from one cell to another to account for similar variations in real life. As an example, we assume that the density in the small cells

corresponding to *k*=1,4,7 is 2 times larger than the density in *k*=2,3,5,6,8,9. From now on, we use the notation $f_{X,Y}(x,y)$ to designate the probability density function, *MC* to designate the area belonging to the considered sector of the macro cell, SC_k to designate the area belonging to the small cell k and MC to designate the surface of the macro cell's considered sector. We can thus write

$f_{X,Y}(x,y) = \frac{3}{2|MC|}$, if (*x*,*y*) is in the small cells corresponding to *k*=1,4,7,

$f_{X,Y}(x,y) = \frac{3}{24|MC|}$, if (*x*,*y*) is in the small cells corresponding to *k*=2,3,5,6,8,9,

$f_{X,Y}(x,y) = \frac{1}{|MC|}$, if (*x*,*y*) is in the area of the macro cell not in the small cells.

Note that $\iint_{MC} f_{X,Y}(x,y)dxdy = 1$, as $f_{X,Y}(x,y)$ is a probability density function. The weight w_{k_0} for any $k_0 \in \{1,\dots,K\}$ is thus given by

$$w_{k_0} = \iint_{MC} G_{k_0}(x,y) f_{X,Y}(x,y)dxdy, \quad (3.20)$$

which leads to

$$w_{k_0} = \sum_{k=1,4,7} \iint_{SC_k} G_{k_0}(x,y)\frac{3}{2|MC|}dxdy + \sum_{k\neq 1,4,7} \iint_{SC_k} G_{k_0}(x,y)\frac{3}{4|MC|}dxdy + \iint_{MC\setminus \cup_{k=1\dots 9} SC_k} G_{k_0}(x,y)\frac{1}{|MC|}dxdy. \quad (3.21)$$

Knowing the positions of each node *k* and the expression of the gain $G_{k_{\grave{a}}}(x;y)$ from the path loss model, the integrals in the above equation can be computed numerically for each k_0 to obtain the weights $w_1, w_2, \dots, w_{10}$.

Let us see now the results of the simulation. As a first step, we assume that all the links use the same MCS i.e., $m_{k,i} = m, R_{k,i} = R, \forall k,i$. The values of m and R are chosen from the table given below depending on the target rate. The modulation is based on a m-QAM constellation with $m \in \{1,2,4\}$ while error control consists in a CC-HARQ based on a RCPC convolutional code with an initial rate equal respectively to ½ or 1. In other words, $R \in \{1/2,1\}$. In either case, we set $L = 3$.

Table 31 The MCSs used in the simulations

MCS name	MCS1	MCS2	MCS3
***m* [bits]**	1	2	4
R	½	½	½
Max sum rate [Mbps]	10	20	40

Later, we allow the different links to operate with different MCSs selected thanks to the greedy algorithm described in the previous section. Figure 55 shows the gain in percentage for the overall transmit power (all the weights are fixed to 1) obtained of i) our algorithm when MCS is pre-defined and ii) our algorithm coupling with the previously-mentioned greedy MCS selection compared to the overall transmit power associated with the case where all the base stations operate at the maximum allowed power level. Each point was obtained using 20 Monte-Carlo runs, and each interval is associated with a given MCS. For target sum rates larger than 35 Mbps, the resource allocation algorithm becomes infeasible due to the individual transmit power constraints.

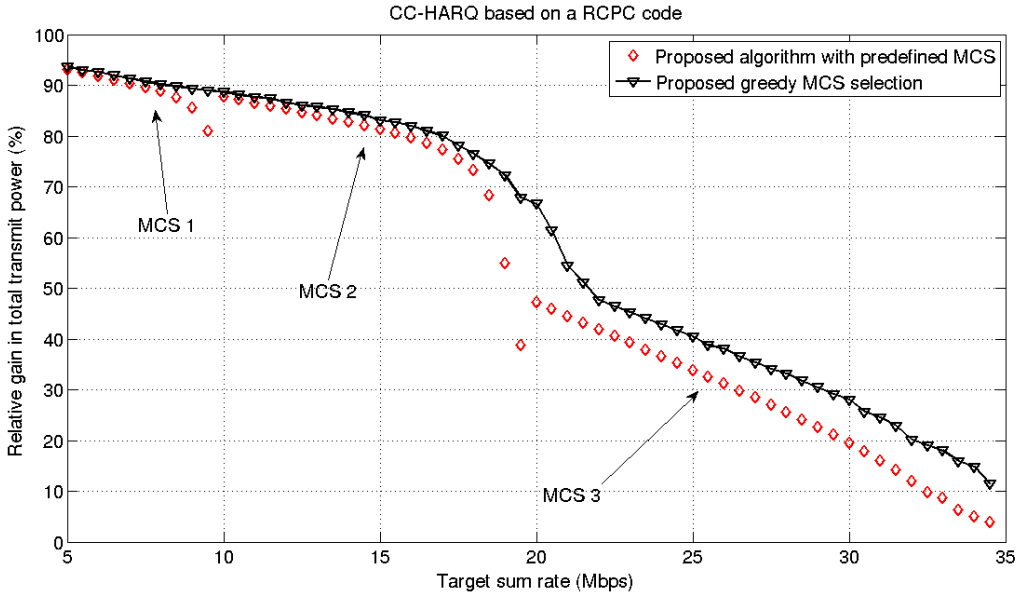

Figure 55 Sum transmit power gain vs. Sum target rate for the proposed algorithms when CC-HARQ is implemented

We now turn our attention to the first step of the evaluation of the EI. For that sake, we assume that there are $N_{population}$=1000 persons in the considered area and we assume that their positions are randomly generated in accordance with the density $f_{X,Y}(x,y)$ defined earlier. Our objective now is to evaluate the KPI as above-defined which is well approximated with $\frac{1}{N_{population}}\sum_{k=1}^{K} G_k(X,Y)\sum_{i=1}^{I_k}\gamma_{k,i}P_{k,i}$. The results presented in Figure 56 show the advantage of using our proposed resource allocation scheme as compared to the trivial case when the base stations are forced to operate with their maximum allowed transmit power.

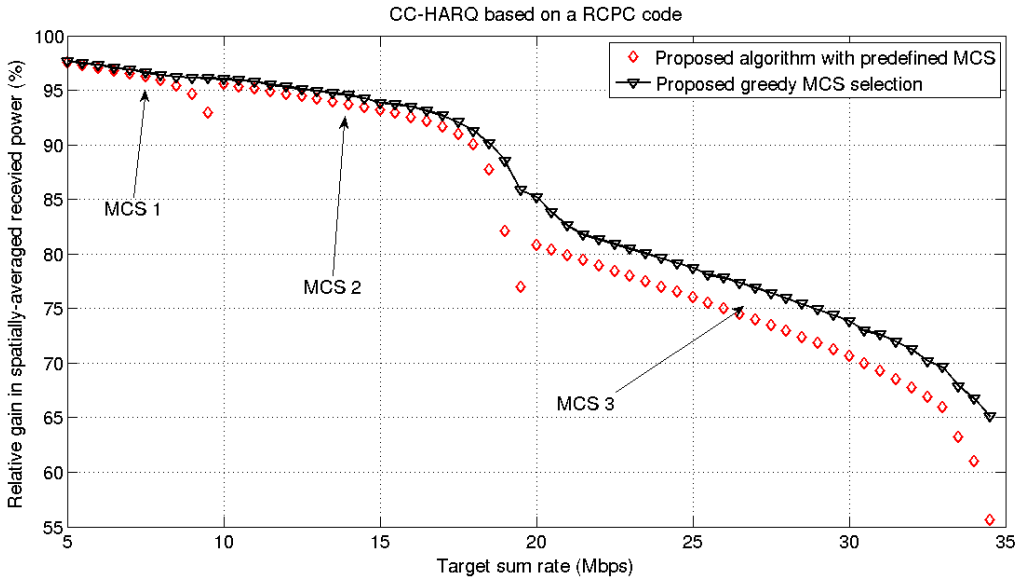

Figure 56 Spatially-averaged received power (KPI) gain vs. Sum target rate for the proposed algorithms when CC-HARQ is implemented

3.5.5 Future Work

The next step in our work will be the evaluation of the reduction in the EI due to the use of the proposed resource allocation schemes. This evaluation will be done for the case where the UEs do not have the same throughput requirements, as opposed to the equal-throughput case addressed in this report. In addition, we have to fix the step 5 where the traffic is time-depended.

4 CONCLUSION

This deliverable D4.2 has presented the WP4 common exposure evaluation methodology (Chapter 1) and its implementation for six radio component solutions (Chapter 2) and five radio link ones (Chapter 3). For each of these solutions, the objective is to reduce the global EM exposure through the EI metric by maintaining QoS. Despite a large diversity of technical domains, the 5-step EI evaluation methodology has been defined to be sufficiently generic for any scenarios and any kinds of solutions. Based on this, solutions performances have been assessed in the light of several quantitative performance indicators which are all related with the three variables (SAR, Tx power, and exposure duration, Table 3) that composed the global EI metric defined in WP2. However, the QoS metric is not imposed in the adopted method. A key advantage to simply assess performances is to consider the EI ratio by comparing the 'with LEXNET solution' versus the 'without LEXNET solution' (i.e. SotA or standard) baseline configurations.

The innovation is first in the adaptation of these mechanisms to the EM exposure lowering and secondly in the analysis itself to globally assess the exposure (UL and DL, over a population) thanks to modified or developed tools.

Thus reported performance assessments have shown a large range of exposure reduction. The macro-cell DTX amplifier deactivation has shown non-significant impact on EI (far below 1%). This technique has been given up for the following step despite interesting improvement in term of energy consumption.

At the opposite, the three antenna solutions seem very promising as they success to focus radiated energy only in useful directions. For instance the implementation of different structures of metamaterials on the terminal board close to the antenna can absorb surface current that radiate towards the body. This solution reaches SAR reduction better than 20% in bands from 2.6 to 5GHz, but the two last steps of the methodology are still in progress to consolidate this promising result.

Beamforming techniques, assuming implementation of SAR modulation alphabet, were analysed for EI reduction. LTE parameters were used in a measurement campaign. Comparing 10g whole body SAR for the case of LEXNET proposed solution, and without LEXNET solution, it turns out that 80% of EI reduction is achieved. However, realization of the SAR modulation alphabet comes at the expense of throughput, as it requires implementation of an Alamouti space-time (or frequency) block coding scheme. The coming step 4 of the methodology will allow appreciating this trade-off.

Regarding the last antenna solution, the small and directive antenna exploits a smaller beamwidth at the small cell antenna which increases the global SINR of the HetNet. Average transmitted power on UL was used as KPI for exposure metric. By deploying the proposed miniature and directive antenna, a 5.2 dB average transmitted power reduction can be reached in the dense SC sub-scenario by maintaining constant the QoS level obtained with a standard omnidirectional antenna. Almost the five steps of the methodology have been followed in this study.

For low noise receiver architecture developed for a SC sub-scenario, the theoretical analysis, using datasheets of COTS components, has shown that EI reduction between 10% (for NF reduction of 0.5dB) and 50% (for NF reduction of 0.5dB) can be achieved. The practical work is focused on design of reconfigurable BPF. However, the prototypes don't obtain the desired selectivity and NF in preliminary results.

In propagation of sleep/idle mode study in a mesh gateway deployment, a 3 dB (50%) gateway transmit power reduction is achieved with only 2% coverage outage on a typical office deployment. For future work, the dynamic part of the system-level simulator, which means the ability to analyse idle algorithms with ongoing stations/traffics for instance, instead of relying only on static parameters (coverage…) will be developed.

Concerning the radio transmission solutions, other promising exposure reductions are shown. A reduction of the "transmission overhead" reference symbol is considered for a specific amount of data in LTE RS design. The main idea is to reduce DMRS usage and to consider that CRS are reconfigured to become DMRS. In a Small-Cell scenario, between 5.7% and 9.1% of RE reduction can be theoretically obtained depending on the different ways of configuring the new DMRS patterns.

Concerning the Wi-Fi and Zigbee interference mitigation, the impact of a low power WSN on Wi-Fi throughput has been demonstrated with an experimental campaign for different proximity between both systems. Wi-Fi can be brought to a halt (even losing association) with WSN frames transmitted in close proximity. EI improvements are calculated with respect to the modification of the time spent transmitting. Tests show PRR of 0.1 to 0.9 for WSN (ZigBee) nodes, which would lead to 10-90% EI reduction. For Wi-Fi, common PRRs of 0.4 to 0.9 lead to 10-60% EI reduction with the Interference Mitigation module. Another studied WSN solution consists in scheduling node transmissions at appropriate times, by locally buffering data to reduce exposure. A significant EI reduction may be attained, depending on the buffer size and update rate..

An interesting study has analysed the impact on EI of the dual-hop OFDM based relay system, with a focus on implementing decode-and-forward (DF) relaying, which is the solution adopted in LTE-A systems. In order to decrease EI on DL communication link, it is proposed to implement BTB SCM scheme at R station. Simulation results, obtained using 3GPP defined parameters for relay systems in rural scenario, have shown that implementing BTB SCM brings EI reduction between 3% and 16%, depending on the channel conditions between BS and R and between R and the user. In future research work power allocation techniques will be combined with BTB SCM in OFDM DF relay systems, in order to achieve further EI reduction on DL.

At last retransmission mechanism Type-II HARQ is considered in a LTE HetNet. The relations between resource allocation parameters and EI are presented. Results on spatially averaged received power, show the advantage of using the proposed resource allocation scheme as compared to the trivial case when the BSs are forced to operate with their maximum allowed transmit power. The future work will comprise

the analysis of the more realistic scenario, where the users will not have the same throughput. Also, the goal will be to quantify the EI global impact reduction reached with the proposed retransmission mechanisms in LTE HetNets.

At the end of the project year 2, all the studies have reached step 3 of the common methodology. All these reported performances are intermediate. They have to be consolidated whether by more realistic assumptions on the analysis, by further developments, by prototype validation, or by widening the scenario to demonstrate a more general relevancy of a solution. The last year will be dedicated to go through step 4 and 5 (global impact on EI). Thus, some prioritization via comparison of their effectiveness will be possible. Steps 1 and 2 also allow to highlight some compatibility or at the opposite some conflicts between these solutions. This last point is a mandatory step to prepare the global exposure reduction assessment and will be addressed during year 3.

REFERENCES

[1] LEXNET, Project Deliverable D4.1, “Promising low exposure index solutions for components and transmission techniques”, http://www.lexnet.fr/, October 2013

[2] LEXNET, Project Deliverable D2.4, “Global Wireless Exposure Metric Definition”, https://www.ict-earth.eu/publications/, October 2013

[3] Emmanuelle Conil, Yoann Corre, Nadège Varsier, Abdelhamid Hadjem, Günter Wermeeren, Luc Martens, Luis M. Correia, Joe Wiart, ‘Exposure index of EU project LEXNET applicated to a LTE macro urban scenario’, Eucap 2014 Conf. Proc., April 2014

[4] O. Kivekas et all, “Bandwidth, SAR, and efficiency of internal mobile phone antennas", Electromagnetic Compatibility, IEEE Transactions on, Vol. 46, No. 1, 71-86, 2004.

[5] A.H. Kusuma et all, “A new low SAR antenna structure for wireless handset applications”, Progress In Electromagnetics Research, Vol. 112, 23-40, 2011

[6] M. I. Kitra et all, “Low SAR Ferrite Handset Antenna Design”, IEEE Transactions on Antennas and Propagation, vol. 55, no. 4, pp 1155-1164, April 2007.

[7] A. C. Lepage, X. Begaud and J. Sarrazin, Microwave and Millimeter Wave Circuits and Systems: Emerging Design, Technologies and Applications, chapter 3 : Wideband directive antennas with High Impedance Surfaces. Wiley, 2012.

[8] Grelier, 2011] M. Grelier, F. Linot, A. C. Lepage, X. Begaud, J. M. Le Mener, and M. Soiron, “ Analytical methods for AMC and EBG characterizations”, Applied Physics A: Materials Science & Processing, 102(2), Feb.2011.

[9] F. Linot, X. Begaud, M. Soiron, C. Renard, and M. Labeyrie, “Characterisation of a loaded high impedance surface”, International Journal of Microwave and Wireless Technologies, 1(9):483–487, Dec. 2009.

[10] Y. Pinto, X. Begaud, A. C. Lepage, “Monopole Antenna with Metamaterial Structures”, EuCAP 2014 - The 8th European Conference on Antennas and Propagation, April 2014.

[11] K. C. Chim, K. C. L. Chan, and R. D. Murch, “Investigating the impact of smart antennas on SAR,” IEEE Trans. Antennas Propag., vol. 52, no. 5, May 2004.

[12] K. C. Chim and R. D. Murch, “Investigating the effect of smart antenna on SAR,” in Proc. IEEE Antennas and Propagation Society International Symposium, vol. 1, 2002, pp. 432–435.

[13] B. M. Hochwald, D. J. Love, S. Yan, and J. Jin, “SAR codes,” in Proc.Information theory and applications workshop (ITA), Feb 2013, pp. 1–9.

[14] N. Czink, N., B. Bandemer, G. Vazquez-Vilar, L. Jalloul, C. Oestges, A. Paulraj, "Spatial separation of multi-user MIMO channels," in Proc. IEEE 20th International Symposium on Personal, Indoor and Mobile Radio Communications, 2009, pp.1059,1063, 13-16 Sept. 2009.

[15] J. Blumenstein, J. C. Ikuno, J. Prokopec, and M. Rupp, “Simulating the long term evolution uplink physical layer,” in Proc. 53rd International Symposium ELMAR, Sep 2011, pp. 141–144.

[16] G. Vermeeren, S. Aerts, D. Plets, W. Joseph, L. Martens E. Conil, N. Varsier, J. Wiart, Y. Core, C. Oliveira, D. Sebastião, L. Correia, R. Agüero, L. Diez, L Rodríguez, M. Koprivica, A. Nešković, M. Popović, J. Milinković, S. Nikšić, “D2.3 Scenarios”, LexNet project, 2014.

[17] Y. Fang, S. Bories, D. Dragomir, A. Voinescu, E. Kocan, M. Pejanovic-Djurisic, P. Ciblat, “IR4.2 Evaluation Methodology and Initial Performance Assessment: Transmission Techniques” LexNet project, 2014.

[18] M.-C. Gosselin, G. Vermeeren, S. Kuhn, V. Kellerman, S. Benkler, T.M.I Uusitupa, W. Joseph, A. Gati, J. Wiart, F.J.C. Meyer, L. Martens, T. Nojima, T. Hikage, Q. Balzano, A. Christ, N. Kuster, N., "Estimation Formulas for the Specific Absorption Rate in Humans Exposed to Base-Station Antennas," IEEE Trans. Electromagn. Compat., vol.53, no.4, pp.909-922, Nov. 2011.

[19] M. Pigeon, C. Delaveaud, L. Rudant, and K. Belmkaddem, “Miniature directive antennas,” *Intern. J. Microwave Wireless Techn.*, 2014.

[20] J. E. Hansen, “Spherical Near-Field Antenna Measurements,” IET, 1988.

[21] A. Clemente, M. Pigeon, L. Rudant, and C. Delaveaud, “Super directive compact antenna design using spherical wave expansion,” *IEEE Antennas Propag. Soc. Int. Symp.* (*APS 2014*), Jul. 2014.

[22] R. F. Harrington, “On the gain and beamwidth of directional antennas,” *IEEE Trans. Antennas Propag.*, vol. 6, no.3, pp. 219-225, Jul. 1958.

[23] R. F. Harrington, “Effect of antenna size on gain, bandwidth and efficiency,” *J. Res. Nat. Bur. Stand*, vol. 64-D, pp 1-12, Jan./Feb. 1960.

[24] 3GPP TSG RAN, “TR 36.872, Small cell enhancements for E-UTRA and E-UTRAN-Physical layer aspects (Release 12),” V12.1.0, Dec. 2013.

[25] 3GPP TSG RAN, “TR 36.814, Evolved Universal Terrestrial Radio Access (E-UTRA); Further advancements for E-UTRA physical layer aspects (Release 9),” V9.0.0, Mar. 2010.

[26] I. Guvenc, et al., “Range expansion and inter-cell interference coordination (ICIC) for picocell networks,” in IEEE Vehicular Technology Conference (VTC Fall), pp. 1–6, Sep. 2011.

[27] EU FP7 LEXNET, D2.4 Global Exposure Metric Definition, Nov. 2013.

[28] 3GPP TR 36.932 “Scenarios and requirements for small cell enhancements for E-UTRA and E-UTRAN”, (Release 12), 2013.

[29] X. Huang, Q. Feng, L. Zhu, Q. Xiang, “A constant absolute bandwidth tunable filter using varactor-loaded open-loop resonators”, Microwave Conference Proceedings (APMC), 2013 Asia-Pacific, November 2013.

[30] W. Tang, J. Hong, “Varactor-Tuned Dual-Mode Bandpass Filters”, IEEE Transactions on Microwave Theory and Techniques (Vol. 58, nº 8), August 2010.
[31] G. Ghaudhary, Y. Jeong and J. Lim, “Dual-band bandpass filter with independently tunable center frequencies and bandwidths”, IEEE Transaction on Microwave Theory and Techniques (Vol. 61, nº 1), January 2013.
[32] Y. Chen, S. Chang, W. Chen and B. Huang “Packaged tunable bandpass filters based on varactor-loaded spiral combline topology”, IEEE microwave magazine, Vol.14, January 2013.
[33] Q. Xiang, Q. Feng, X. Huang and D. Jia “Electrical tunable microstrip LC bandpass filters with constant bandwidth”, IEEE Transactions on Microwave Theory and Techniques, Vol. 61, nº 3, March 2013.
[34] http://www.skyworksinc.com/uploads/documents/SMV1247_SMV1255_Series_200061O.pdf
[35] B. Kapilevich, “A varactor-tunable filter with constant bandwidth and loss compensation”, Microwave Journal, April 2007.
[36] 3GPP TR 36.942 “Evolved Universal Terrestrial Radio Access (E-UTRA); Radio frequency (RF) system scenarios”, (Release 11), 2012.
[37] EARTH, Project Deliverable D4.3, “Final report on green radio technologies”, https://www.ict-earth.eu, June 2012.
[38] EARTH, Project Deliverable D4.1, “Most Promising Tracks of Green Radio Technologies”, https://www.ict-earth.eu, December 2010.
[39] LEXNET, Project Deliverable D6.1, “Validation platform framework and initial assessment”, http://www.lexnet.fr/, Apr 2014.
[40] ns-3. Available online at: http://www.nsnam.org/
[41] ITU-R M2135, “Report ITU-R M2135, Guidelines for evaluation of radio interface technologies for IMT-Advanced”, 2008.
[42] 3GPP TR 36.872, “Small cell enhancements for E-UTRA and E-UTRAN-Physical layer aspects (Release 12),” V12.1.0, Dec 2013.
[43] IEEE 802.11 TGax, “TGax Simulation Scenarios”, doc: IEEE 802.11-14/0980r3, Jul 2014.
[44] IEEE 802.11-2012, “IEEE Standard for Information technology - Telecommunications and information exchange between systems Local and metropolitan area networks - Specific requirements, Part 11: Wireless LAN Medium Access Control (MAC) and Physical Layer (PHY) Specifications”, 2012.
[45] [IEEE 802.11-03/0940r4] IEEE 802.11 TGn, “TGn Channel Model”, doc: IEEE 802.11-03/0940r4, May 2004.
[46] IEEE 802.15.4 specification, Available online at http://standards.ieee.org/getieee802/download/802.15.4d-2009.pdf
[47] Zheng, Jun, and Abbas Jamalipour. Wireless sensor networks: a networking perspective. Wiley-IEEE Press, 2009

[48] [ATMega128RFA1 2012] ATMega128RFA1 Datasheet, Available online at http://www.atmel.com/Images/doc8266.pdf

[49] [ATmega256RFR2 2013] ATmega256RFR2 Datasheet, Available online at http://www.atmel.com/Images/Atmel-8393-MCU_Wireless-ATmega256RFR2-ATmega128RFR2-ATmega64RFR2_Datasheet.pdf

[50] IEEE 802.11 specification, available online at http://standards.ieee.org/getieee802/download/802.11-2012.pdf

[51] deRFmega128 Datasheet, Available online at http://www.dresden-elektronik.de/funktechnik/products/radio-modules/avr-single-chip-modules/description/?L=1&eID=dam_frontend_push&docID=1203

[52] IEEE 802.15.4 specification, Available online at http://standards.ieee.org/getieee802/download/802.15.4d-2009.pdf

[53] E. Kocan, M. Pejanovic – Djurisic, D. S. Michalopoulos, G. K. Karagiannidis, „Performance evaluation of OFDM Amplify-and-Forward Relay System with Subcarrier Permutation“, IEICE Trans. on Communications, Vol.E93-B, No.05, pp. 1216-1223, May 2010.

[54] E. Kocan, M. Pejanovic-Djurisic, C. Mecklenbräuker, “On the Ergodic Capacity of Dual-Hop OFDM based DF Relay System with Subcarrier Mapping”, in Proc. of IEEE conf. ICCSPA'13, Sharjah, UAE, February 2013.

[55] E. Kocan, M. Pejanovic-Djurisic, Z. Veljovic, “On the Optimal Subcarrier Mapping Scheme in OFDM Decode-and-Forward Relay Systems”, In Proceedings of IEEE WTS 2011, pp. 1-5, New York, USA, April 2011.

[56] 3GPP TR 36.826 v11.3.0 (2013-07) Relay radio transmission and reception (Release 11)

[57] H. Holma, A. Toskala, LTE for UMTSL: Evolution to LTE-Advanced, 2nd edition, Wiley, March 2011

[58] W. Wang, S. Yang and L. Gao, “Comparison of schemes for joint subcarrier matching and power allocation in OFDM decode-and-forward relay systems,” in Proc. of IEEE ICC’08 Conference, pp. 4983-4987, May 2008, Beijing.

[59] Y. Li, W. Wan, J. Kong, M. Peng, “Subcarrier pairing for amplify-and forward and decode-and-forward OFDM relay links”, IEEE Comm. Letters, vol. 13, no. 4, pp. 209-211, April 2009.

[60] C.-N. Hsu, H.-J. Su, P.-H. Lin, “Joint subcarrier pairing and power allocation for OFDM transmission with decode-and-forward relaying”, IEEE Trans. on Signal Proc. vol. 59, no. 1, pp. 399-414, Jan. 2011.

[61] IST-WINNER D1.1.2 P. Kyösti, et al., "WINNER II Channel Models", ver 1.1, Sept.

[62] 3GPP TR 36.932 “Scenarios and requirements for small cell enhancements for E-UTRA and E-UTRAN”, (Release 12), 2013.

[63] N. Ksairi, P. Ciblat, and C. Le Martret: Optimal Resource Allocation for Type-II HARQ-based OFDMA ad hoc networks, IEEE Global Signal Processing Conference (GLOBALSIP), Austin (USA), December 2013.

[64] [3GPP TR 36.104] 3GPP TR 36.104 “Evolved Universal Terrestrial Radio Access (E-UTRA); Base Station (BS) radio transmission and reception”, (Release 12), 2013.

APPENDIX 1: INTERNAL REVIEW

	Reviewer 1: Filipe Cardoso (INOV)			Reviewer 2: Massinissa Lalam (SC)		
	Answer	**Comments**	**Type***	**Answer**	**Comments**	**Type***
1. Is the deliverable in accordance with						
(i) the Description of Work?	☒ Yes ☐ No		☐ M ☐ m ☐ a	☒ Yes ☐ No		☐ M ☐ m ☐ a
(ii) the international State of the Art?	☒ Yes ☐ No		☐ M ☐ m ☐ a	☒ Yes ☐ No		☐ M ☐ m ☐ a
2. Is the quality of the deliverable in a status						
(i) that allows to send it to EC?	☐ Yes ☒ No	Globally the relevant contents/results are there but in some cases the methodology and the analysis of results needs to be reworked in order to be easy to follow. Also, the whole document needs to be checked for English spelling, formatting and consistency. Links between chapters should also be improved.	☒ M ☐ m ☐ a	☐ Yes ☒ No	Content is fine, but editorial revision is "strongly" needed in some parts	☒ M ☐ m ☐ a
(ii) that needs improvement of the writing by the editor of the deliverable?	☒ Yes ☐ No		☒ M ☐ m ☐ a	☒ Yes ☐ No	Harmonisation across the sections should be performed before EC delivery	☐ M ☒ m ☐ a
(iii) that needs further work by the partners responsible for the deliverable?	☒ Yes ☐ No		☒ M ☐ m ☐ a	☒ Yes ☐ No	Some sections need a bit more details (e.g. reference to IR4.2 should be avoided, addition of descriptions …)	☐ M ☐ m ☒ a

* Type of comments: M = Major comment; m = minor comment; a = advice

APPENDIX 2: STUDY CASES - ANTENNAS

The aim is to study a simplified model of a terminal mobile. The model consists on a metallic plane with an antenna located in three different positions (center, middle of the edge and corner). The metallic plane size represents a current smart phone with dimensions around 125 x 60 mm. This size can be bigger to represents another mobile terminal as a tablet, however the study is performed taking in account the smallest dimensions because is the critical case.

Initially, three antennas, monopole, IFA (Inverted-F Antenna) and ILA (Inverted-L Antenna) have been chosen to be analyzed. However, the ILA study is not performed because it presents low bandwidth.

The monopole and IFA antennas are designed to work à 5GHz.

4.1 Monopole Antenna

The dimensions of the monopole antenna are shown in Figure 57. l_d parameter is around λ/4 to fix the resonant operating frequency. The *d* parameter allows fixing the bandwidth; this is fixed to 1mm to be manufactured. This antenna is connected to the source by a coaxial input with a characteristic impedance of 50Ω.

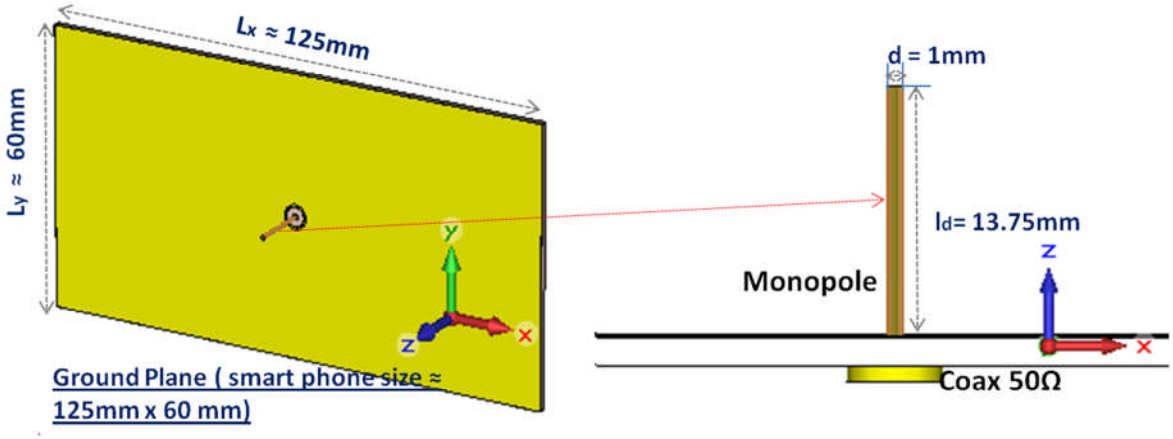

Figure 57 Monopole antenna configuration.

4.2 IFA Antenna

The IFA antenna is shown in Figure 58. This antenna is printed on a dielectric substrate with ε_r = 2.17 and thickness equals to 0.706 mm. This antenna is optimised following guidelines design of Woosung reference[3]. *L* and *h* parameters fix the resonant operating frequency; the matching of the antenna depends of *s* parameter. The frequency bandwidth can be modified by changing by w_1 and w_2 parameters.

[3] Woosung Lee; Manjung Ko; Jaeheung Kim; Young Joong Yoon, "Analysis of the shorting pin effects on an Inverted-F Antenna using a equivalent model for impedance matching," Antennas and Propagation (EuCAP), 2010 Proceedings of the Fourth European Conference on , vol., no., pp.1,5, 12-16 April 2010

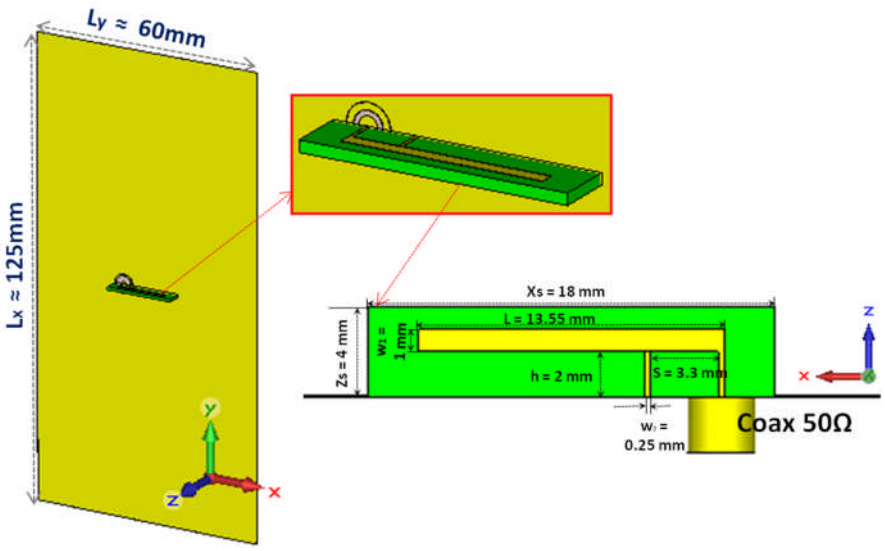

Figure 58 IFA Antenna configuration

4.3 Metamaterial structures

The metamaterial structures are simulated and optimized using CST Microwave Studio™ (Frequency Solver). Only a unit cell is considered because periodic boundaries are applied to simulate an infinite array. Each structure consists of an array of square patches above a grounded dielectric slab with thickness equals to 2.3622 mm and a relative dielectric permittivity of 2.2. The patch length is 9.7 mm and the patches gap is 0.25 mm.

4.3.1 AMC (ARTIFICIAL MAGNETIC CONDUCTOR)

First configuration is the monopole antenna with AMC. The AMC bandwidth (defined as the frequency band where the phase of the reflection coefficient is between 90° and -90°) ranges from 4.42 to 5.65 GHz, where the phase difference is zero at 5GHz (Figure 59).

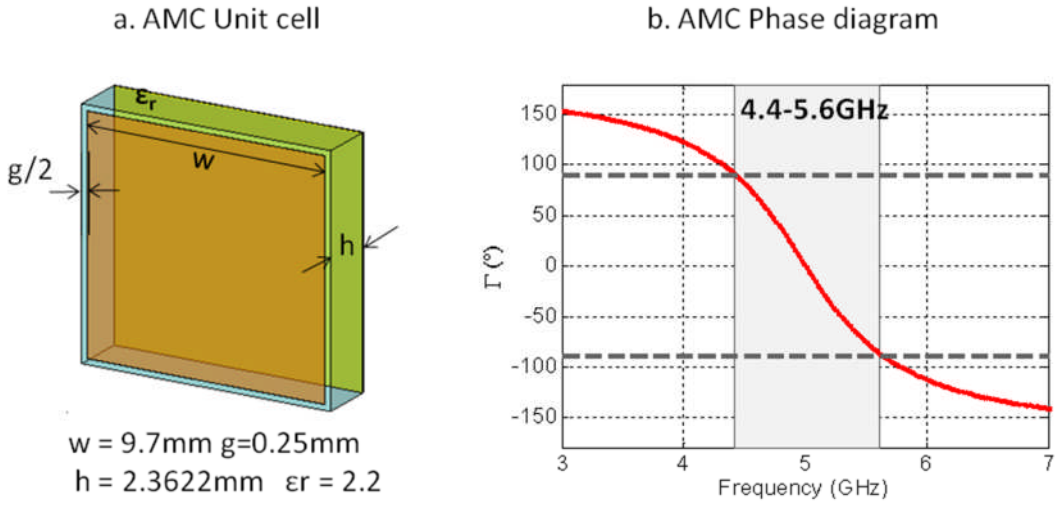

Figure 59. AMC Unit cell and Phase diagram

4.3.2 EBG (ELECTROMAGNETIC BAND GAP)

In the case of EBG structure the patches are connected to ground by a metallic via with 0.5 mm of diameter. The band gap (defined by the bandwidth when |S21| < -20dB) is 3.6-6.11 GHz. (Figure 60).

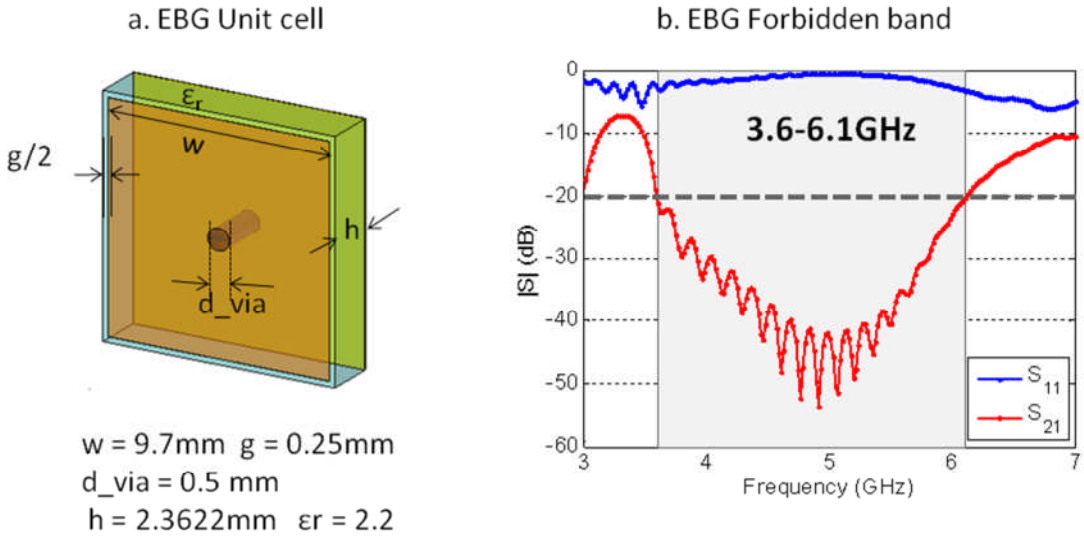

Figure 60. EBG structure and bandwidth

4.3.3 RHIS (RESISTIVE HIGH IMPEDANCE SURFACE)

In the RHIS structure, the squared patches (without via) are interconnected by a resistor. The optimal resistor value depends on both angle of incidence and wave polarization[4]. Figure 61 shows the RHIS unit cell structure and the absorption band for three different structures; they are optimized to absorb incident waves at normal incidence (angle of incidence equals to 0°) and oblique incidence (60° and 85°) in TE polarization. The maximal absorption at normal incidence is obtained when the resistor (R) value is 377 Ω, the patch length (w) is 9.7mm and the gap (g) is 0.25 mm. In the case of incidence oblique at 60°, the resistor value is 800 Ω and the patch length is 11.7 mm. For maximal absorption at 85°, the resistor value is 5000 Ω and the patch length is 12 mm.

[4] Y. Pinto, J. Sarrazin, A. C. Lepage, X. Begaud, N. Capet, " Resistive high-impedance surfaces (RHIS) as absorbers for oblique incidence electromagnetic waves", Applied Physics A, 2014; DOI: 10.1007/s00339-014-8724-5

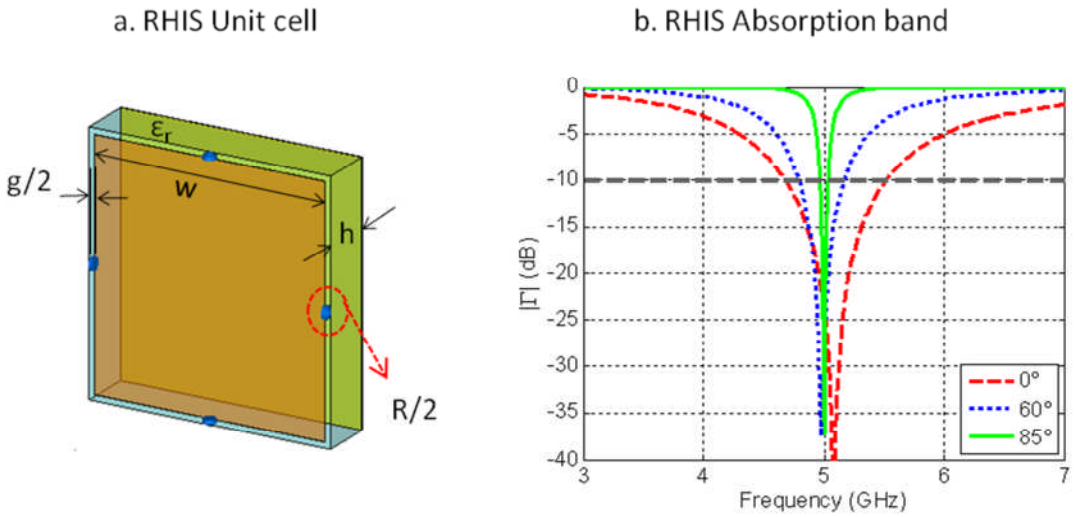

Figure 61. RHIS configuration and Absorption bandwidth

4.4 Antennas with metamaterial structures

The antennas with metamaterial structures are simulated and optimized using CST Microwave Studio™ (Time Solver).

4.4.1 Monopole Antenna

The monopole antenna is surrounded with the metamaterial structures. Four cells are removed around the antenna. The solutions with metamaterials are compared to the reference antenna (monopole with a metallic plane without metamaterials). The results for three positions (centre, middle of the edge and corner) of the monopole antenna are displayed in Figures 61,62, 63, 64 , 65, and 66.

Figure 62 shows the antenna matching for the three position cases. It is observed that the EBG solution is not appropriate because the antenna matching is not preserved (criteria: $|\Gamma| < -10$dB) when antenna is located at the centre and at the corner however the antenna is matched when located on the middle of edge. Solutions with AMC and RHIS (for normal incidence) give some shifts in frequency bandwidth but keep antenna matched. Solutions with RHIS optimized at oblique incidence (60° and 85°) shifts slightly the frequency band when the antenna located on the centre but the antenna is not matched when located on the side (corner or middle of the edge).

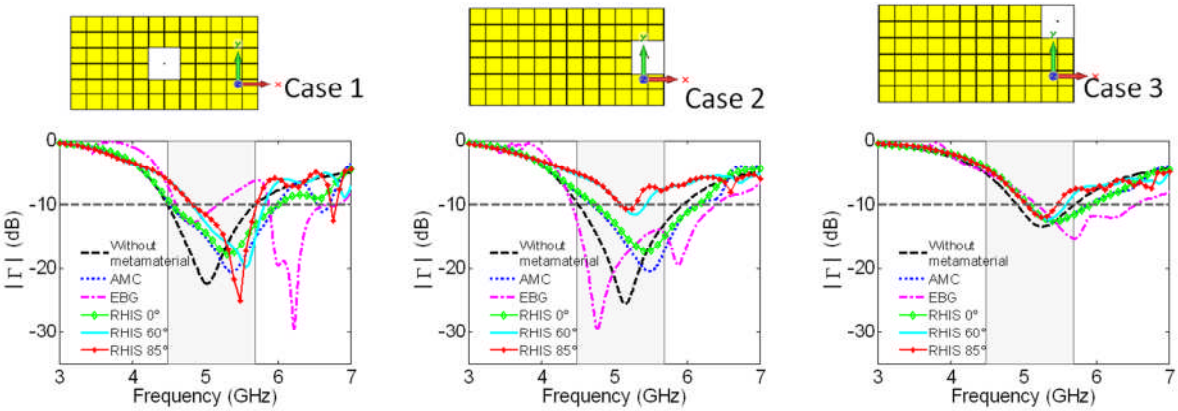

Figure 62 Impedance matching. Case 1: antenna at centre. Case 2: antenna at middle of the edge. Case 3: antenna on the corner

Figure 63 displays the total efficiency results. Efficiency is preserved when AMC and EBG are used. In the case of the RHIS solutions the efficiency and the gain Figure 64) are decreased due to the presence of resistors but remain acceptable in the operating bandwidth.

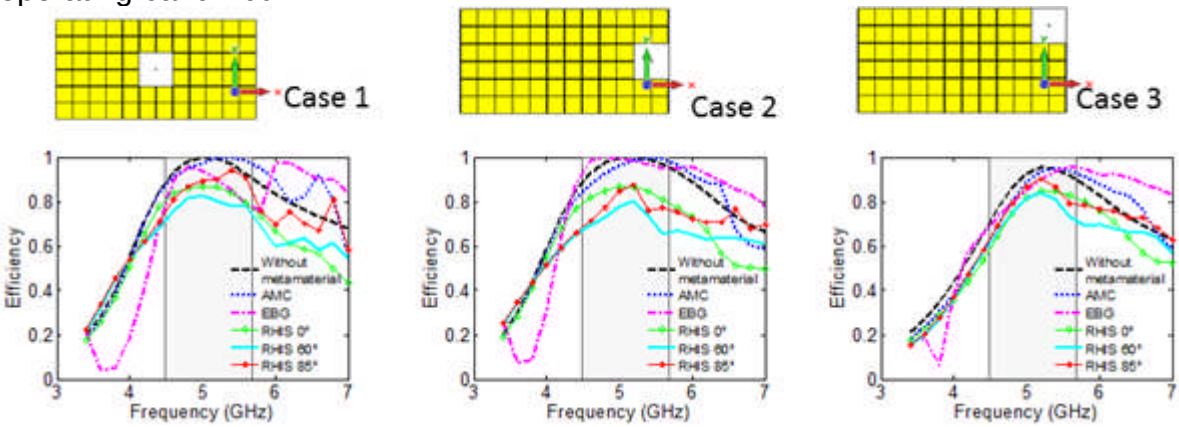

Figure 63 Efficiency. Case 1: antenna at centre. Case 2: antenna at middle of the edge. Case 3: antenna on the corner

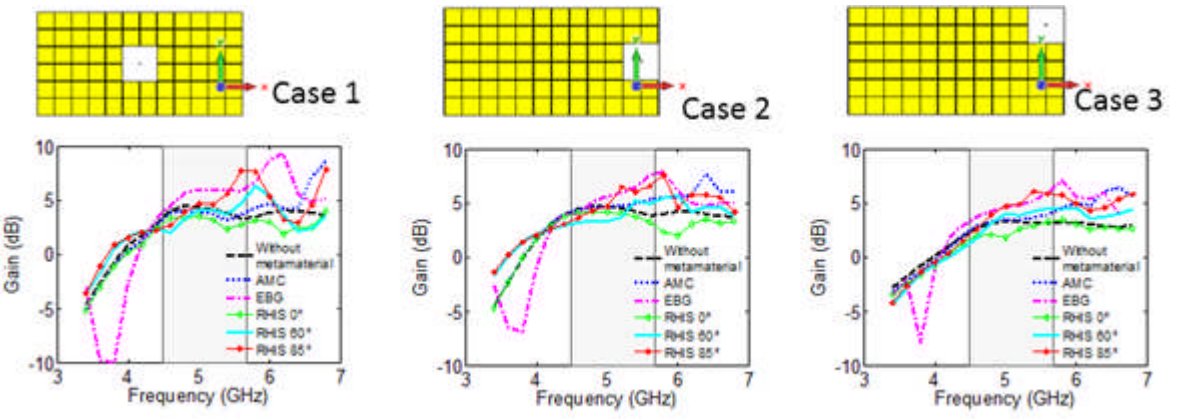

Figure 64 Realised Gain. Case 1: antenna at centre. Case 2: antenna at middle of the edge. Case 3: antenna on the corner

In all configurations, EBG structure modifies the radiation and changes the omnidirectional antenna into a directive one. In the case of AMC solution the radiation pattern seems to be preserved. When RHIS solutions are implemented, the

gain decreases and the radiation pattern is slightly modified but it remains acceptable. The radiation pattern is displayed in Figures 64, 65 and 66.

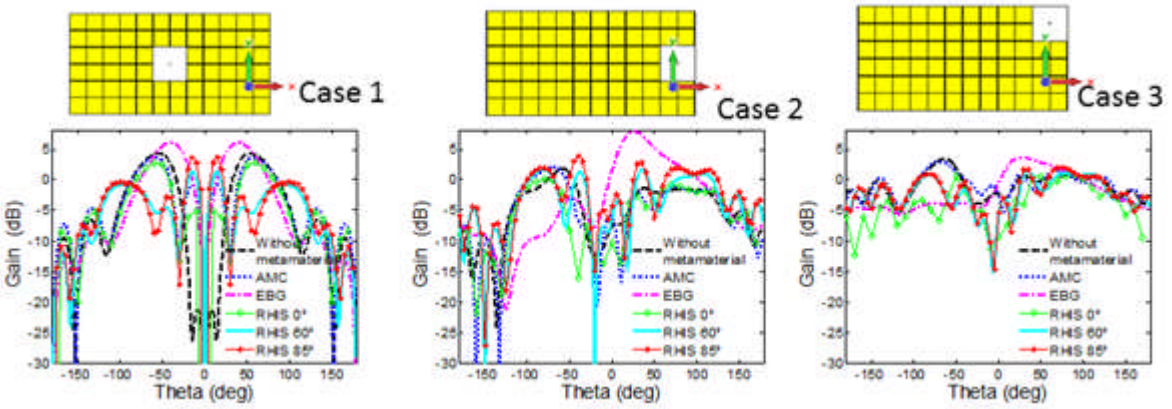

Figure 65 Gain Radiation pattern. Plane phi = 0°. Case 1: antenna at centre. Case 2: antenna at middle of the edge. Case 3: antenna on the corner

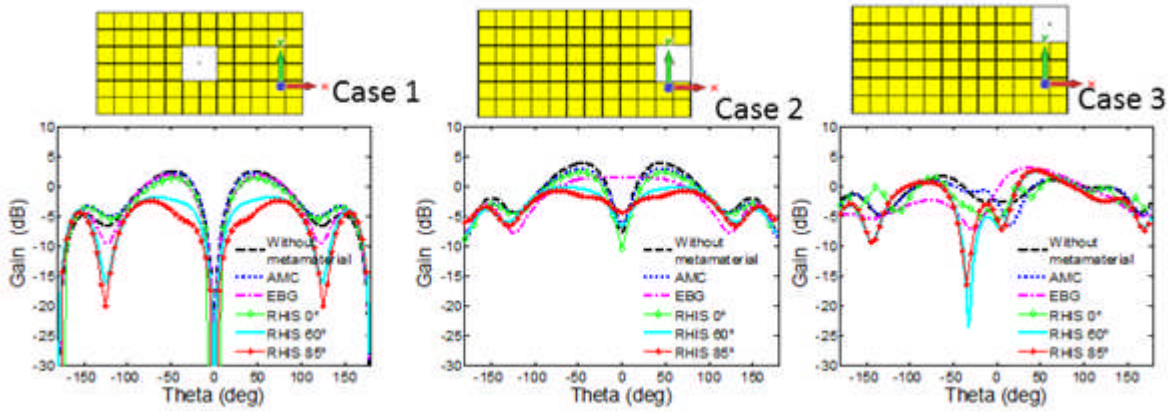

Figure 66 Gain Radiation pattern. Plane phi = 90°. Case 1: antenna at centre. Case 2: antenna at middle of the edge. Case 3: antenna on the corner

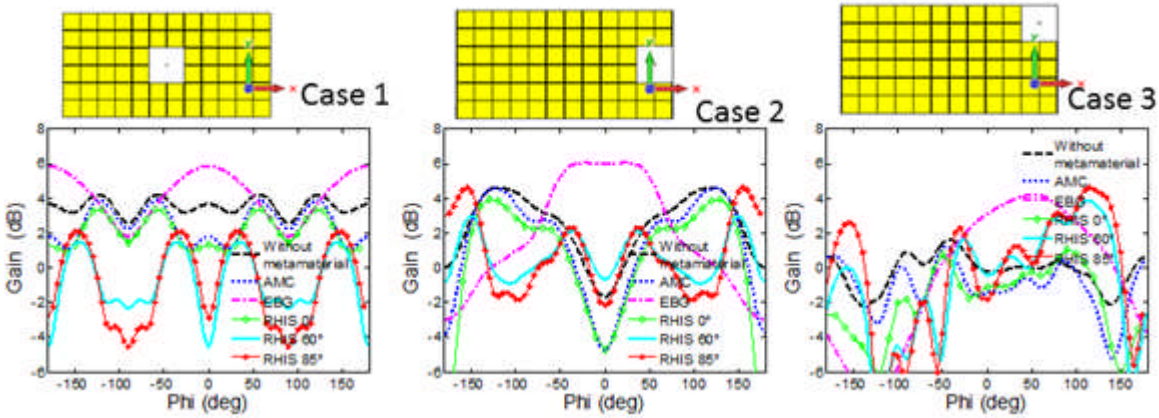

Figure 67 Gain Radiation pattern. Plane theta = 45°. Case 1: antenna at centre. Case 2: antenna at middle of the edge. Case 3: antenna on the corner

The best solution is defined as the antenna where impedance matching and omnidirectional radiation are preserved. In the case of monopole antenna, the case where the antenna is at centre is analyzed as reference case. The exposure taking into account the solutions with AMC and RHIS has been analyzed (see section

2.1.2.2). AMC and RHIS solutions are selected because they preserve the antenna matched and don't significantly modify the radiation of the reference antenna.

4.4.2 IFA Antenna

The IFA is surrounded with the metamaterial structures without four cells like previously for the monopole antenna. In the case of the RHIS solution, results with the structure optimized for oblique incidence are not available at the moment. The results for three positions (centre, middle of the edge and corner) of the monopole antenna are displayed in the next paragraphs.

In the case of the IFA antenna, the antenna size is reduced due to influence of the metamaterials.

Figure 68 displays the antenna matching. The antenna is matched for solutions with AMC and RHIS in all configurations. In the case of the EBG solution the antenna matching is not preserved.

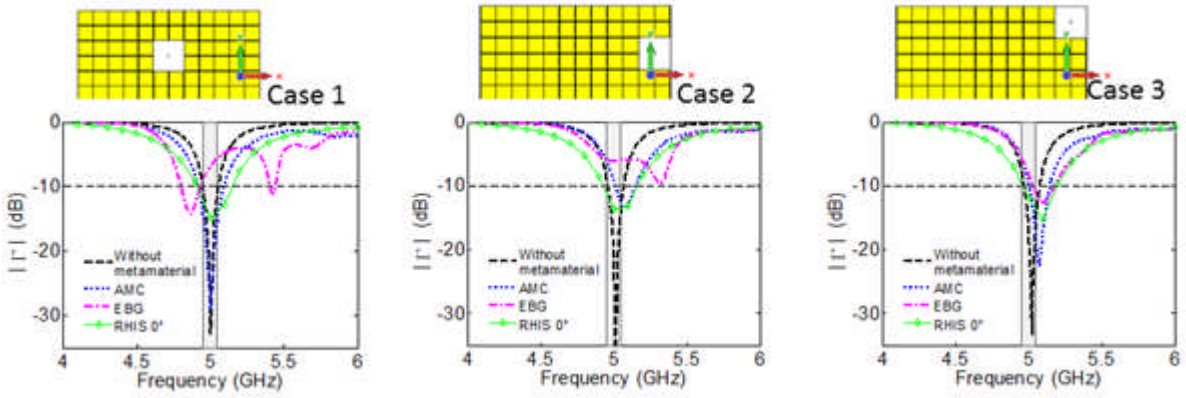

Figure 68 Impedance matching. Case 1: antenna at centre. Case 2: antenna at middle of the edge. Case 3: antenna on the corner

Regarding the efficiency and the gain (Figure 69 and Figure 70). The solution with RHIS reduces slightly the total efficiency and the gain. In the case of the AMC, efficiency is preserved but the gain is increases in the cases where the antenna is located on the side.

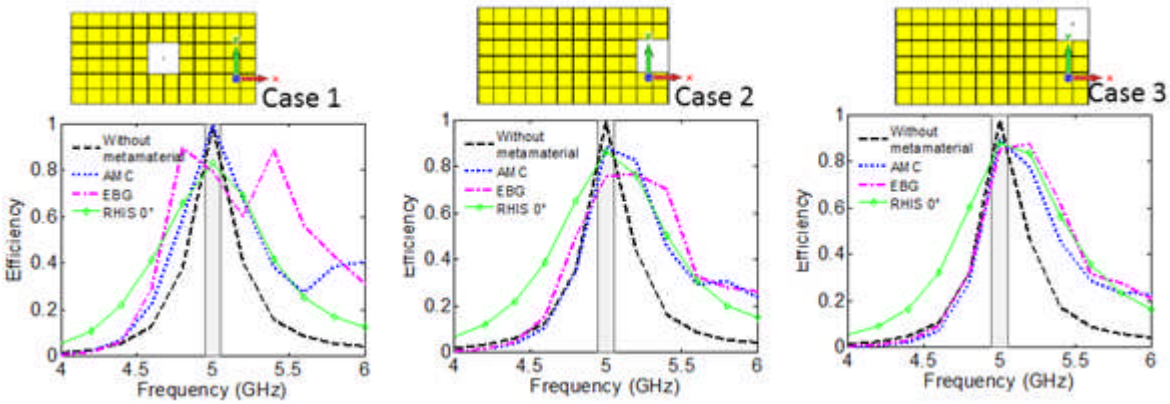

Figure 69 Efficiency. Case 1: antenna at centre. Case 2: antenna at middle of the edge. Case 3: Antenna on the corner

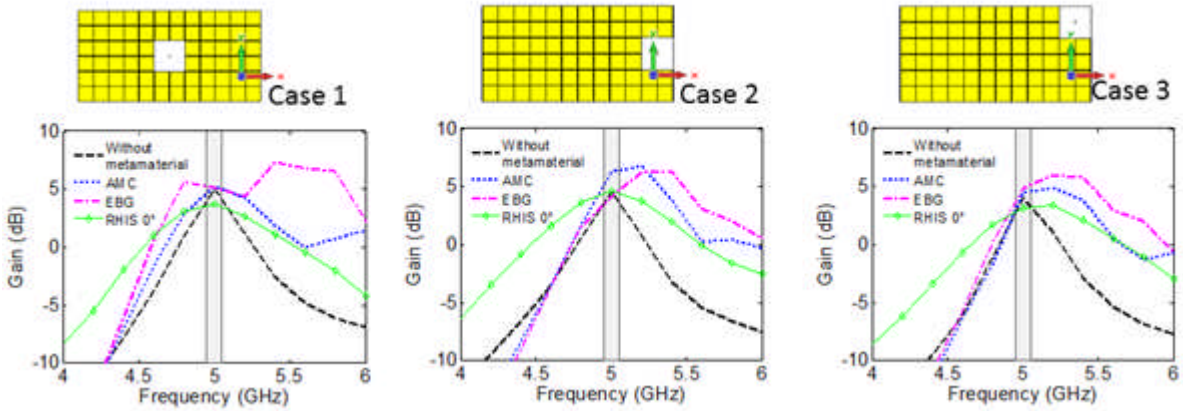

Figure 70 Realised Gain. Case 1: antenna at centre. Case 2: antenna at middle of the edge. Case 3: antenna on the corner

If we consider the radiation pattern, the RHIS solution appears to be the appropriated because the radiation pattern of the IFA antenna without metamaterials is slightly modified in all configurations. In the case of the AMC and EBG, radiation pattern changes are observed. So, AMC solution is rejected also.

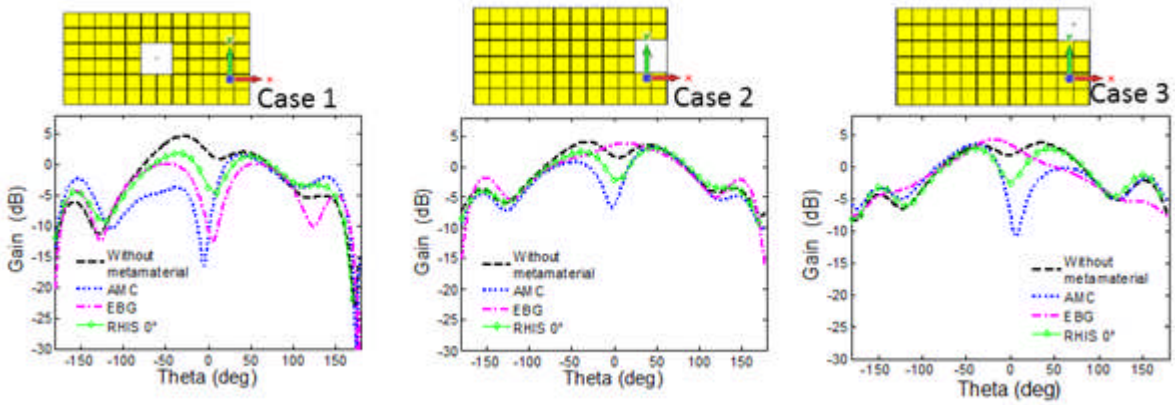

Figure 71 Gain Radiation pattern. Plane phi = 0°. Case 1: antenna at centre. Case 2: antenna at middle of the edge. Case 3: antenna on the corner

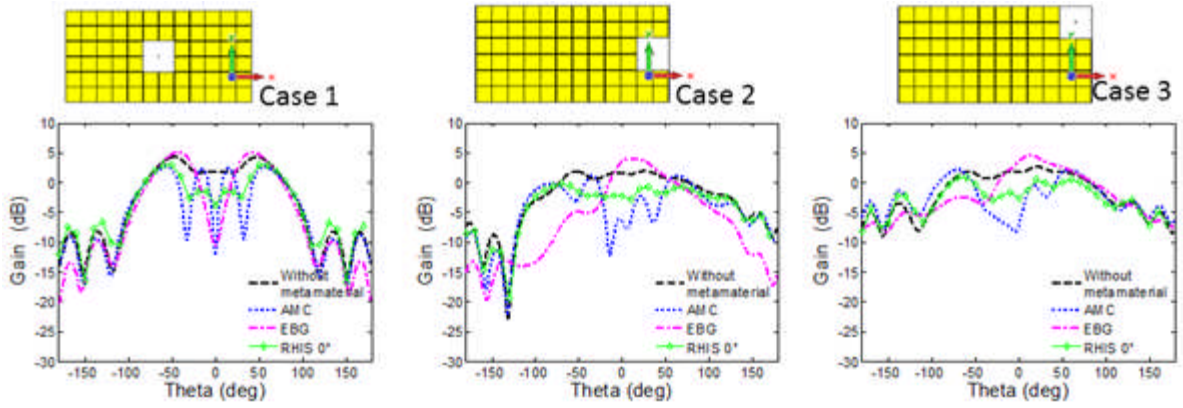

Figure 72 Gain Radiation pattern. Plane phi =9 0°. Case 1: antenna at centre. Case 2: antenna at middle of the edge. Case 3: antenna on the corner

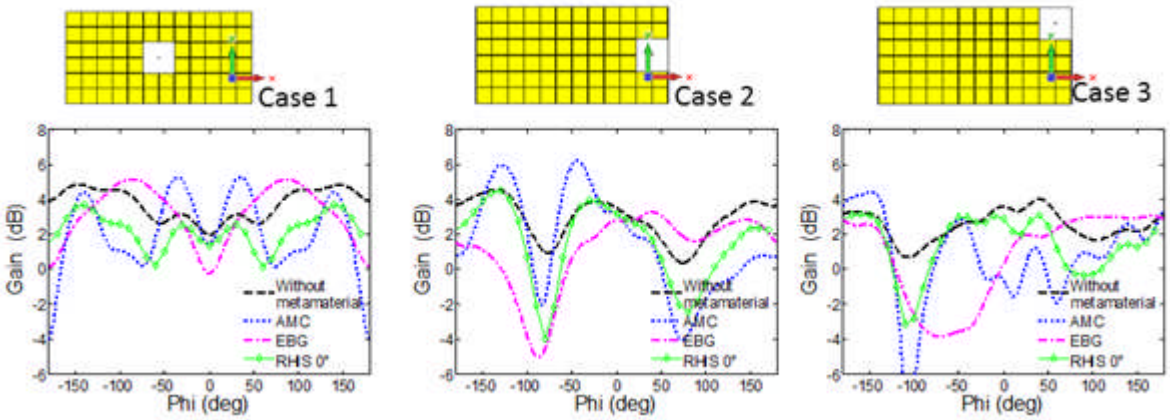

Figure 73 Gain Radiation pattern. Plane theta = 45°. Case: Antenna at centre. Case 2: Antenna at middle of the edge. Case 3: Antenna on the corner

The IFA antenna has been to represent a realistic case of mobile antennas. Then, the case of the antenna located on the middle of edge is selected as realistic case for our study. Exposure is analyzed for this position case in section 2.1.2.2. RHIS solution is selected to reduce the exposure because it preserves antenna matched and radiation pattern of the antenna without metamaterials.

APPENDIX 3: EXPERIMENTAL VALIDATION – MONOPOLE ANTENNA

The antenna reference case presented in section 2 has been realized. The objective is to confirm the performances given by simulation (impedance matching and radiation).

The reference case consists of a monopole antenna placed at the center of a grounded dielectric slab. Two solutions with and without metamaterials have been realized. In the case of the antenna with metamaterials, only the RHIS optimized to absorb incident waves at 85° in TE polarization is realized because it has been proved that was the best solution to reduce the exposure.

Figure 74 shows the prototype of the reference antenna without metamaterials. The monopole antenna is placed at the center of a grounded FR-4 laminate with thickness equals to 1.6 mm and relative permittivity of 4.2. Figure 75 shows the prototype of the reference antenna with RHIS 85°. The RHIS structure is manufactured using the substrate Arlon Diclad 880 with thickness equals to 2.36 mm and a relative dielectric permittivity of 2.2. The resistances are the surface mounted chip resistors that are soldering between the patches. The resistance value is 5600 Ω.

The size (~74 x 150 mm) of the prototypes is representative of a last generation mobile phone.

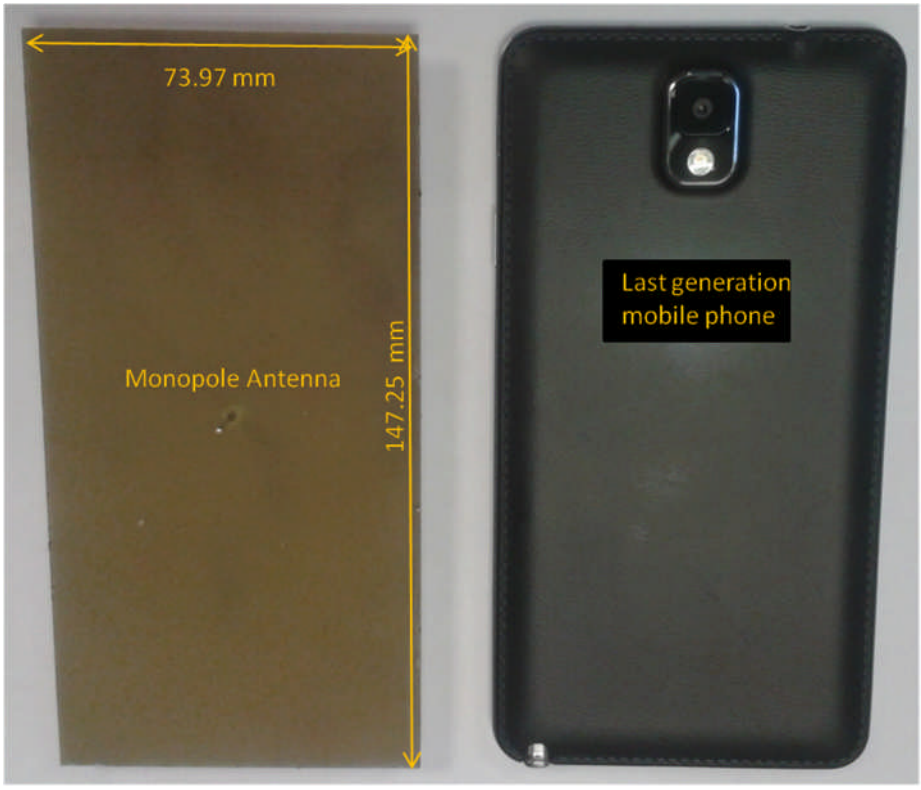

Figure 74 Monopole antenna without metamaterials

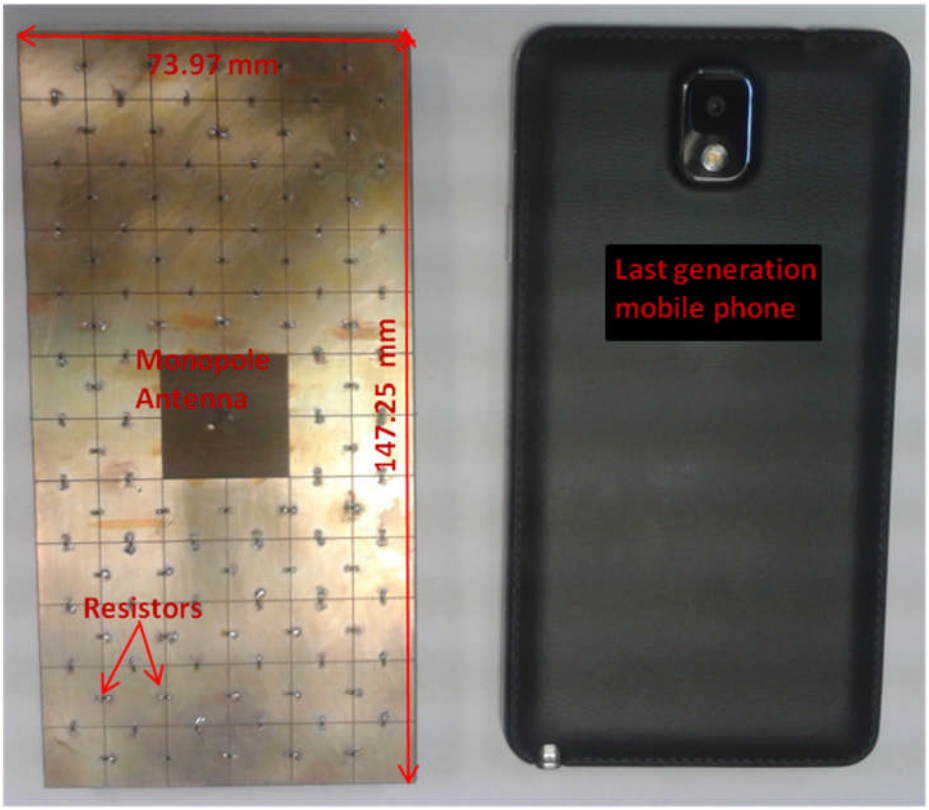

Figure 75 Monopole antenna with RHIS structure

First, the impedance matching is validated. Figure 76 and Figure 77, show the simulation and measurement results. For the monopole without metamaterial (Figure 76), a very good agreement between simulation and measurement is obtained.

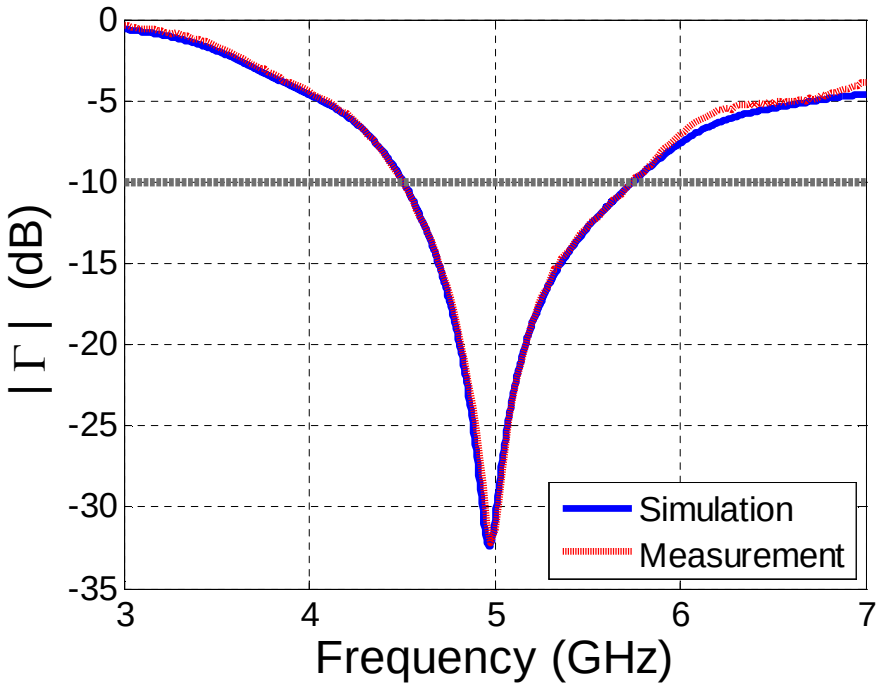

Figure 76 Impedance matching monopole antenna without metamaterial

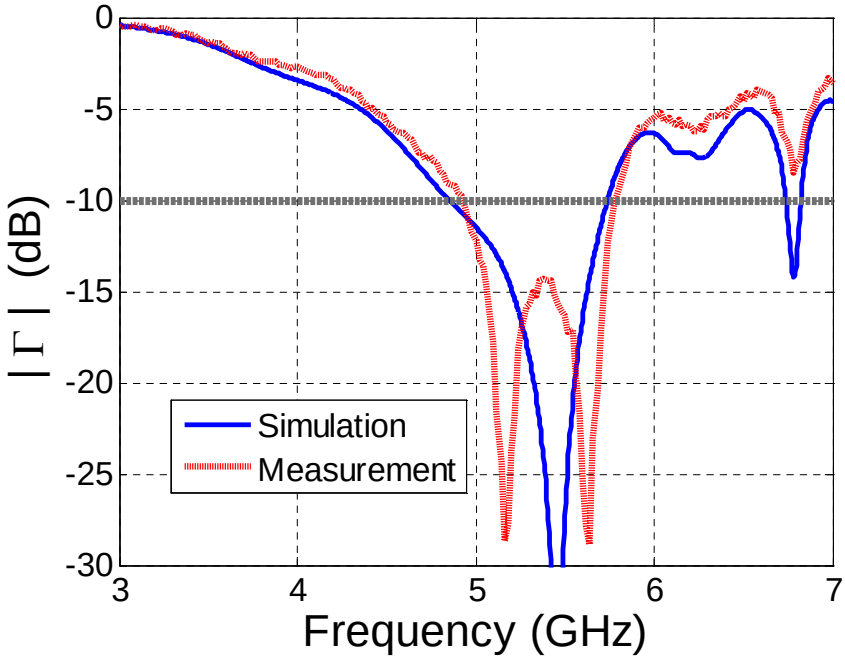

Figure 77 Impedance matching monopole antenna with RHIS

In the case of the monopole with RHIS (Figure 77), a good agreement between simulations and measurements is observed with some little differences at low level.

Next, the radiation performances are validated by the measurement of the realized gain in two main planes. Figure 78 and Figure 79 display the results. A very good agreement between simulations and measurements is observed in both cases.

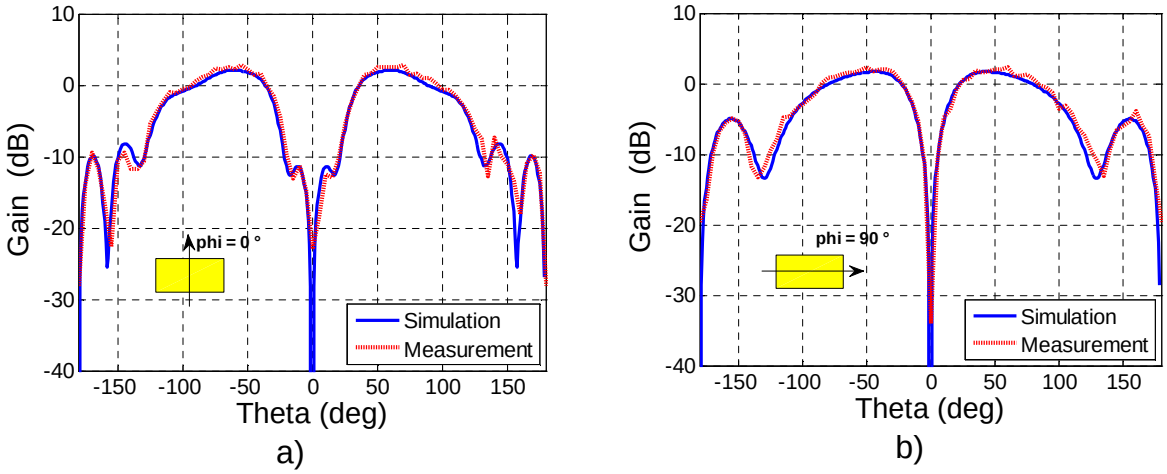

Figure 78 Gain, monopole antenna without metamaterial. a) Plan phi = 0°. b) Plan phi = 90°.

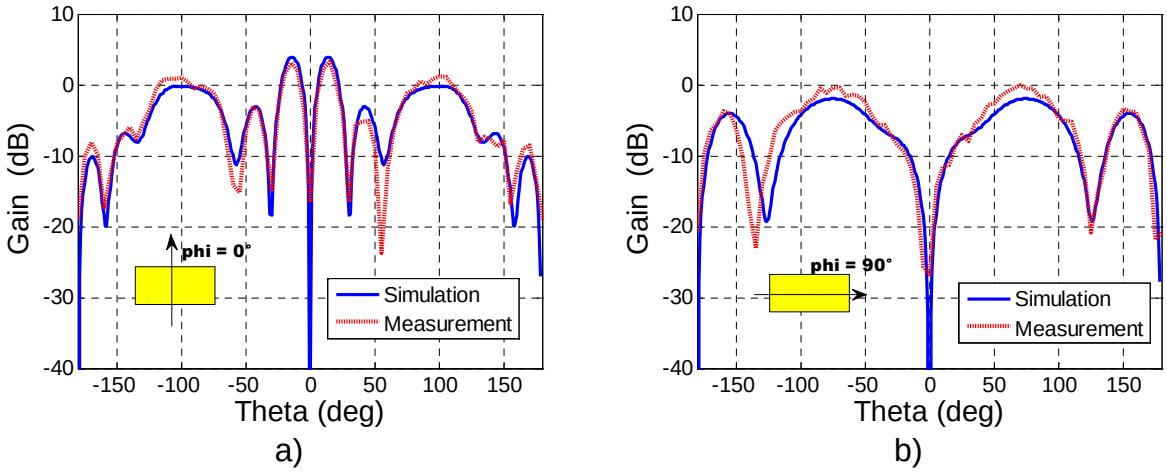

Figure 79 Gain, monopole antenna with RHIS. a) Plan phi = 0°. b) Plan phi = 90°.